

POLITECNICO DI TORINO

**Corso di Laurea Magistrale
In Mechanical Engineering
A.A. 2022/23
Sessione di Laurea 10/2023**

Tesi di Laurea Magistrale

Simulation of the behaviour of tracked vehicles on soft soils using multibody software



**Politecnico
di Torino**

Relatori:

Enrico Galvagno
Luca Dimauro
Mauro Velardocchia
Antonio Tota

Candidati:

Gaetano Prezioso

¹ Politecnico di Torino, Department of Mechanical and Aerospace Engineering
² Politecnico di Torino, Department of Management and Production Engineering
Corso Duca degli Abruzzi, 24 – 10129 Torino, Italy

Index

Index.....	2
Abstract	3
Introduction	4
Chapter 1 Soft soil description	5
1.1 Vertical/normal forces.....	5
1.1.1 Loading curves parametrization analysis	6
1.1.2 Unloading curves parametrization	10
1.1.3 Repetitive loading and loading cycles analysis	12
1.1.4 Vertical-normal force magnitude and direction calculation.....	19
1.1.5 Approximation hypotheses verification	22
1.2 Longitudinal and Lateral Forces	29
1.2.1 Selection threshold between internal shearing and bulldozing	34
1.2.2 Grouser height sensitivity analysis	35
1.2.3 Optimal grouser number and spacing analysis	40
1.2.4 Longitudinal force calculation.....	44
1.3 Segment forces	44
Chapter 2 Tracked vehicle analyses.....	45
2.1 Assembly description and soil-controller setup.....	45
2.2 First analyses	51
2.2.1 Soil parameters and behaviour	53
2.3 Vehicle parameters on different soils.....	55
2.3.1 Similar soils from the 2 types	58
2.3.2 Segment forces analysis	60
2.4 Issue with total track forces.....	63
2.5 ATV pressure-sinkage analysis over time.....	64
2.6 Drawbar pull testing.....	66
2.6.1 Drawbar characteristics	67
2.6.2 Grouser height tuning	72
2.7 Tensioner tuning	74
2.7.1 Drawbar performance analysis	95
Chapter 3 Conclusions	98
Chapter 4 References	99

Abstract

This document analyses the behaviour of tracked vehicles on soft soils, firstly looking at how it has been modelled through literature, with the aid of software tools such as MATLAB and the Adams Car plugin “Adams Tracked Vehicle”, or ATV.

Using MATLAB, the various equations modelling soft soil behaviours were tested, and some ideal loading scenarios, like repetitive or continuous loading, and optimizations, like grouser height and spacing, were proposed.

Using ATV instead, it was possible to simulate the full behaviour of a tank moving through different soils, such as sand, clay or snow. Extrapolating interesting values such as input torque and power or track slip, these optimizations were tested and the influence of different parameters like track tension and geometry was shown.

Introduction

Off road locomotion is a topic of interest in many fields, such as the automotive industry and transport, agriculture, military. Because of this, it has been studied for many years, pioneered by Bekker [3] (1956) and still in development when regarding simulating and analysing the behaviour of a wheeled or tracked vehicle in soft soils.

Gathering information from literature and articles that studied terramechanics, the aim of this document was to explain how soft soil modelling works and illustrate the trends of all forces related to contact and interactions with many different terrains using the tools provided.

The book “Terramechanics and off-road vehicle engineering – Wong” [1], combined with the guide provided with the ATV software tool, was useful in laying the groundwork on what the most important parameters of a terrain and vehicle are and how the rigid bodies of a tracked vehicle and soft soils engage with each other. It also gives the reader ideas regarding what was already tested and discussed and what could be instead an interesting study to develop.

Using such sources, the first steps in the development of this document were made, in describing the forces present in the interaction between a track segment and a deformable terrain, and these were analysed to understand the interactions that different soils generated in the same conditions, and using the results of these analyses would give inputs on what to work on when simulating the whole body of the vehicle.

Wong’s book also describes the different approaches used in the modelling of this topic [1]:

- The empirical methods: Vehicles are tested in a range of terrains considered to be representative, all while identifying terrain variables and measuring them via field observations.
- Computational methods: The finite element method (FEM) and discrete element method (DEM) involve intensive computation, and can be used to predict the behaviour of tyre performances on soft soil, but don’t provide enough complexity to analyse the performance of tracked vehicles, which have many more elements involved in the calculations.
- Methods for parametric analysis: These are mathematical models developed in lieu of the limitations of the empirical and computational models mentioned. These methods include performance evaluations of vehicles with different characteristics, like flexible tracks, or off road wheeled vehicles.

The ATV plugin uses the third category of methods. It gives the user flexibility in designing a vehicle and modifying most parameters, from geometry of the hull or all wheels, the sprocket wheel, the track segments, and all other significant components, and with it the user is able to simulate and hence predict the performance of a vehicle with the modification of the aforementioned components.

By understanding the way the plugin makes calculations and creates outputs, and optimizing the analyses once done, the results can be discussed and conclusions can be made on the various ways to optimize the performance of a tracked vehicle cruising on soft terrain.

Chapter 1 Soft soil description

As stated in the introduction, our simulations are done in the Adams Car ATV module environment, so it's important to understand of how the program handles soft soil interactions.

1.1 Vertical/normal forces

The vertical forces acting on the track are modelled based on the formula proposed by Bekker [1], which, for continuous loading ($z > z_{max}$) is:

$$P = \left(\frac{K_c}{b} + K_\Phi \right) \cdot z^n \quad (1.1.1)$$

where:

- Z [m] is the penetration.
- $K_\Phi \left[\frac{N}{m^3} \right]$, $K_c \left[\frac{N}{m^2} \right]$ and n are material dependent sinkage parameters.
- b [m] is the lesser dimension of the tool penetrating the soil (track width in our case).

For unloading, which means when the penetration is less than the maximum one ($z < z_{max}$), the equation becomes [1]:

$$P = P_{max} - (K_0 + A_u \cdot z_{max})(z_{max} - z) \quad (1.1.2)$$

where:

- $P_{max} \left[\frac{N}{m^2} \right]$ is the maximum pressure calculated using (1.1) at the maximum penetration.
- $K_0 \left[\frac{N}{m^3} \right]$ and $A_u \left[\frac{N}{m^4} \right]$ are ground property parameters.

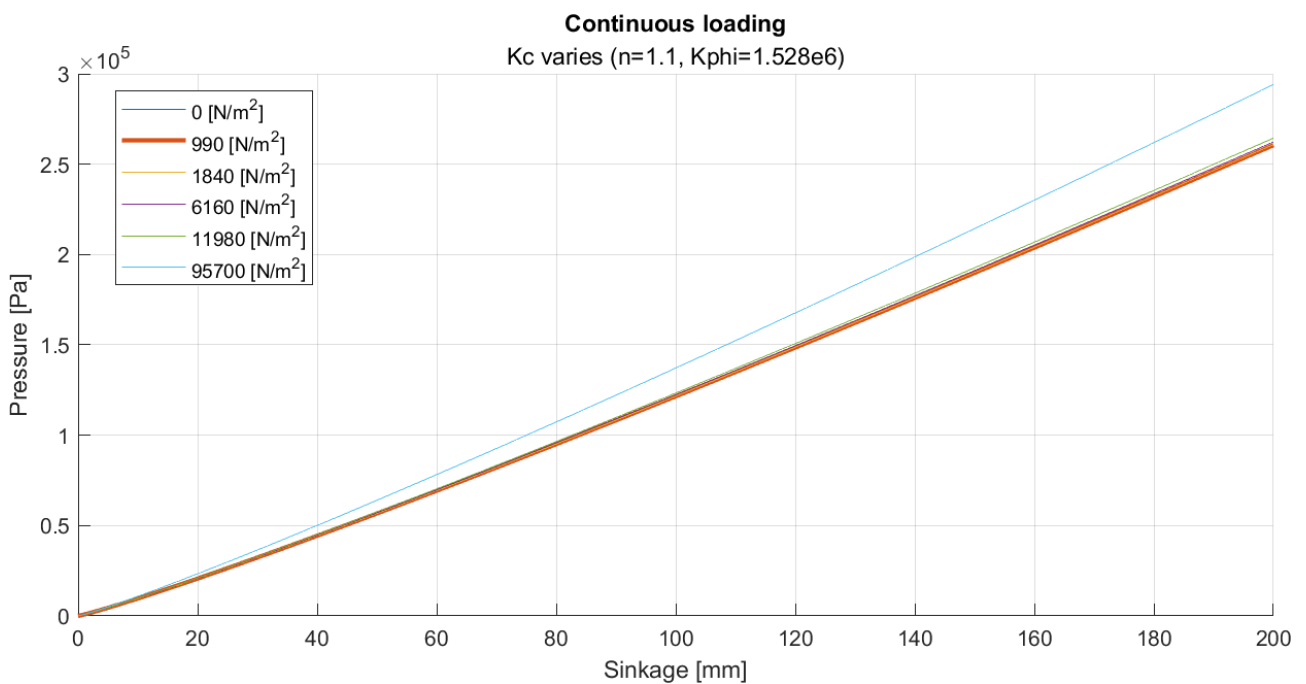
1.1.1 Loading curves parametrization analysis

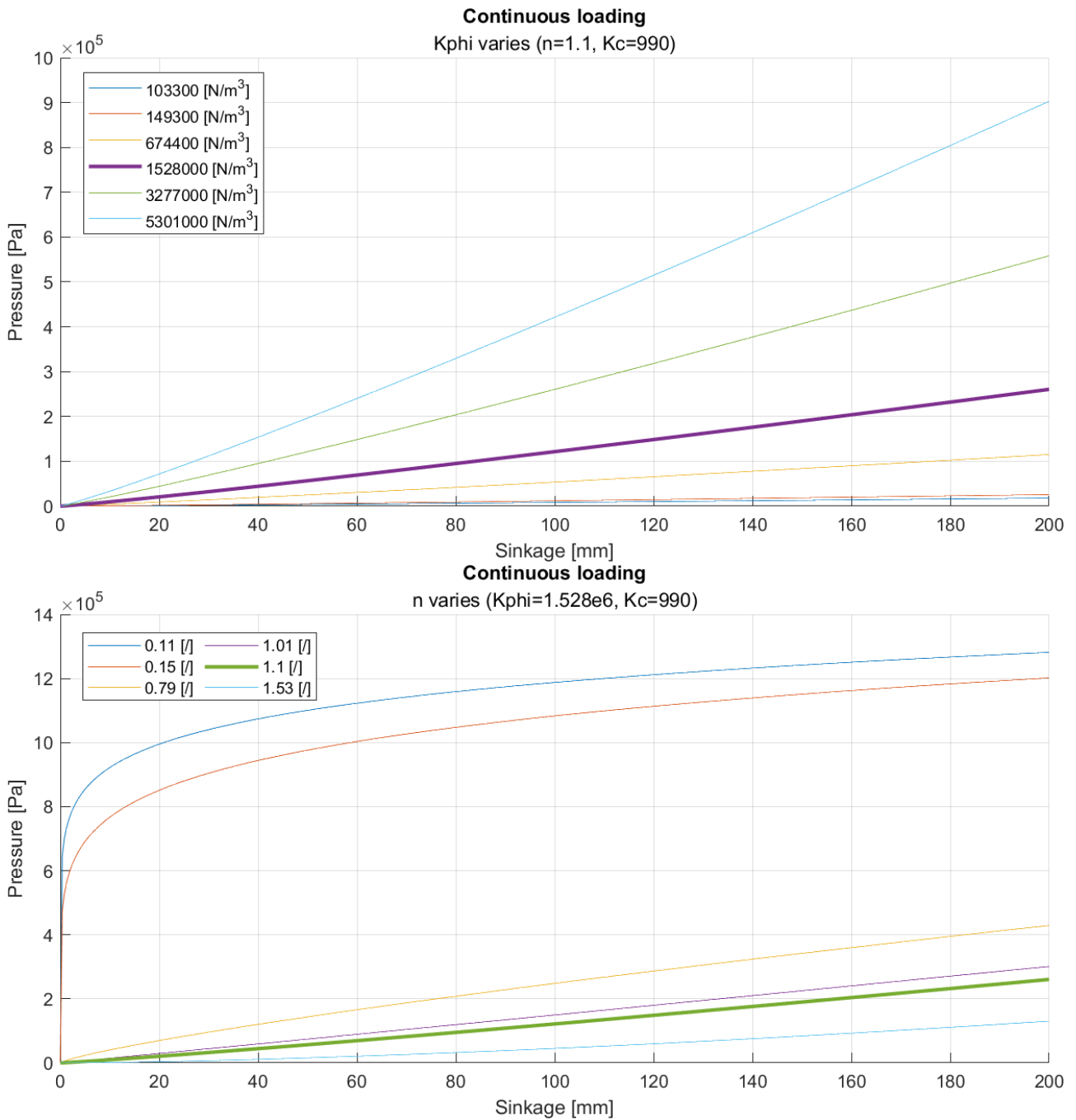
Now knowing these equations, a sensitivity analysis on each parameter was done;

In the script there are a few parameters that needed to be set before actually going into the parametrizations of soil values, and those are mainly the geometric parameters of our tank track (track width and grouser height) and a range of sinkage that could be acceptable. Since our starting soil is sand, I chose a sinkage range of 0-200 mm, which seems to be a good range when looking at simulation results.

Having done that, a set of 6 different values for each vertical parameter was chosen according to what the minimum and maximum values of different soils were, choosing again dry sand as base soil and varying only one parameter per graph to see what effect each one had on the pressure curves.

Let's see what continuous loading equations give:





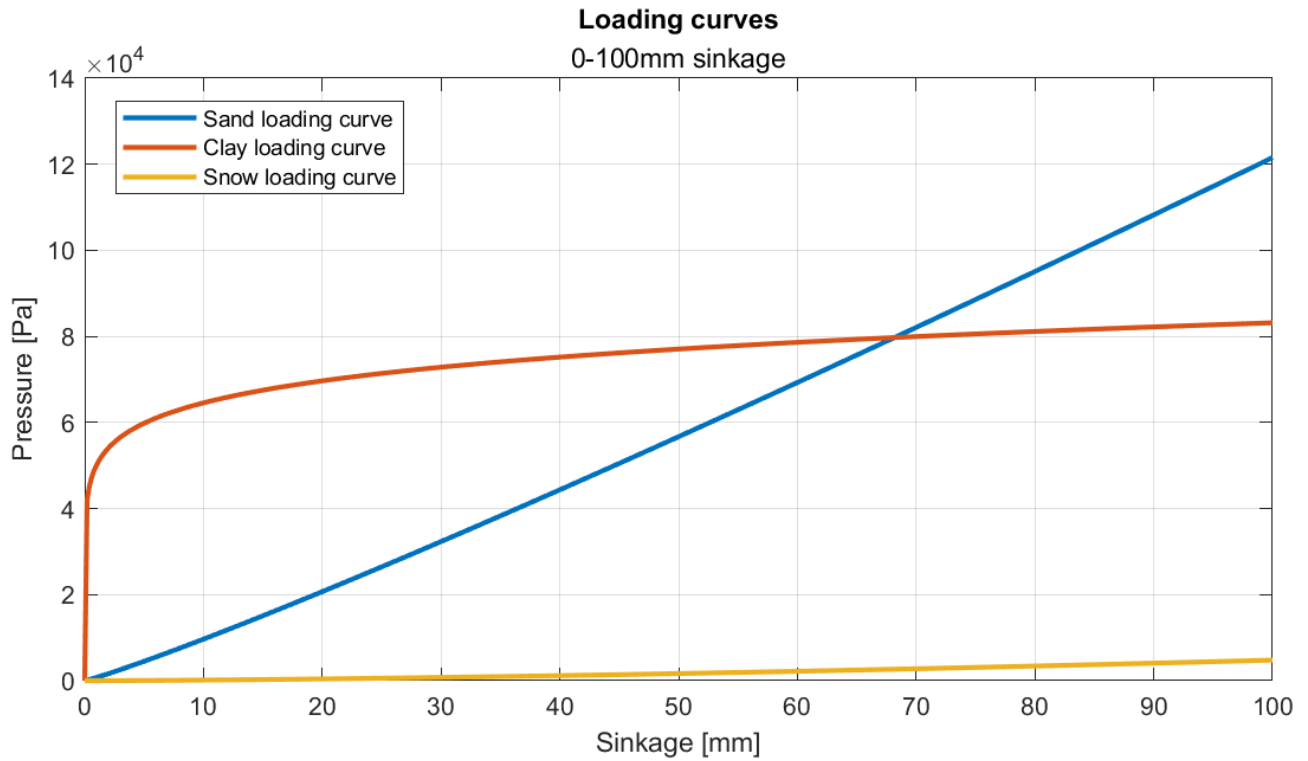
Figures 1.1.1-3 – Continuous loading parameters tuning

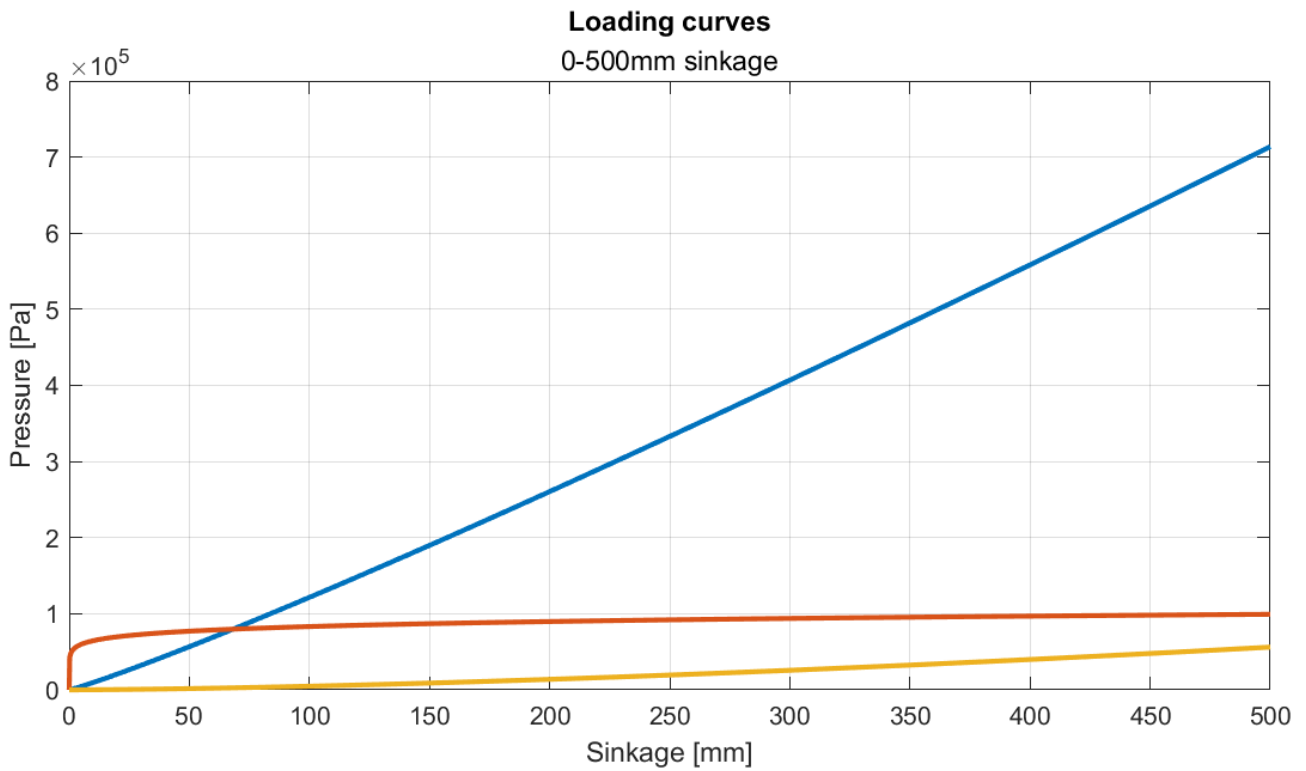
We can immediately see how varying K_c has little to no effect on the values of pressure linked to the sinkage compared to other parameters. The most interesting one seems to be the value of n , which controls the nonlinearity of the trend: a value of one implies a linear trend while different values that could be less or greater than one introduce a nonlinear pressure-sinkage relation. We can also see how K_{phi} controls the slope of the curve in close to the same way K_c does, but in a much more significant way, due to the fact that values are in general much higher for this parameter, for the soils we're taking into consideration.

To make things a bit clearer, in the next plot there are displayed the loading curves of the 3 soils we're experimenting with, being dry sand, heavy clay 40%, and soft snow:

	Dry sand LLL	Heavy clay WES 40	soft snow	
spec weight	1.525E+04	1.726E+04	3.000E+03	N/m ³
Kc	9.900E+02	1.840E+03	6.160E+03	N/m ²
Kphi	1.528E+06	1.033E+05	1.493E+05	N/m ³
n	1.100E+00	1.100E-01	1.530E+00	\

Table 1.1.1 – Sand, clay and snow loading parameters



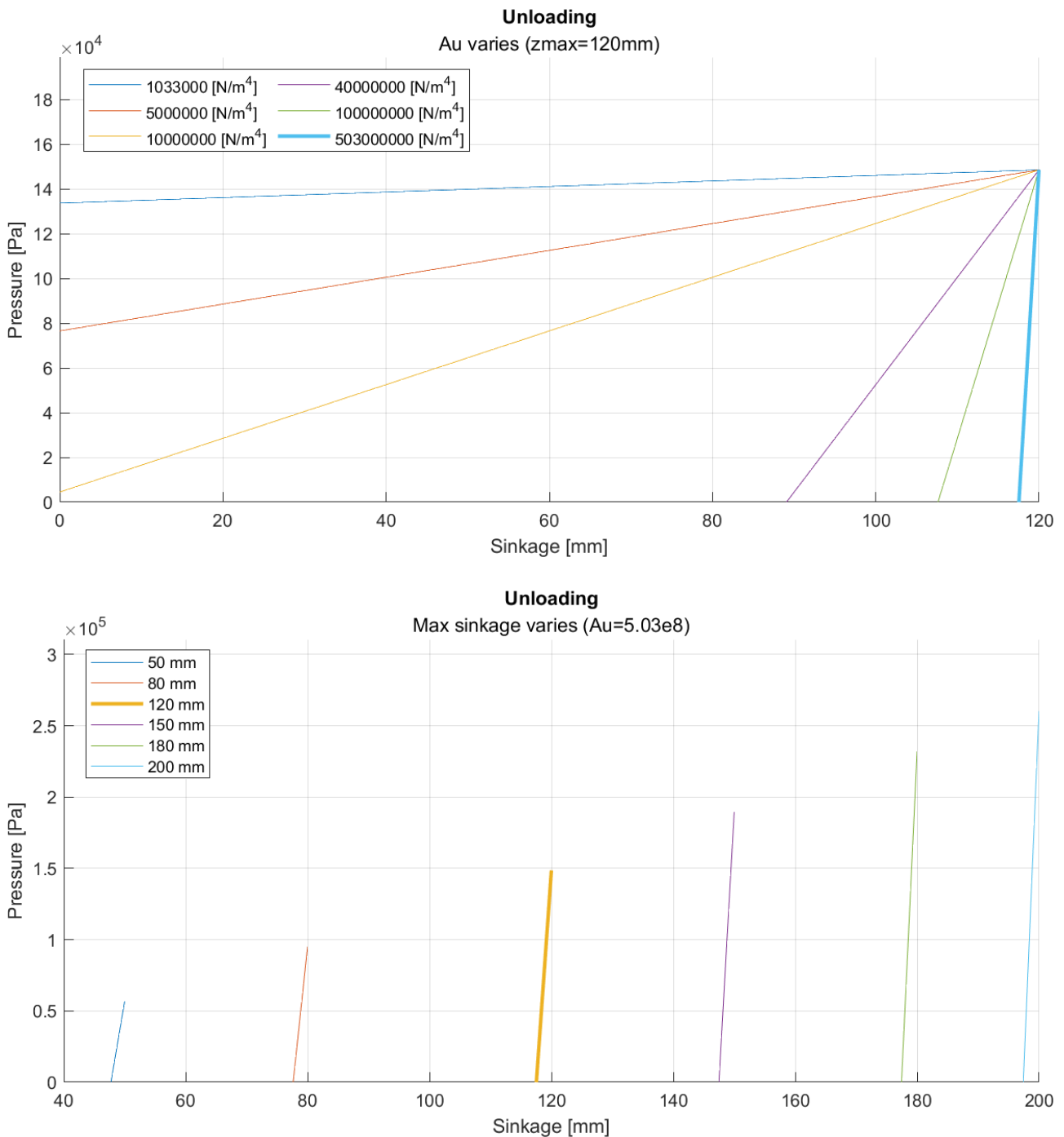


Figures 1.1.4-5 – Loading curves of real soils

As we can see, the sand curve is almost linear, and grows at a much faster rate compared to snow, having an order of magnitude higher K_{phi} , while clay has a very non-linear behaviour, and grows to a high pressure almost instantly but then the curve flattens and the sand pressure surpasses it quite quickly.

1.1.2 Unloading curves parametrization

The same was done for the unloading curves described in chapter 1.1:



Figures 1.1.6-7 – Unloading parameters tuning

It seems interesting to see the Au variation, and how it's the main parameter affecting the slope of the unloading curve: We can see that with other parameters as default, The Au values $<4e7$ evoke a different behaviour; since it would require negative sinkage to get to 0 pressure, which wouldn't make any sense, the software is able to compare the unloading and loading curves, and if the unloading curve goes above the loading one, the unloading pressure will follow the loading curve back to 0 pressure and sinkage. This happens if the values of Au are too low or if unloading

happens too early on a loading curve having an exponent n lower than 1. We can see that the higher A_u is, the more “memory” the soil has, meaning even really low variations in sinkage generate really steep pressure curves. Basically, this means that as soon as the track segment rises of a few millimetres above the maximum sinkage, no load is any longer applied to it until it re-sinks very close, or surpassing, the maximum one; the minimum value of A_u chosen in the graph is proprietary to clay, which causes, as it will be shown in the next tests, a behaviour that is very different compared to sand and snow. The last plot instead highlights how there’s a small slope variation also linked to what the minimum sinkage, where pressure is null, is. As we can see from Figure 2.1.8, the “active” part of the soil is always around 3 mm below max sinkage for this soil (there’s some error due to discretization).

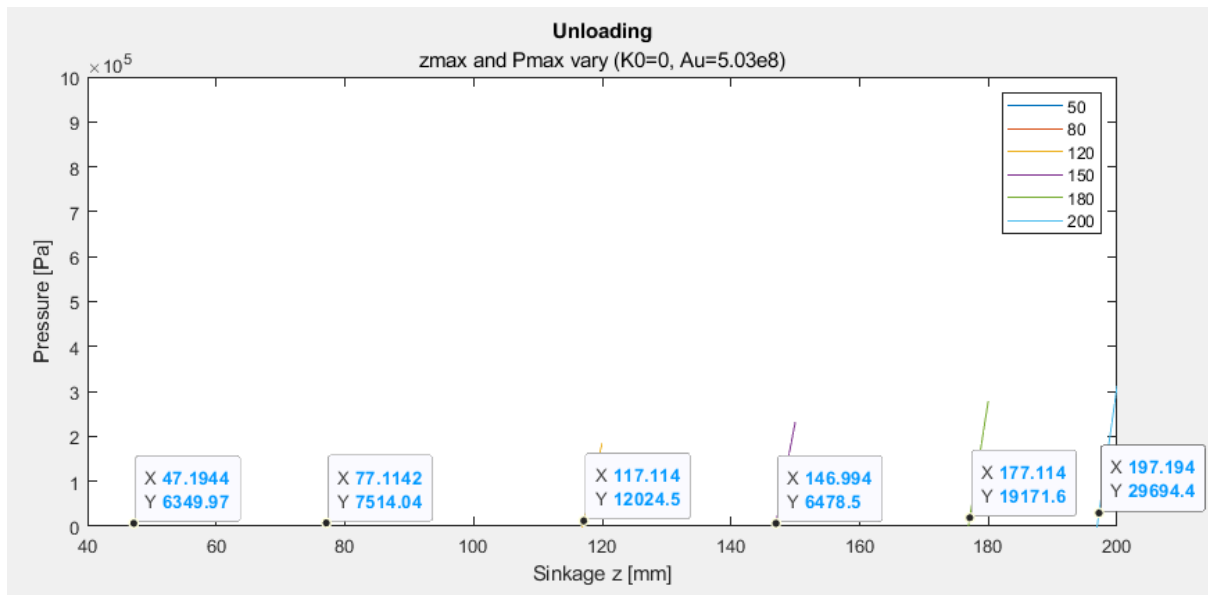


Figure 1.1.8 – Minimum pressure points for unloading

The ATV module remembers the sinkage and pressure values for each road segment, to be able to then use one or the other formulas when needed.

1.1.3 Repetitive loading and loading cycles analysis

Considering the case of a tracked vehicle, a road element is initially subject to load when the first road wheel comes in contact with it, passing over and generating a pressure. Once the wheel has passed, the load on the element is reduced, and it is applied again as a succeeding road wheel rolls over the same element. The unloading-reloading cycle continues until the rear roadwheel of the vehicle has passed.

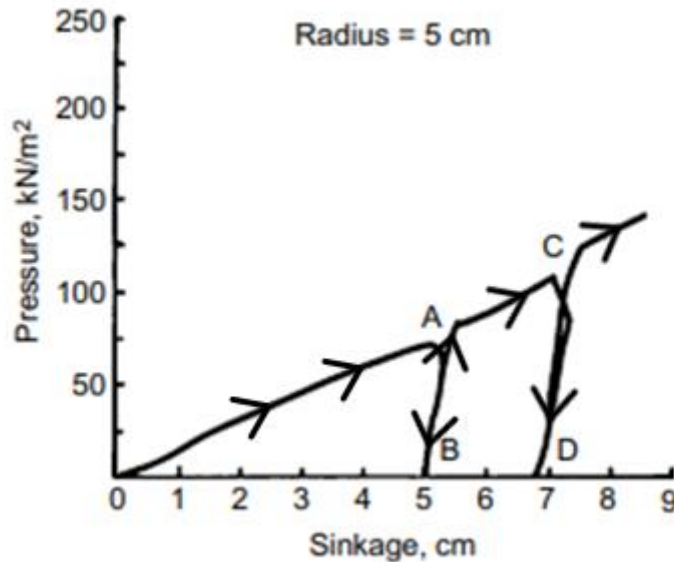


Figure 1.1.9 – Response to repetitive normal load [1]

In figure 1.1.9 we can see a typical response of terrain to repetitive loading. Pressure first increases along curve OA, but when load is reduced at point A, the pressure-sinkage relationship then follows curve AB. When load is reapplied, it follows more or less the same path, and if pressure then exceeds the maximum one reached previously (point A), additional sinkage results, following the original OA direction, then follows CD in unloading, having a very similar characteristic to AB. To summarize, the soil exerts pressure following equation (1.1.1) as it sinks, reaching a certain value; during unloading and successive loading, until a new sinkage/pressure maximum value is reached, the relationship follows equation (1.1.2).

The graph from figure 1.1.9 was recreated in MATLAB using the soft soil equation for the 3 different soils we will be using in the report, which are sand, clay and snow.

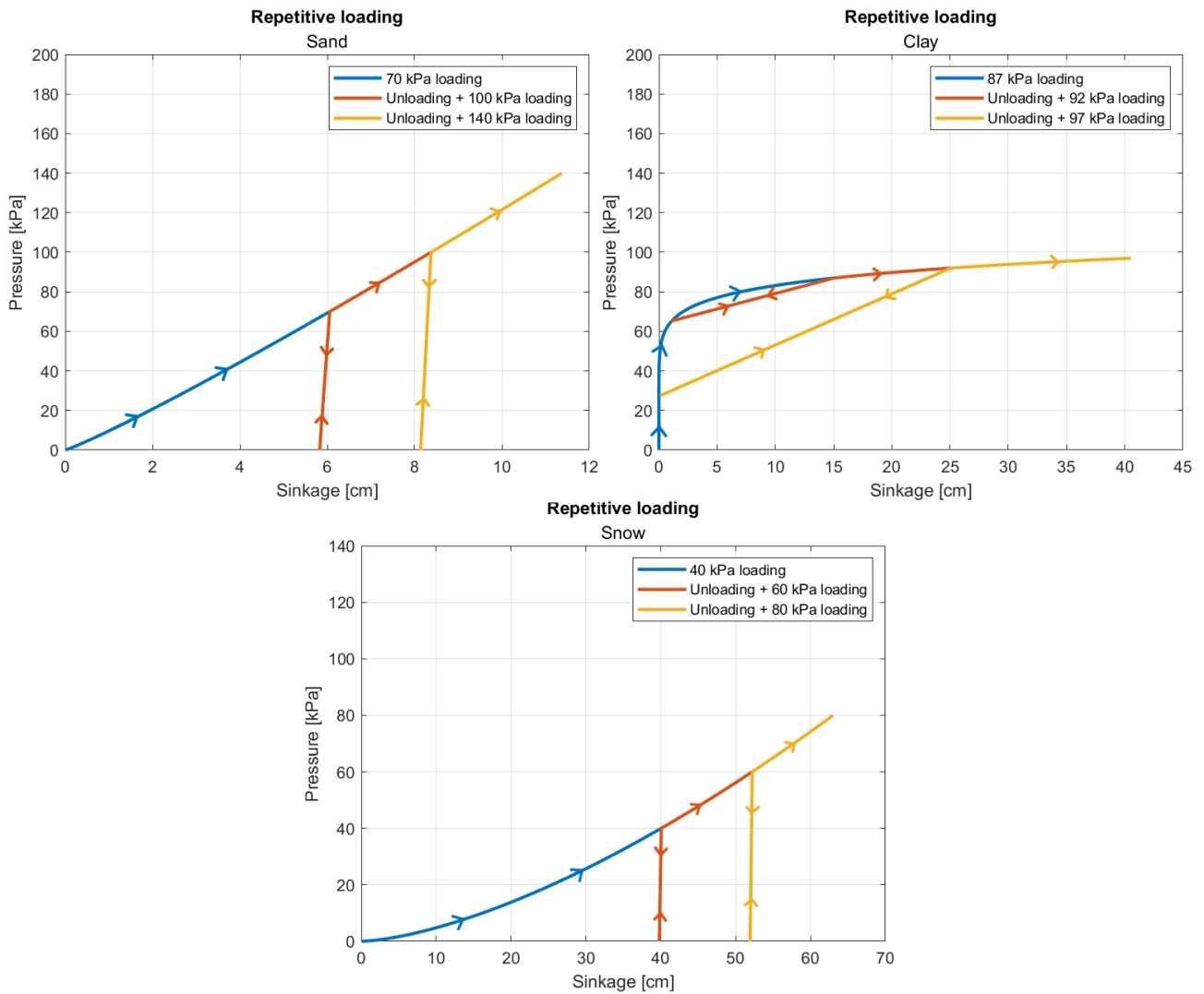
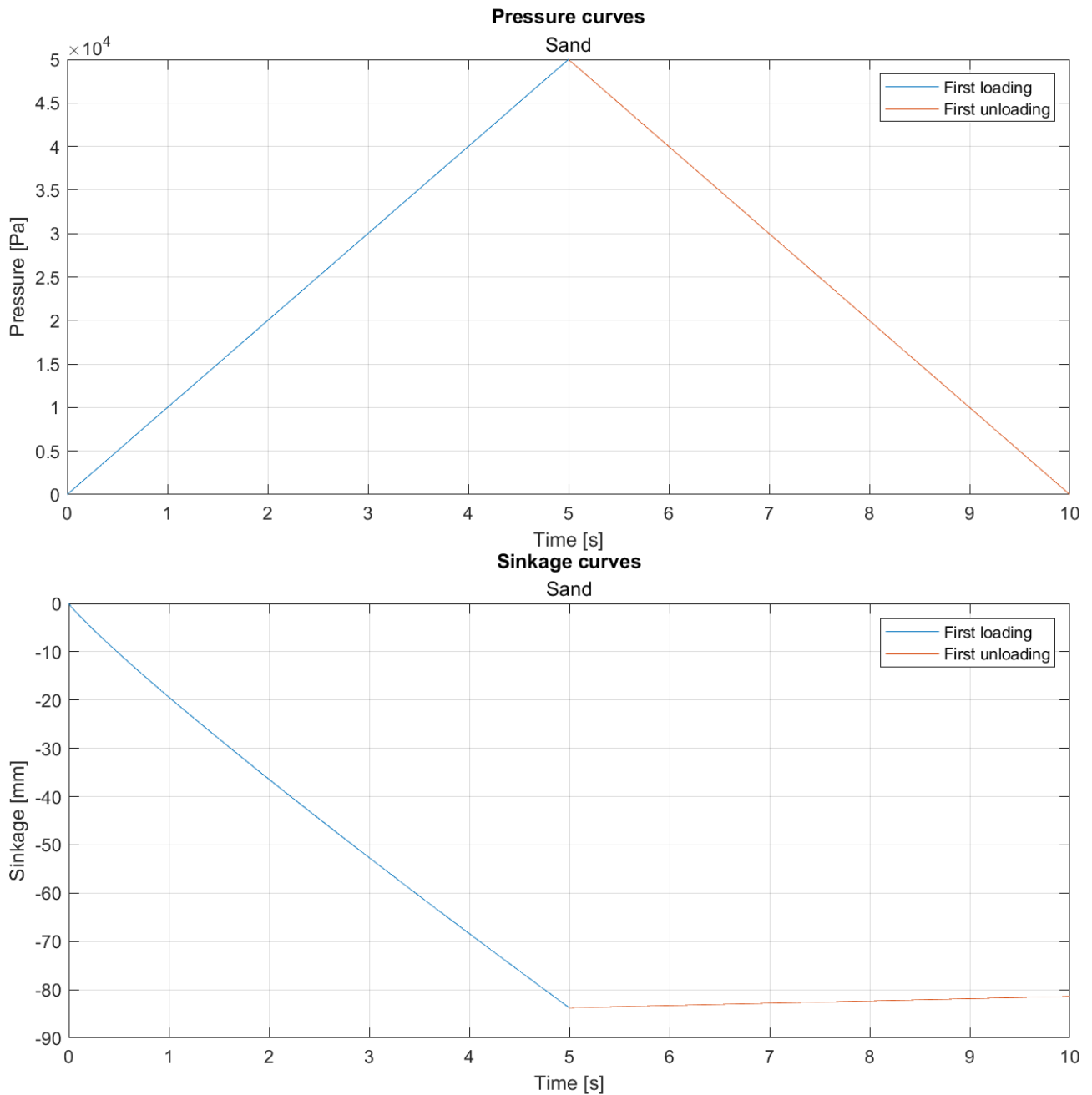


Figure 1.1.10 – Repetitive loading for different soils

As it can be seen, sand and snow have a very similar behaviour, with snow having even more “memory” of the load, with a steeper unloading curve. Clay however, behaves differently: The unloading curves are far less steep, and in fact, until a certain load is reached, intersect with the loading curve. The unloading follows firstly the linear unloading curve, then once it intersects the non linear loading, it follows the latter instead.

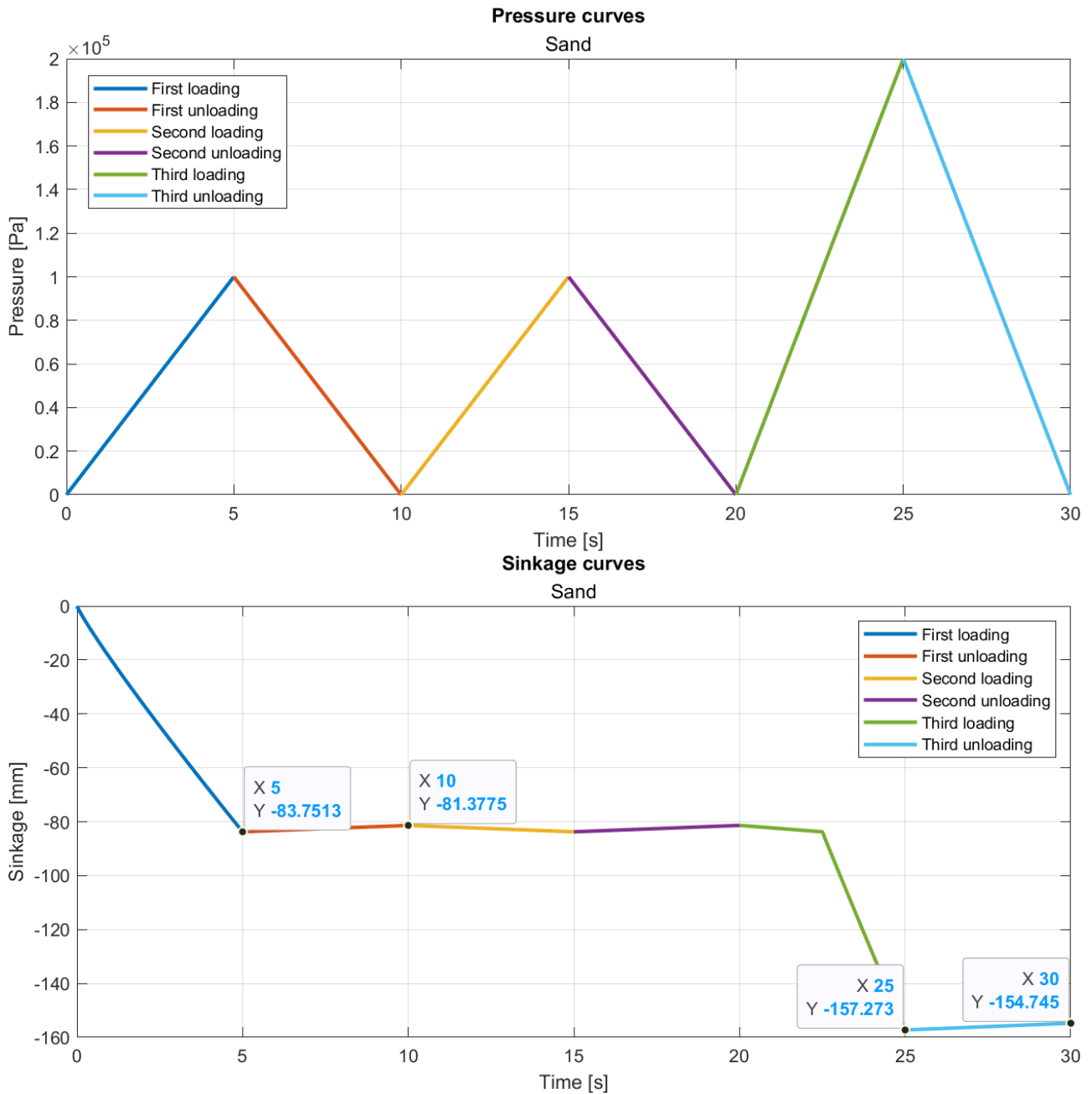
For a better understanding of how this works, a graph showing how pressure and sinkage are linked was plotted, assuming first a linear trend in time for pressure and then the same for sinkage. Sinkage will be plotted in the negatives to better represent the downward deformation of the terrain. Here are the results:



Figures 1.1.11-12 – Linear pressure trend and sinkage response

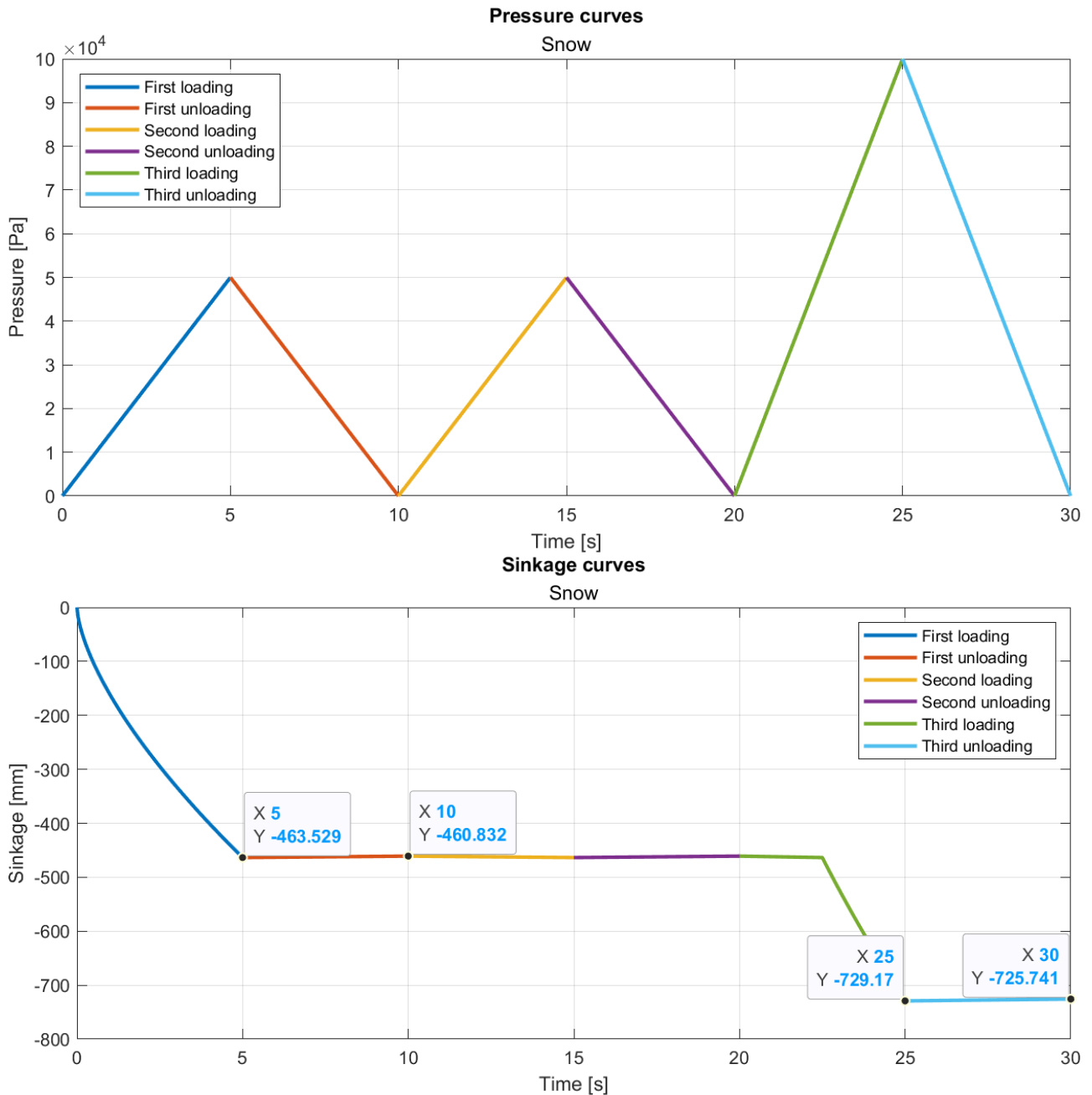
As we can see, supposing a linear charge and discharge of the track segment pressure, the unloading sinkage varies very little in comparison with the loading one. Also, as seen before, the difference between maximum sinkage and the zero pressure one in unloading is once again around 3 mm.

What can now be done is apply a second pressure wave equal to the first one and then a third pressure wave that surpasses the first 2, and check the behaviour of the 3 main soils the focus is on, so sand, clay and snow, analysing each independently.



Figures 1.1.13-14 – Repetitive loading response, Sand

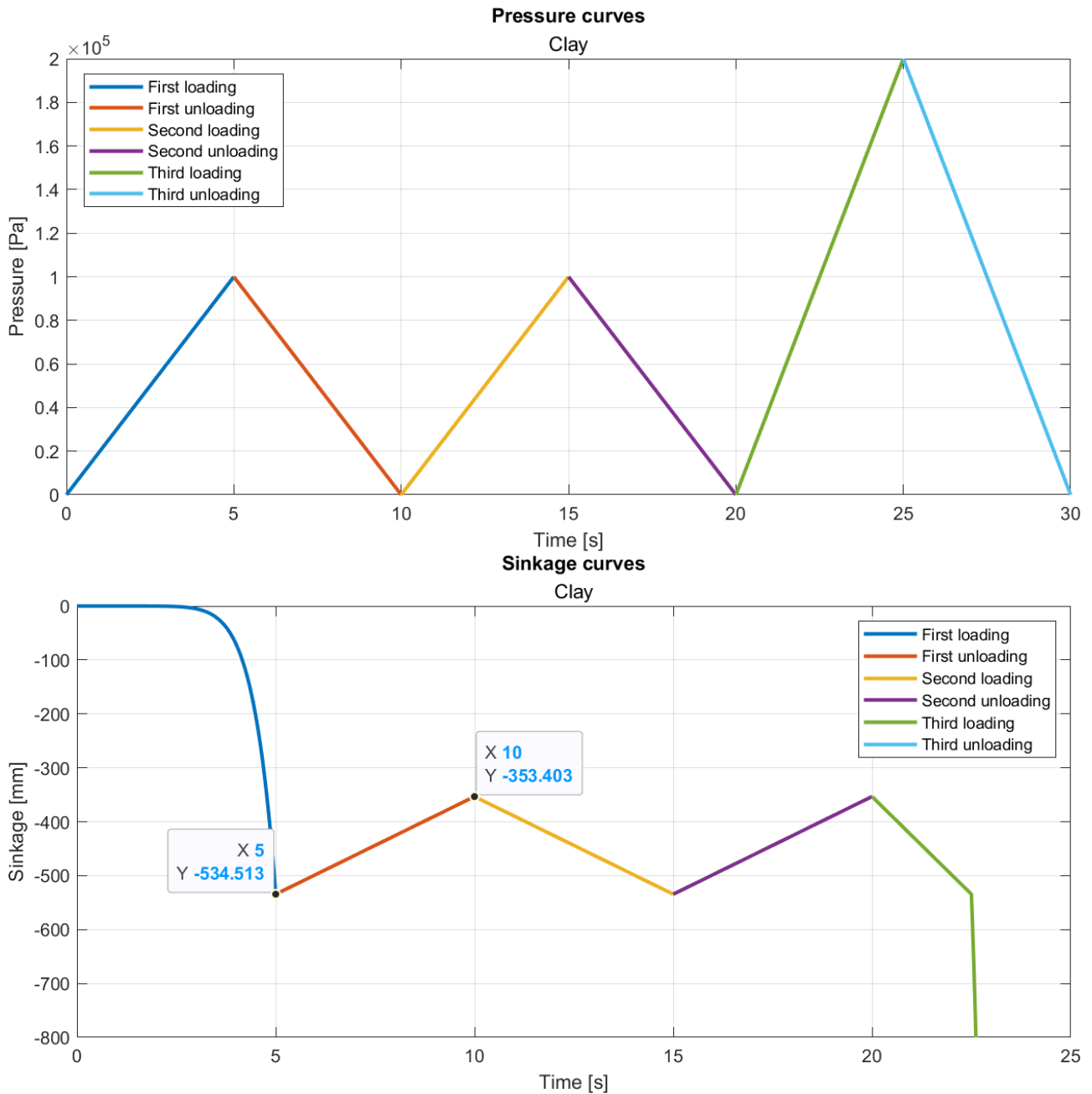
Applying a second pressure wave that reaches the peak as the previous one, we can see how the reloading has very little effect on the sinkage if we don't reach the threshold value of what was the previous peak pressure, or, as seen in the third curve, until we do. With this soil (dry sand LLL) the "memory" effect is quite pronounced, with the sinkage oscillations being extremely low (~ 2.37 mm for the 1 bar delta and ~ 2.52 for the 2 bar delta) for both the unloading curves and for the first part of the 2nd loading curve, so the curves affected by equation 1.1.2.



Figures 1.1.15-16 – Repetitive loading response, Snow

As we can see here, the behaviour of snow is very similar to that of sand, with the exception of a less linear loading characteristic ($n=1.53$ compared to sand's $n=1.1$) and much higher values of sinkage even at half the pressure applied to sand. Also, unloading shows a variation of 2.73 mm with a 0.5 bar delta and of 3.43 mm with a 1 bar delta, so a very similar behaviour to sand's, with a slightly steeper slope, but not too influent in the magnitude of what we're working with.

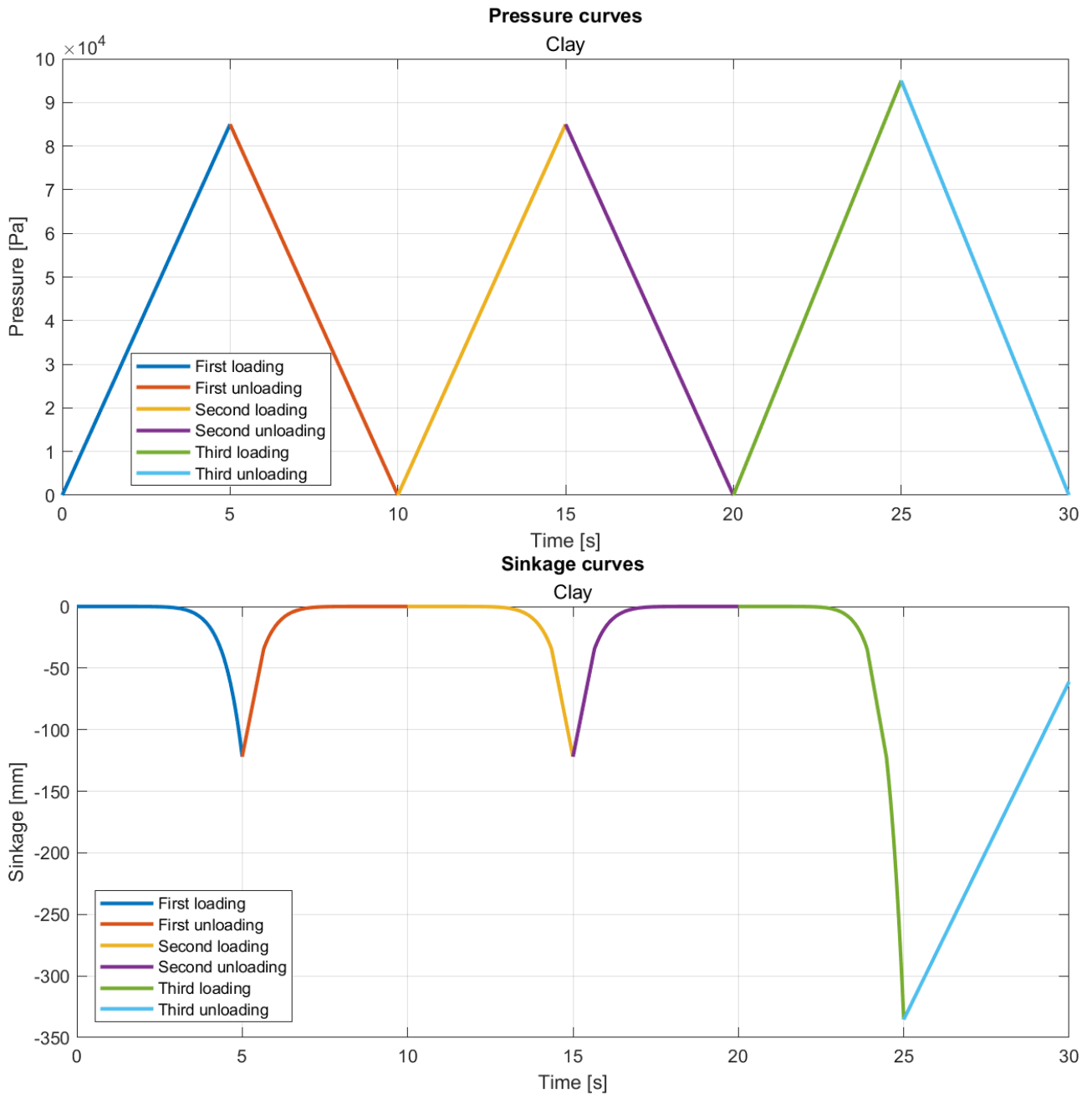
Clay on the other hand has a very different behaviour from both sand and snow, due to both the very high non-linearity of loading and the way steeper slope of unloading, as shown in the following images.



Figures 1.1.17-18 – Repetitive loading response, Clay

First thing to notice is how here the sinkage values are very unrealistic when compared to the simulations run in Adams, meaning the pressure peaks are too high, at least for the model used in the simulations, having a weight of around 16000kg. Also we can see how the unloading slope, as said, is extremely steep when compared to snow's or sand's, showing a 180 mm variation. The unloading curve is modelled linearly, and this creates, with highly non linear loading curves, a strange behaviour that here is not shown, but in simulations is evident, which is the fact that unloading is more responsive to pressure variations with respect to loading.

To highlight this clearly, another test was run with different pressure oscillations and a way smaller gap between the first 2 peaks and the third one.



Figures 1.1.19-20 – Lower pressure clay behaviour

Like shown in figure 1.1.10, the unloading behaviour of clay is peculiar. The unloading curve is in fact followed until it intersects with the loading one, then following the latter. This happens until the load is small enough to make the 2 intersect; after a certain load in fact the relation follows only the unloading curve, like shown here in the third unloading.

1.1.4 Vertical-normal force magnitude and direction calculation

Having seen how pressure is calculated, the normal force calculation on a track segment is straightforward:

$$F_n = P \cdot A \quad (1.1.3)$$

Where:

- $P \left[\frac{N}{m^2} \right]$ is the pressure according to either (1.1.1) or (1.1.2).
- $A \left[m^2 \right]$ is the area of the track segment.

To calculate the normal force the ATV module splits the track segment into 8 areas, chosen by the software and not editable by the user, and for each of them the force between segment and road is calculated by measuring soil sinkage at the centre of the segment area [2].

Road deformation is then calculated for all road elements under the track segment, one for each road element [2].

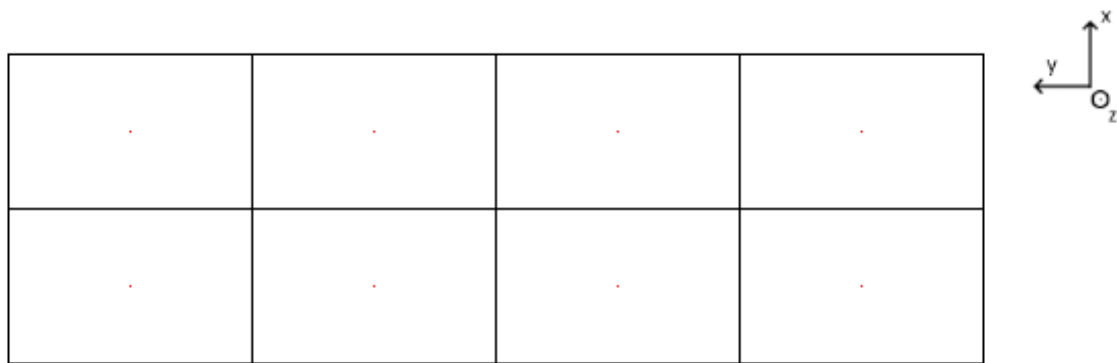


Figure 1.1.24 – Track segment discretization.

In the figure above, the outer rectangle represents the track segment, split in 8 parts as the module requires. The red dots represent the point (midpoint) where the forces coming from the ground are computed and applied to the segment.

Because of this, it's a requirement that the road element size is less than the segment area that the singular track element is split into, meaning it should be less than 0.5 times the track segment length and less than 0.25 times its width. This is because otherwise the road element could be compressed by more than one track segments, leading to errors [2]. In figure 1.1.24 we could imagine the ground segments being as big as the split, these being the maximum value dimensions they could have. In figure 1.1.25 we can instead see how a road segment can also be smaller.

For example, the road elements here represented (in green) are 1/4 the length and 1/8 the width of our track segments.

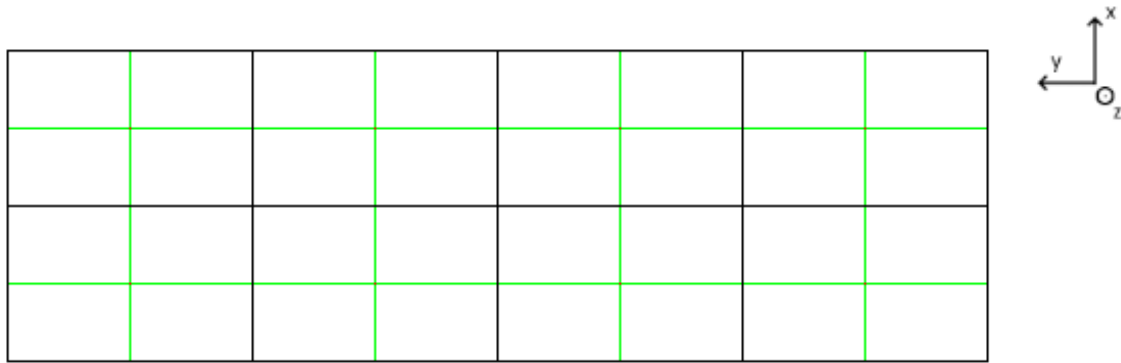


Figure 1.1.25 – Road element dimensions

To check what are the effects of different road element dimensions, 3 analyses were run, imposing road elements either 1/2,1/4,1/8 of the length or 1/4,1/8,1/16 of the width. Here the comparison is between the same quantity (pressure on the segment tip) evaluated in the 3 cases, to see how refined the mesh should be to get a good compromise between computational speed and result accuracy.

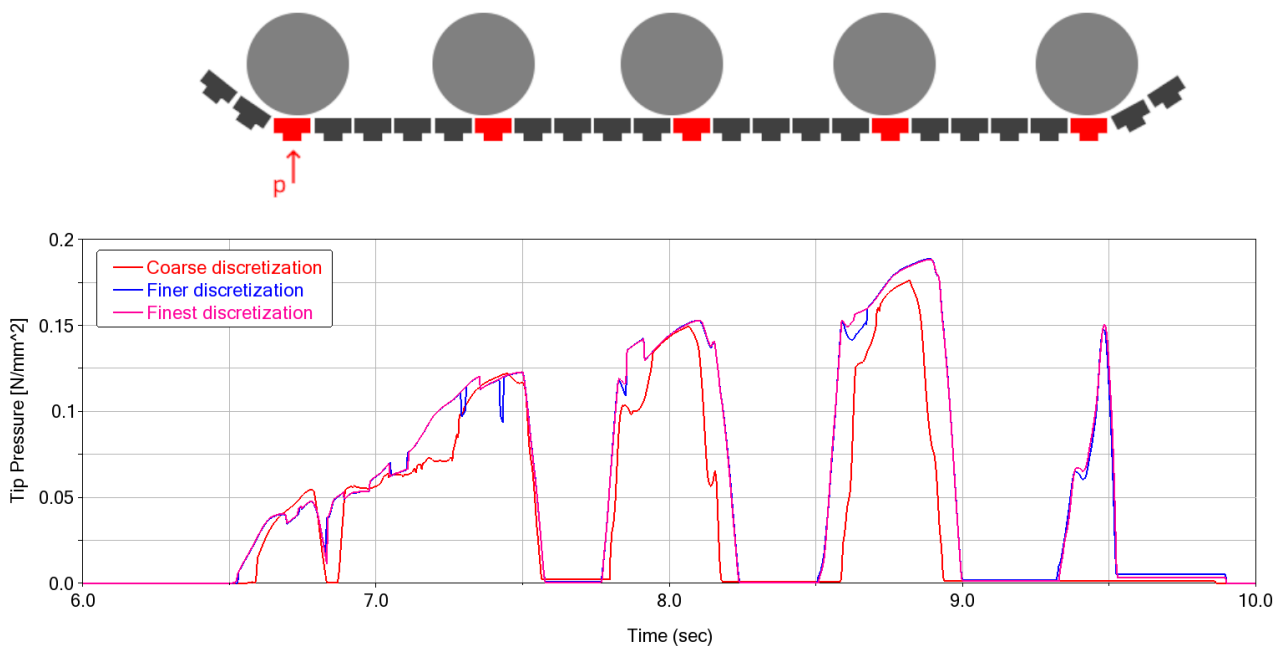


Figure 1.1.26 – Pressure on the segment tip

The red line refers to the coarsest road mesh, at half the length and a quarter of the width, but as we can see here it generates non negligible errors, as it doesn't detect the fifth road wheel (rightmost pressure peak) and also exhibits considerably big discrepancies in values (that in general are underestimations) elsewhere. The other two cases, with a finer mesh, show almost the same behaviour. Summarizing, the mid mesh revealed to be small enough to prevent errors but not too small to significantly increase the computational times.

Since the segment in most cases is rotated with respect to the ground in most cases, this method of calculation is based upon an approximation, since only 8 discrete forces are calculated on each segment instead of computing an integral of the pressure trend along the whole surface of our segment.

We can see that if a segment is subject to cycles of loading and unloading, it could oscillate heavily, since there is no damping in the standard Bekker equations. In dynamic models the ATV module therefore introduces some viscous damping, added to the vertical force equation [2]:

$$F_n = P \cdot A - c \cdot V_n \quad (1.1.4)$$

Where:

- $c \left[\frac{Ns}{m} \right]$ is the viscous damping coefficient.
- $V_z \left[\frac{m}{s} \right]$ is the vertical velocity of the track segment centre of mass, positive if directed upwards.

Ideally the damping coefficient should be low enough not to significantly influence the force calculation but still enough to stabilize the dynamic behaviour.

One more particularity about the “vertical” forces is the direction; as we know a soft soil is able to deform and change its shape according to loads to which it is subject. This means that our track segment points into the ground with a normal direction that could be different from the vertical. Keeping the road normal as undeformed and using the track segment normal pointing into the soil, the force vector direction is calculated by the ATV module as this [2]:

$$u_{force} = 0.5 \cdot u_{road} - 0.5 \cdot u_{segment} \quad (1.1.5)$$

where u_{road} is the vertical (z) versor, while $u_{segment}$ points into the ground with a negative vertical component (-z) of magnitude $\cos(\alpha)$ and an horizontal one of magnitude $\sin(\alpha)$.

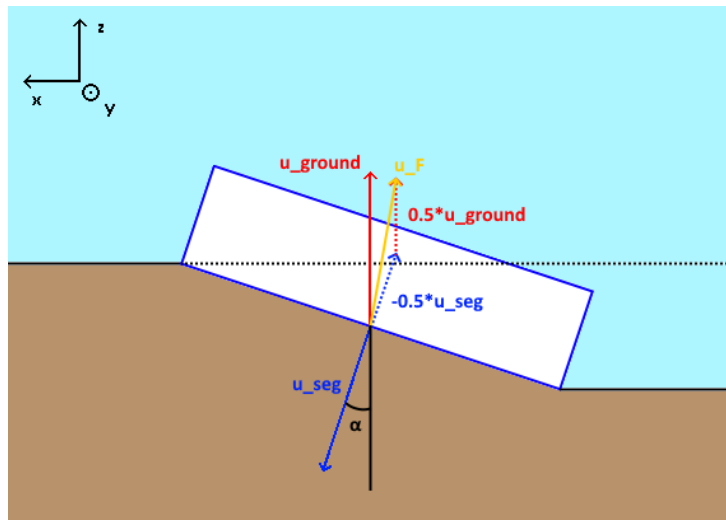


Figure 1.1.27 – Force direction representation

1.1.5 Approximation hypotheses verification

The calculation of said forces shown in the previous section makes a lot of approximations and simplifying assumptions. To see the effect of said approximations an analysis was done using an ATV simulation and MATLAB, to highlight the differences between an ideal calculation and how the software does it.

To do so, the default grouser geometry was used, running a simulation of 6 seconds at 2m/s or 7.2km/h, so as to make the tank stabilise and to make every track segment come in contact with the road. The soil chosen was dry sand.

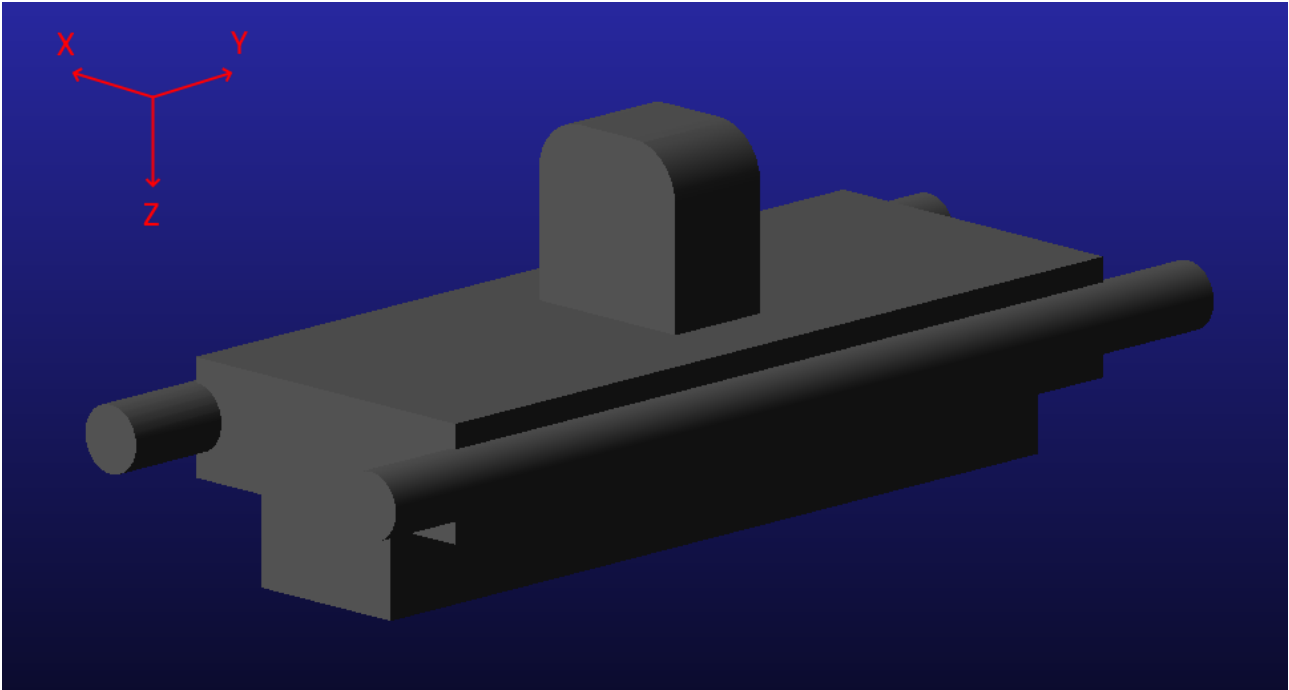


Figure 1.1.28 – Track segment geometry

The segment length, in the X direction, is 152.4 mm, the width, in the Y direction, is 480 mm, with the grouser being 380 mm wide, meaning that the grouser doesn't span the whole width of the segment. The height of the grouser is 40 mm. The assumption made for the MATLAB analysis was that the segment can be rotated around the Y direction but not around X and Z, making the pressure distribution constant in the Y direction but variable along X.

Second step was to take a random point in time to extrapolate data from the simulation.

Data at this time step:

Simulation data	Value	
Pressure at grouser tip	1.5982E+02	kPa
Pressure at segment	1.0593E+02	kPa
Sinkage at grouser tip	128.26	mm
Sinkage at segment	88.25	mm
Grouser contact area	28956	mm ²
Segment contact area	44196	mm ²
Grouser force	4627.6	N
Segment force	4681.6	N
Total force	9309.2	N
Angle phi	8.09	deg

Since all data extrapolated from the simulation is discrete, the normal force acting on the segment is simply the product of contact areas and pressures; instead, for our analysis we assumed the sinkage at grouser tip value to be at the lowest point of the grouser:

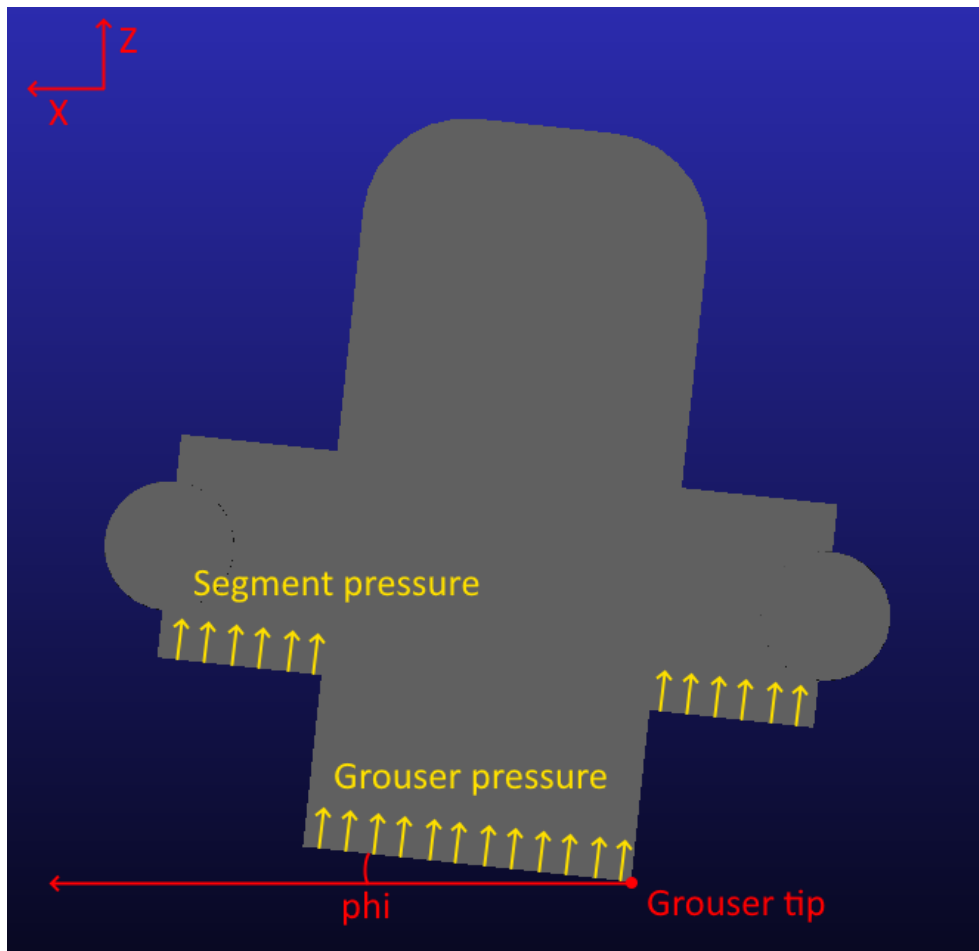


Figure 1.1.29 – Grouser tip location

This way we're able to calculate the sinkage for every other point of the segment using the segment geometry:

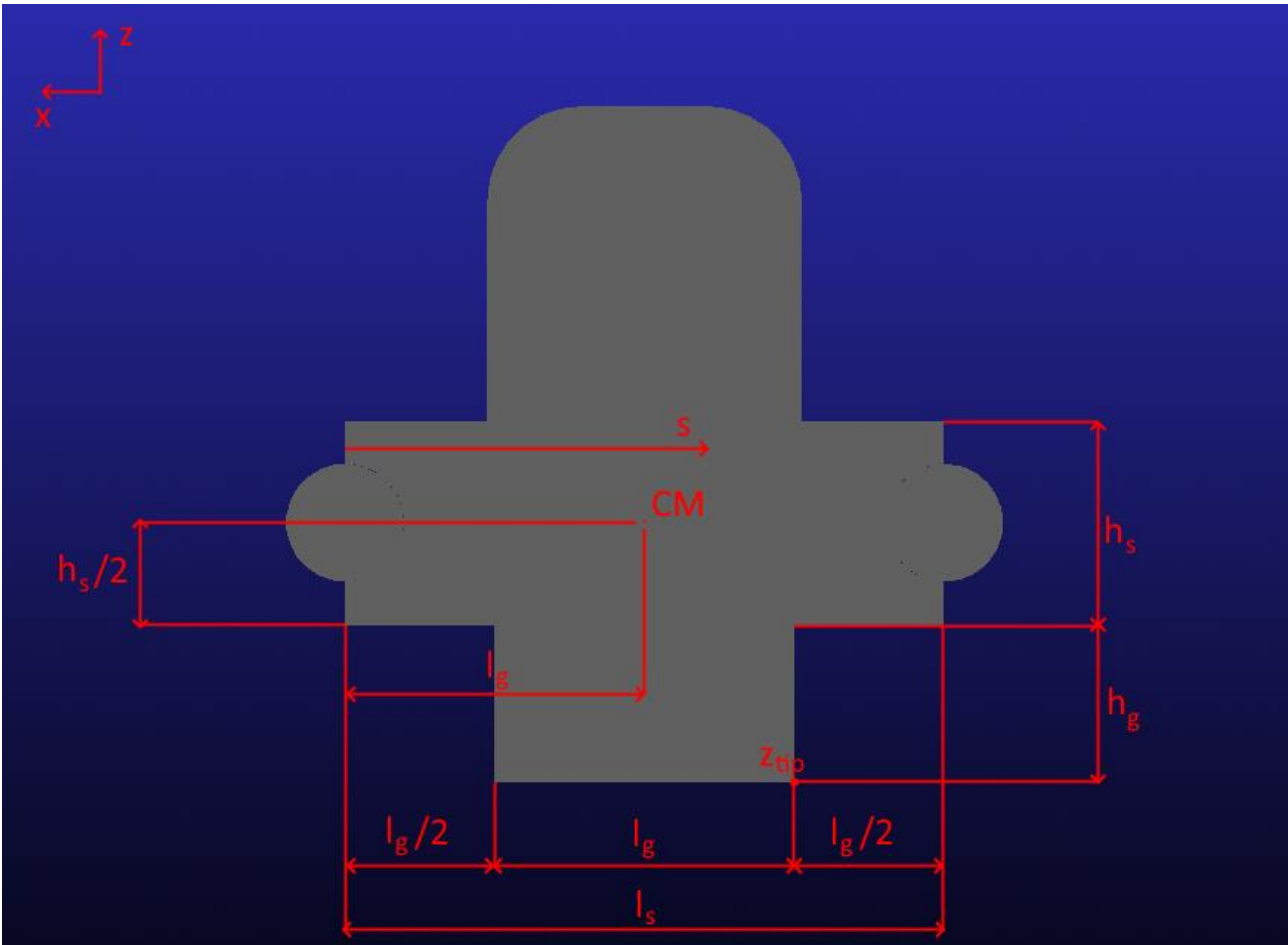


Figure 1.1.30 – Segment xz plane geometry

The equations are then:

$$z(s) = z_{tip} - \left(\frac{3}{2}l_g - s\right) \cdot \text{sen}(\varphi) - h_g \cdot \cos(\varphi) \quad (1.1.6)$$

Valid for $s < \frac{l_g}{2}$ and $s > \frac{3}{2}l_g$

$$z(s) = z_{tip} - \left(\frac{3}{2}l_g - s\right) \cdot \text{sen}(\varphi) \quad (1.1.7)$$

Valid for $\frac{l_g}{2} < s < \frac{3}{2}l_g$

Where s is the independent variable, being the position along the x direction of the segment contact point to the ground, and z being the sinkage applied due to geometry. In our case, z_{tip} , which is the z value of the grouser tip, which also is the point where the sinkage is maximum, is to the right of the grouser because the segment is rotated clockwise as shown in figure 1.1.29.

Now, using equations 1.1.1 and 1.1.2 with all the terrain parameters we can calculate pressure at all segment points:

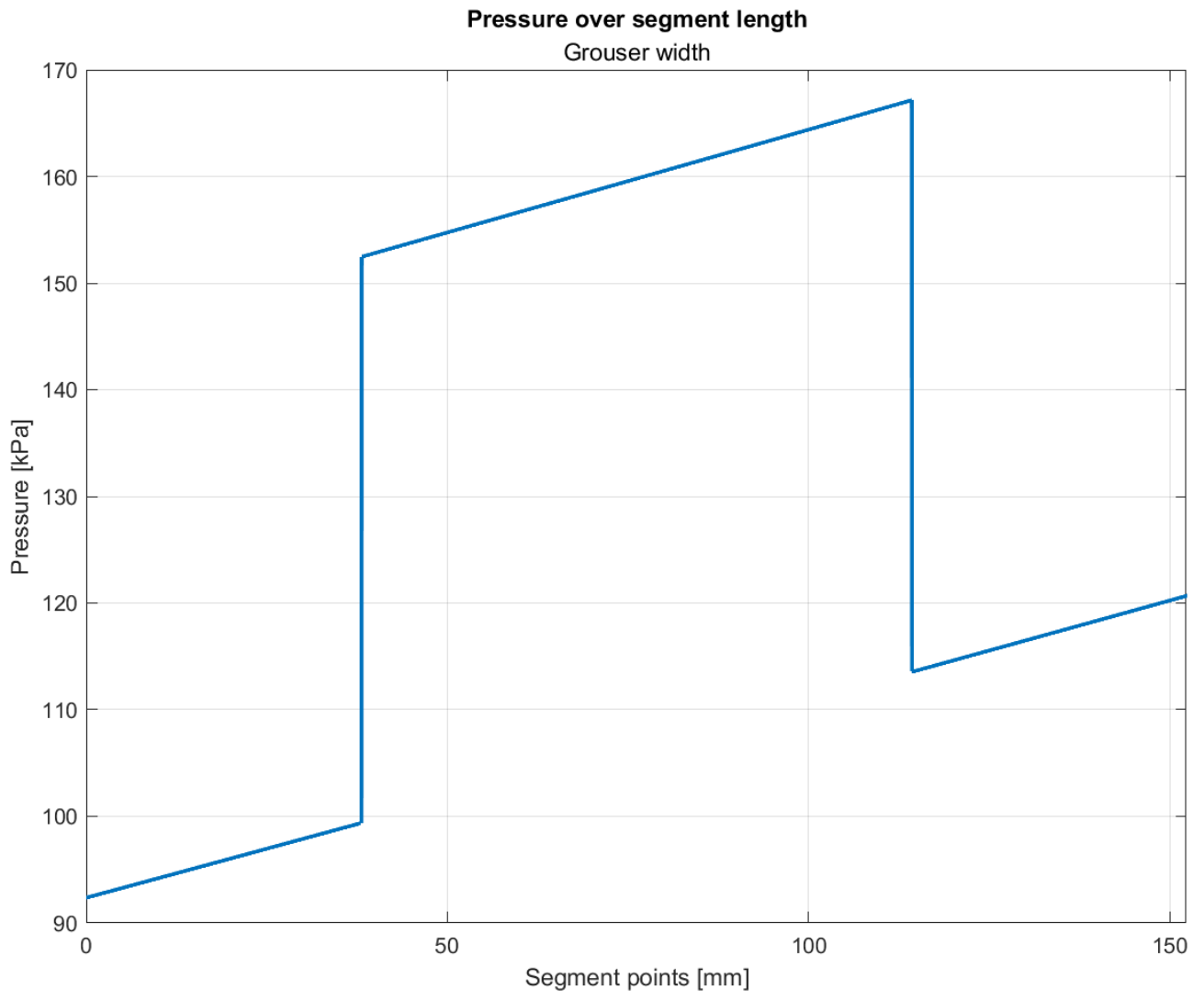


Figure 1.1.31 – Pressure acting along the segment

This is the pressure acting along the width of the segment that includes the grouser, but as said before the grouser is 380 mm wide while the segment is 480 mm. So on the borders the pressure trend will instead be:

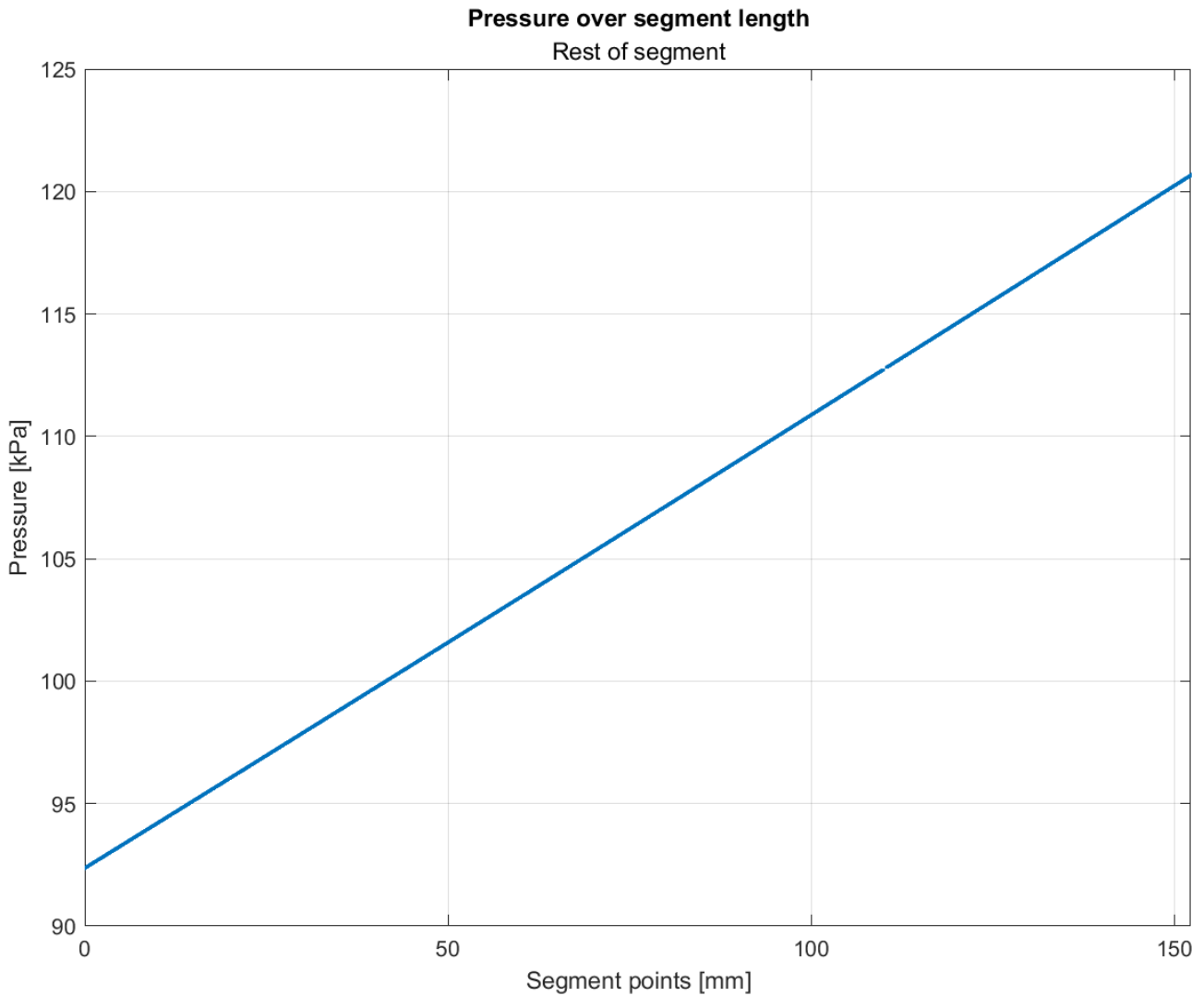


Figure 1.1.32 – Pressure trend on rest of segment

Having these two trends, the calculation of force is just a matter of integration, though we have to be careful regarding what is grouser and what is segment; so for calculating grouser force:

$$F_{gr} = b_g \int_{l_g/2}^{\frac{3}{2}l_g} p_{gr}(s) ds \quad (1.1.8)$$

Where the integral boundaries are the points where the grouser starts and ends, and b_g is the grouser width in the y direction, in meters; this is done because as stated before we assume that the segment cannot rotate around X and Z axes, making pressure constant along grouser width but as seen in the graphs not along the length.

For the segment:

$$F_{gr} = b_s \int_0^{l_g/2} p_{seg}(s) ds + (b_s - b_g) \int_{l_g/2}^{3l_g/2} p_{seg}(s) ds + b_s \int_{3l_g/2}^{l_s} p_{seg}(s) ds \quad (1.1.9)$$

Again because the grouser doesn't span the whole segment width, but segment pressure is calculated for the whole length of the segment.

The last calculation regards the point of application of said force. The point of application of the force is where the total moment about your chosen reference point is zero. This means that the total force (calculated from the integrals shown in equations 1.1.8 and 1.1.9) to the left and to the right of the point of application is equal. In other words, it's the point where the cumulative force calculated is half of the total force. Having done the calculations using matlab, it's easy to extract it, calculated in the s direction used up until now from the start of the segment.

The calculations results are then:

Study results	Value	
Grouser force	4629.6	N
Segment force	4703.7	N
Total force	9333.4	N
Point of application	79.878	mm
Resultant torque	34.328	Nm

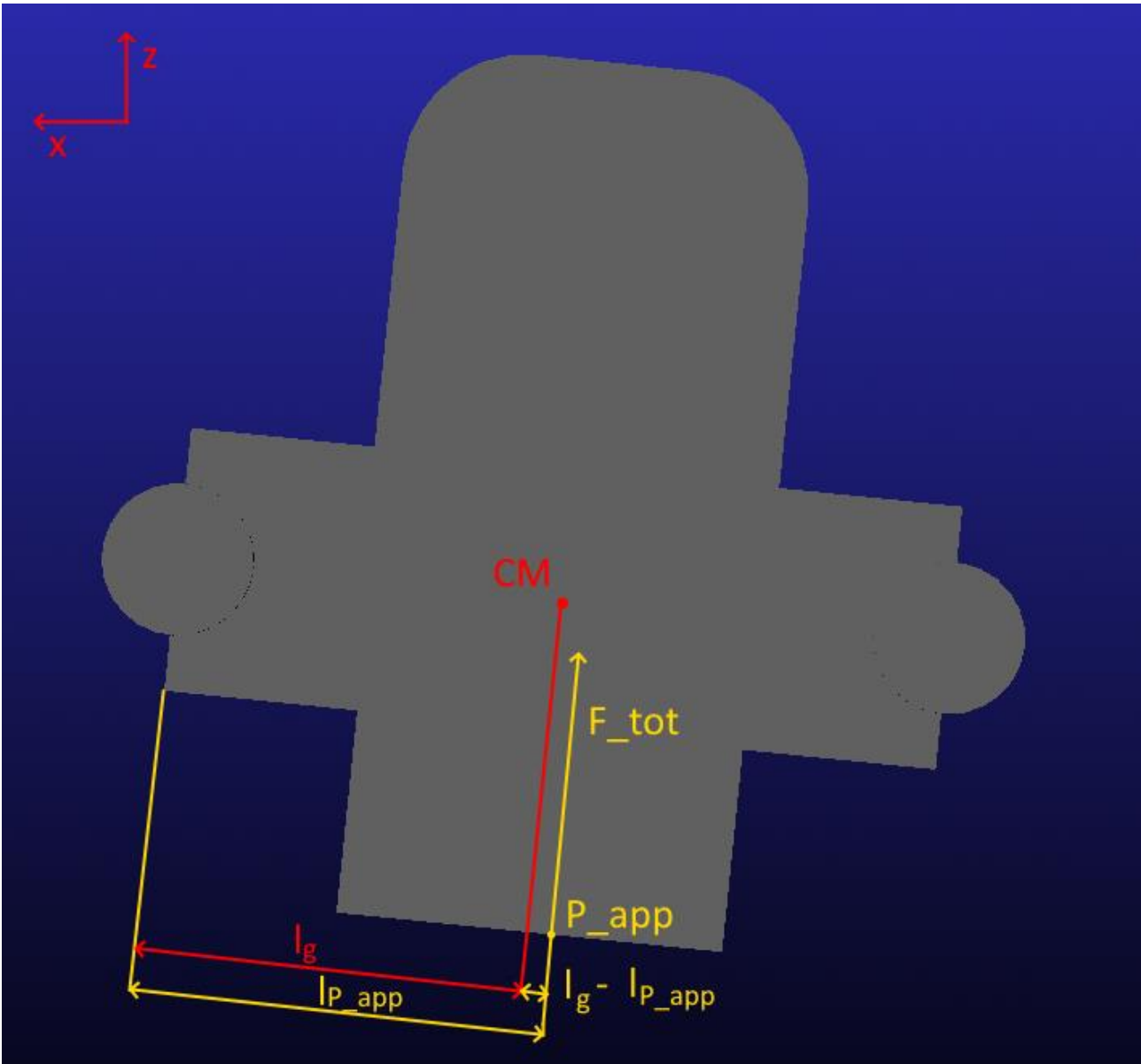


Figure 1.1.33 – Normal force point of application

As it can be seen results are very comparable, the difference in normal force is only circa 24 N, so a 0.257% discrepancy. The torque however is not comparable, since the simulation computes the total torque acting on the segment from the ground, which also includes longitudinal forces like the ones discussed in the next chapter, while this study only focuses on normal forces.

In conclusion, the approximations made by the software appear to be accurate enough and shouldn't lead to significant errors.

1.2 Longitudinal and Lateral Forces

The longitudinal forces exerted by soft soil on a track segment of a vehicle are of different natures, caused by shearing, which acts on the surfaces of the track segment directly in contact with the soil, like grouser tip and side walls of the segment itself, or by exploiting the failure characteristic of the soil, manifesting a phenomenon known as bulldozing force.

The shearing force is the force exerted due to the track sliding on the soil surface. There are 3 types of soils described in literature. Most common soils can be modelled as elastoplastic materials. This type of material exhibits a stress strain relationship of this type [1]:

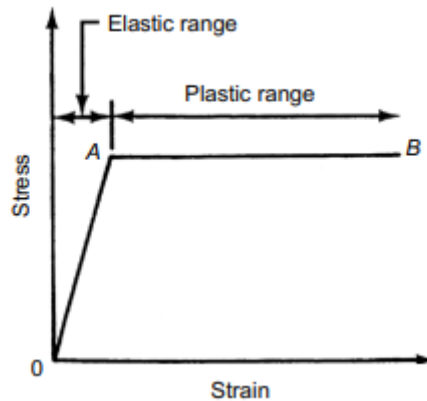


Figure 1.2.1 – Stress-strain in an elastoplastic material

The elastic properties are used to predict a pressure distribution in the soil under a force generated by the track/wheel making contact with the ground. Over a certain boundary of load, represented by “A” in figure 1.2.1, a small increase in stress produces an extremely rapid increase in strain, constituting plastic flow. The state preceding plastic flow is referred to plastic equilibrium; the transition from plastic equilibrium to plastic flow represents the failure of the terrain [1]. One of the most widely used criteria to represent the behaviour of this transition is the Mohr-Coulomb criterion, which postulates that the material will fail if the shear stress satisfies the following condition [1]:

$$\tau_{max} = c + \sigma \cdot \tan\Phi \quad (1.2.1)$$

Where:

- $\sigma \left[\frac{N}{m^2} \right]$ is the normal stress on the shearing surface, so ground pressure.
- $c \left[\frac{N}{m^2} \right]$ is the cohesion.
- $\Phi [rad]$ is the angle of internal shearing resistance of the material.

Cohesion is the bond that unites two particles of the material together, regardless of the pressure present in between the latter. On the other hand, the particles are held together by the pressure present in between them, meaning the shear strength of the material increases linearly with the normal pressure. For terrains like completely saturated clay (clay that has absorbed the maximum amount of water it can absorb), the max shear stress will only depend on cohesion, while for others like dry loose sand, the cohesion will be 0 and the maximum shear stress will only depend on the pressure.

Once we know how to calculate the maximum shear stress, we need to know the shear stress-displacement relationship, which is modelled by Janosi and Hanamoto [1]. The two proposed a behaviour based on an exponential equation (1.2.2):

$$\tau = \tau_{max}(1 - e^{-j/K}) \quad (1.2.2)$$

Where:

- $\tau_{max} [\frac{N}{m^2}]$ is the maximum shear stress and $j [m]$ is the shear displacement.
- $K [m]$ is an empirical value referred to as the shear deformation parameter [1] and is a measure of the magnitude of shear displacement required for the development of max shear stress.

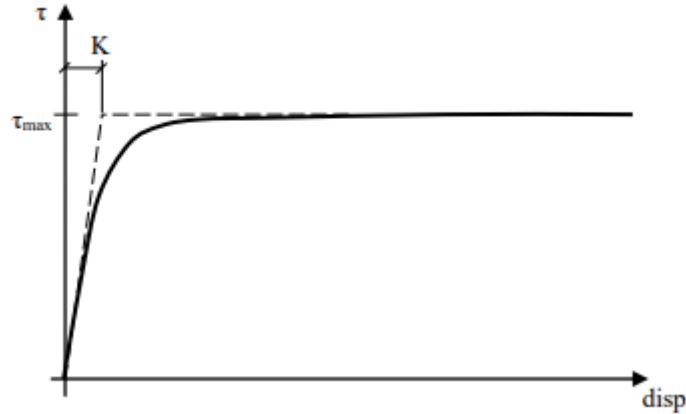


Figure 1.2.2 – Shear stress – shear displacement [2]

The maximum shear stress acting on the segment is strictly linked on the ground pressure acting on it, as equation (1.2.1) explicates, ground pressure which can be evaluated using the equations (1.1.1) and (1.1.2), as we can see in figure 1.2.3:

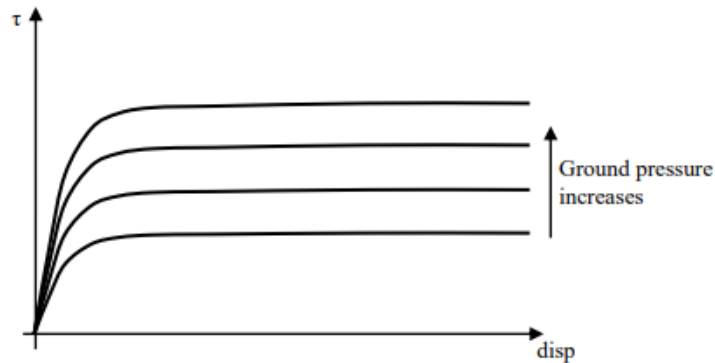


Figure 1.2.3 – Shear stress for different ground pressures [2]

Combining previous equations we obtain the law governing shear stress in a track segment moving on a soft soil [2]:

$$\tau = (c + P \cdot \tan\Phi)(1 - e^{-j/K}) \quad (1.2.3)$$

The ATV software has a tool with which the user is able to simulate the behaviour of a single segment on soft soils, imposing either a force or a displacement in the 6 degrees of freedom, so movement along X,Y and Z axes and rotation about them.

A few tests were made with different normal forces to reproduce figure 1.2.3

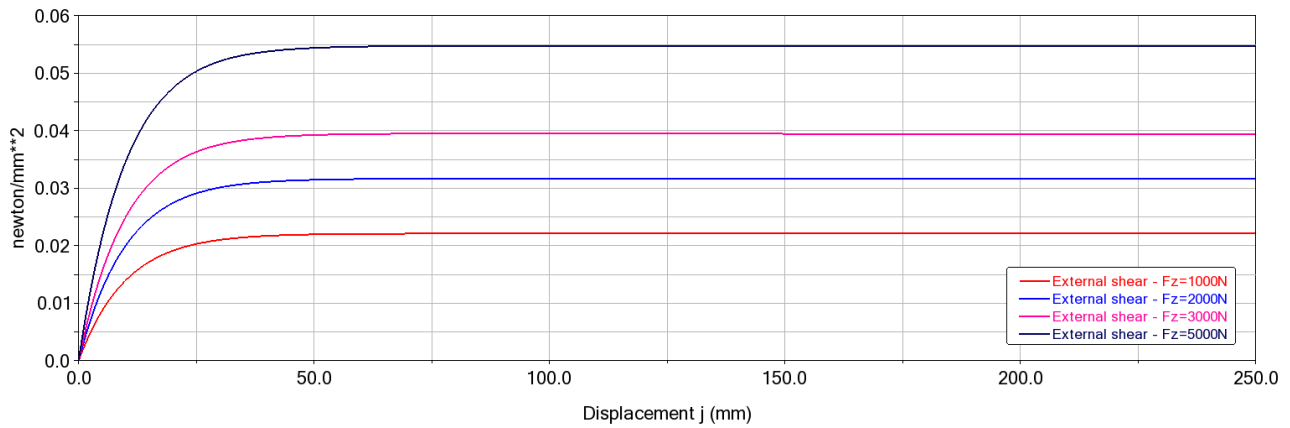


Figure 1.2.4 – Shear curves for different normal loads

For the sake of completeness, we must say that in the literature other two equations for modelling shear stress-displacement behaviour are available, both peaking at the maximum stress at a certain displacement but then decaying at higher j , going to either 0 or a constant value lower than the maximum when approaching infinite displacement. Since the soils analysed in this document are modelled using the type 1, the other 2 types are not going to be discussed, but only qualitatively shown in the following figures:

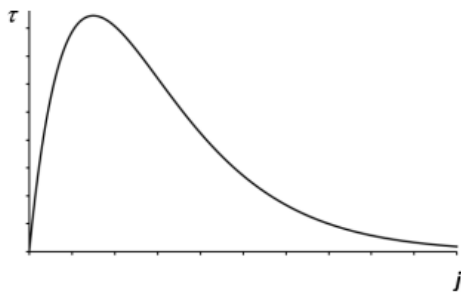


Figure 1.2.5 – Shear eq. type 2

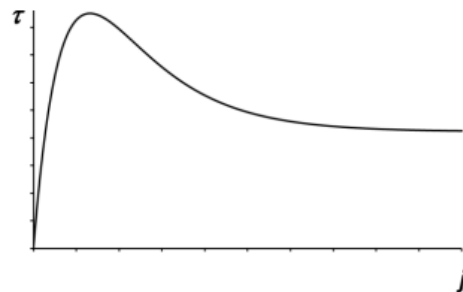


Figure 1.2.6 – Shear eq. type 3

The type 2 shearing equation:

$$\tau = \tau_{max} \cdot (j/K_{\omega}) \cdot e^{1-j/K_{\omega}} \quad (1.2.4)$$

Where:

- K_{ω} is the shear displacement j where the shear stress peaks.

The type 3 shearing equation:

$$\tau = \tau_{max} \cdot K_r \left[1 + \left(\frac{1}{K_r \left(1 - \frac{1}{e} \right)} - 1 \right) \cdot e^{1 - \frac{j}{K_{\omega}}} \right] \cdot \left(1 - e^{-\frac{j}{K_{\omega}}} \right) \quad (1.2.5)$$

Where:

- K_{ω} is again the shear displacement at maximum stress.
- K_r is the fraction of stress at which the curve relaxes at infinite displacement.

The bulldozing force is the force exerted by a grouser moving through the soil. We define the minimum lateral compressive stress required to set the soil element into failure as passive earth pressure [1], which can then be calculated using the following equation:

$$\sigma_p = \gamma_s h N_\phi + q N_\phi + 2c\sqrt{N_\phi} \quad (1.2.6)$$

Where:

- $\gamma_s \left[\frac{N}{m^3}\right]$ is the specific weight of the soil.
- $h [m]$ is the grouser height.
- $N_\phi = \tan^2(45^\circ + \phi/2)$ is called the flow value of the soil.
- $\phi [rad]$ is the angle of internal shearing resistance.
- $q \left[\frac{N}{m^2}\right]$ is the surcharge, i.e. the pressure from what's above the grouser.
- $c \left[\frac{N}{m^2}\right]$ is the cohesion.

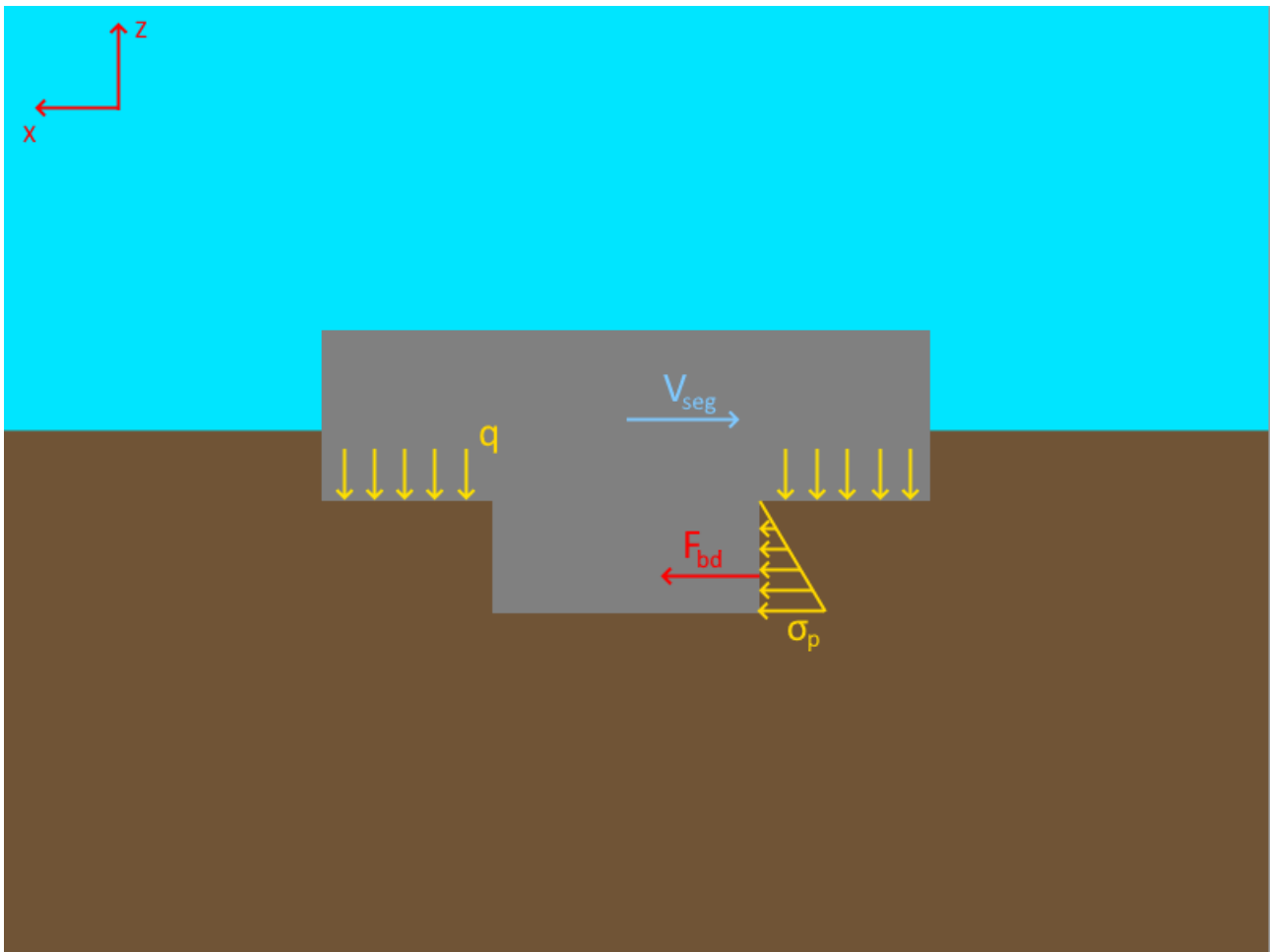


Figure 1.2.7 – Bulldozing forces and stresses

The soil in front of the grouser blade will be brought into a state of passive failure, and if the blade is wide enough in comparison to the height, we can integrate the passive earth pressure over the grouser height, so the force the grouser is exerting can be calculated [1]:

$$F_p = b \left(\int_0^{h_b} (\gamma_s z N_\phi + q N_\phi + 2c\sqrt{N_\phi}) dz \right) = b \left(\frac{1}{2} \gamma_s h_b^2 N_\phi + q h_b N_\phi + 2c h_b \sqrt{N_\phi} \right) \quad (1.2.7)$$

Where h_b is the height of the grouser blade and b is the grouser width. This means that the assumption is that the variables included in the calculation, such as pressure, are constant along the y direction.

This formula, which makes the problem two-dimensional, can be utilized in case the blade is relatively much wider than it is tall, and in case it is perpendicular to the segment surface. In the models proposed by the software, barring big modifications, this is the case, and the simplifying hypotheses are fair to use.

The last longitudinal force calculated by the software is the side wall force. Pressure acting on the track that has sunken into the soil also has an influence, generating a shear stress on the grouser walls and therefore a thrust. This force acting on the side walls of the grouser was described by Bekker [3] with the following equation:

$$H_{side} = 2lhc + W \tan \phi \left(0.64 \frac{h}{b} \cot^{-1} \left(\frac{h}{b} \right) \right) \quad (1.2.8)$$

...

Where:

- l [m] is the length of the grouser along the x axis.
- h [m] is the depth of the grouser going into the soil along the z axis.
- b [m] is the track segment width along the y axis.
- c [$\frac{N}{m^2}$] is the cohesion.
- W [N] is the vertical load on the track segment.
- ϕ [rad] is the angle of internal shearing resistance.

1.2.1 Selection threshold between internal shearing and bulldozing – passive earth failure pattern

For the bulldozing effect to be in play, the terrain between 2 grousers must have enough space to experience the passive failure pattern mentioned in previous chapters. If there is not enough space to make that happen, the soil becomes “trapped” between the 2 consecutive grousers and acts as a solid adjacent to the latter. This phenomenon is called internal shearing. The 2 types of shearing are visualized in the following image:

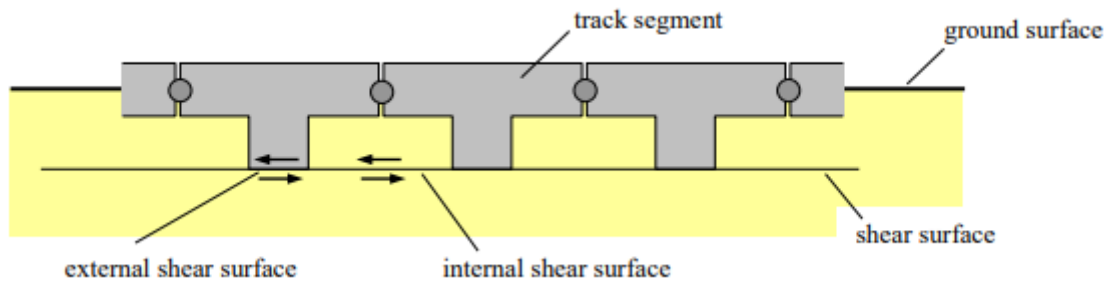


Figure 1.2.8 – Internal and external shearing [2]

Shearing parameters present in equation (1.2.3) for each type should be defined for every soil.

To then produce thrust, the external stress is multiplied by the grouser tip area and the internal is multiplied by the rest of the ground contact area [2]:

$$F_{long} = A_{shoe}(\tau_{ext} * gr + \tau_{int}(1 - gr)) \quad (1.2.9)$$

where gr is the ratio between the grouser tip area and full area of the track segment.

The Rankine passive failure theory [2] defines a minimum spacing between grousers at which the longitudinal force will switch from being generated by means of bulldozing or by means of internal shearing.

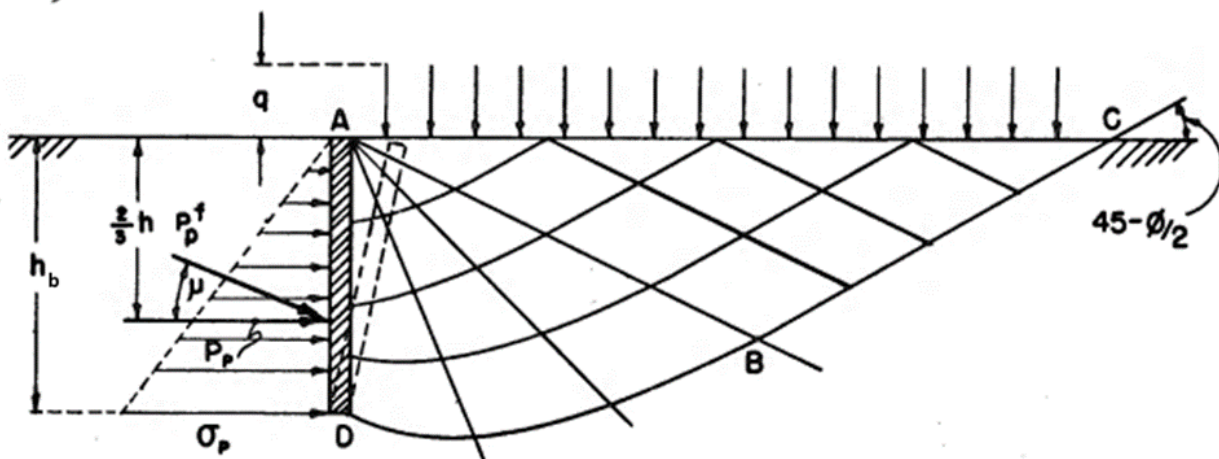


Figure 1.2.9 – Passive earth failure pattern [3]

Having enough space means that the failure zone, represented in figure 1.2.9, with the radial slip zone ABD, and the Rankine stress zone ABC, is able to be generated in front of the grouser, so that bulldozing can take effect, otherwise relying on internal shearing. This limit is calculated as:

$$l_s = \frac{h_b}{\tan(45^\circ - \phi/2)} \quad (1.2.10)$$

If grouser distance is greater than l_s , the bulldozing effect is in action, if it is lesser, then the internal shearing would be active. This switch between the two calculations is not done automatically by the software, meaning the user has to check the soil properties and the grouser geometry used before choosing a calculation method, hence introducing potential errors.

1.2.2 Grouser height sensitivity analysis

Recalling equations 1.2.7 and 1.2.8, a study was done using MATLAB of the relations between grouser height and bulldozing/side wall forces for each of the 3 soils taken into consideration. To better see the effects of terrain parameters, different surcharge pressures were extrapolated from simulation and used for the modelling. Also, as stated in paragraph 1.2.4, there is a limit for which the earth failure pattern manifests and for which bulldozing forces are active, hence a maximum grouser height was calculated for each soil using equation 1.2.10, with the assumption of the segment length being 152.4 mm and grouser length being 76.2 mm, meaning there's a clearance of 76.2 mm between 2 consecutive grousers:

- $h_{b,max} = 45.78 \text{ mm}$ for sand.
- $h_{b,max} = 68.61 \text{ mm}$ for clay.
- $h_{b,max} = 50.24 \text{ mm}$ for snow.

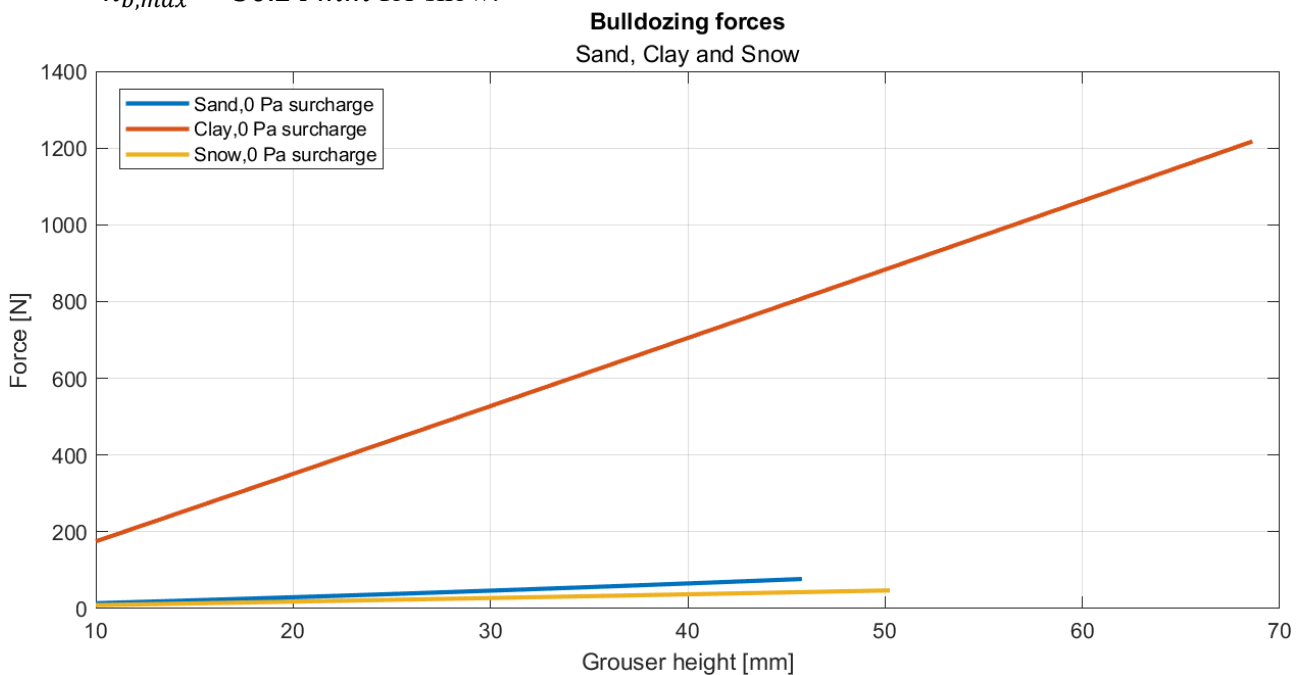


Figure 1.2.10 – Bulldozing force trend with grouser height, no surcharge

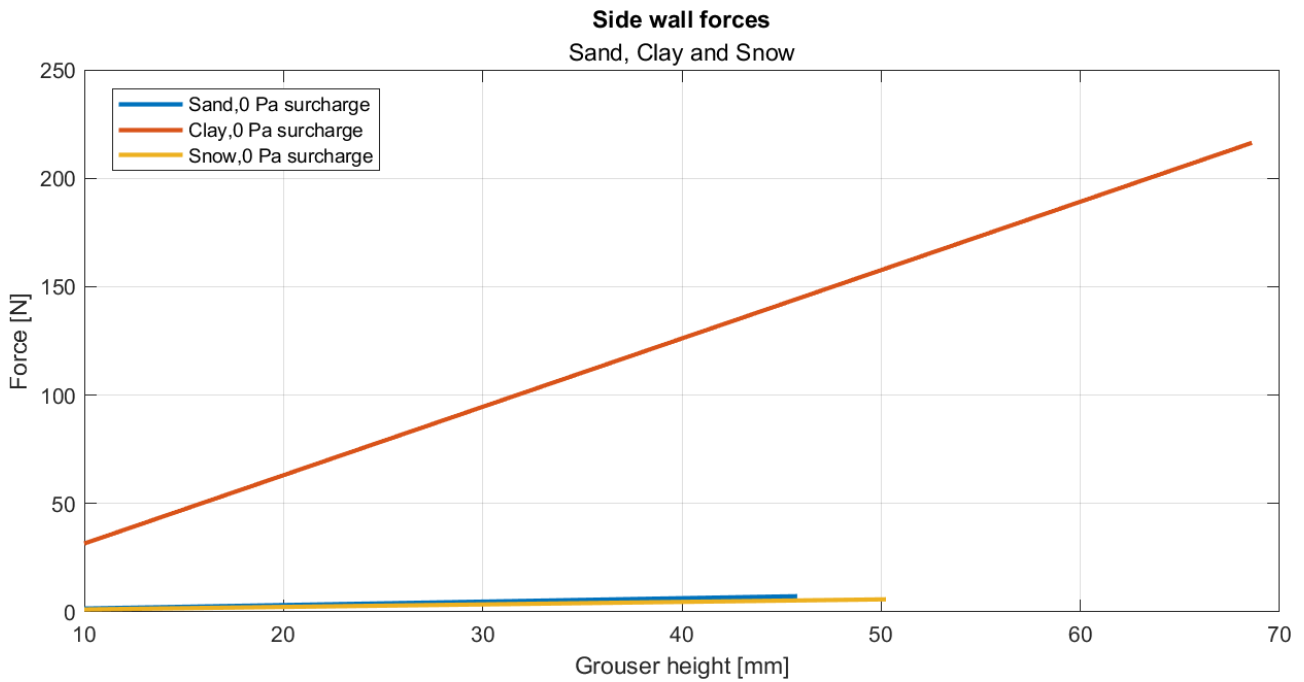


Figure 1.2.11 – Side wall force trend with grouser height, no surcharge

To be able to read this graph, the surcharge concept should be explained. It is simply the pressure acting in front of the grouser, so right at its point of attachment at segment height. This, for longitudinal motion, in soils like sand and snow, can be 0, if the segment is not under one of the roadwheels, meaning the grouser can still exert force without vertical load if the segment is still sunk in the ground, which is possible due to the unloading curves. For clay however, this isn't the case, and the surcharge in real cases will never actually be 0, as figure 1.1.21 shows. So even though the clay values are the highest, due to its cohesion being the highest between the chosen soils, the curve has no meaning for the longitudinal direction. It has however meaning in the lateral direction, because soil is not compressed on the side of the track, meaning the vehicle is more stable and follows a straight trajectory easier. This could be relevant in case of a road that is sloped in a direction which is not that of travel. For this reason, with no surcharge it's better to only look at the sand and snow curves:

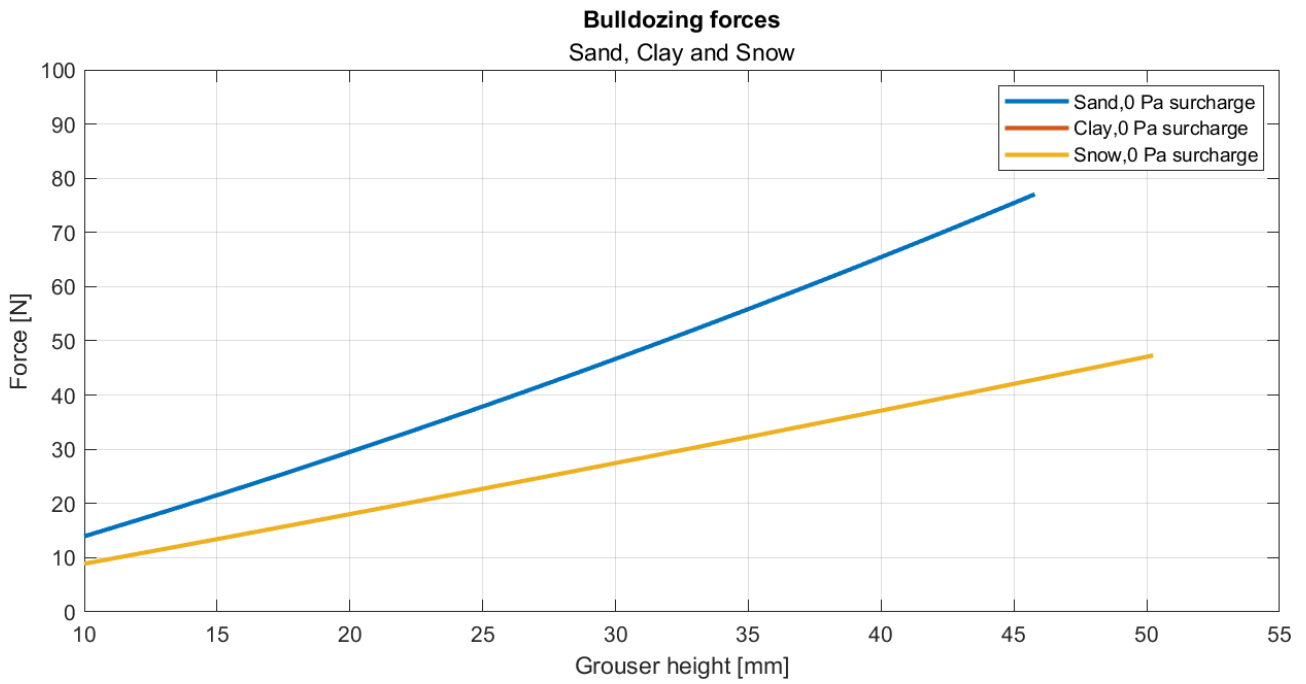


Figure 1.2.12 – Sand and snow bulldozing with no surcharge

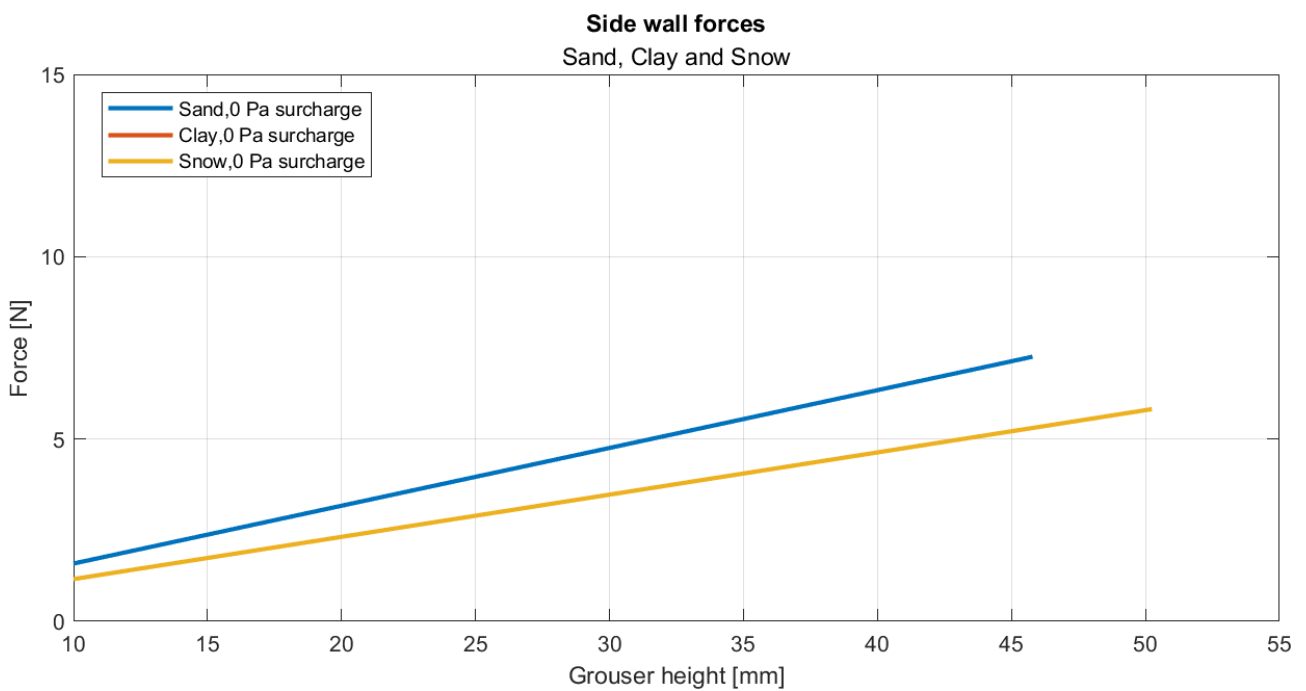


Figure 1.2.13 – Sand and snow side wall forces with no surcharge

Having said this, we can see how the magnitude of the bulldozing force is around 1 order of magnitude higher than the side wall force.

Now let's compare forces with surcharge present:

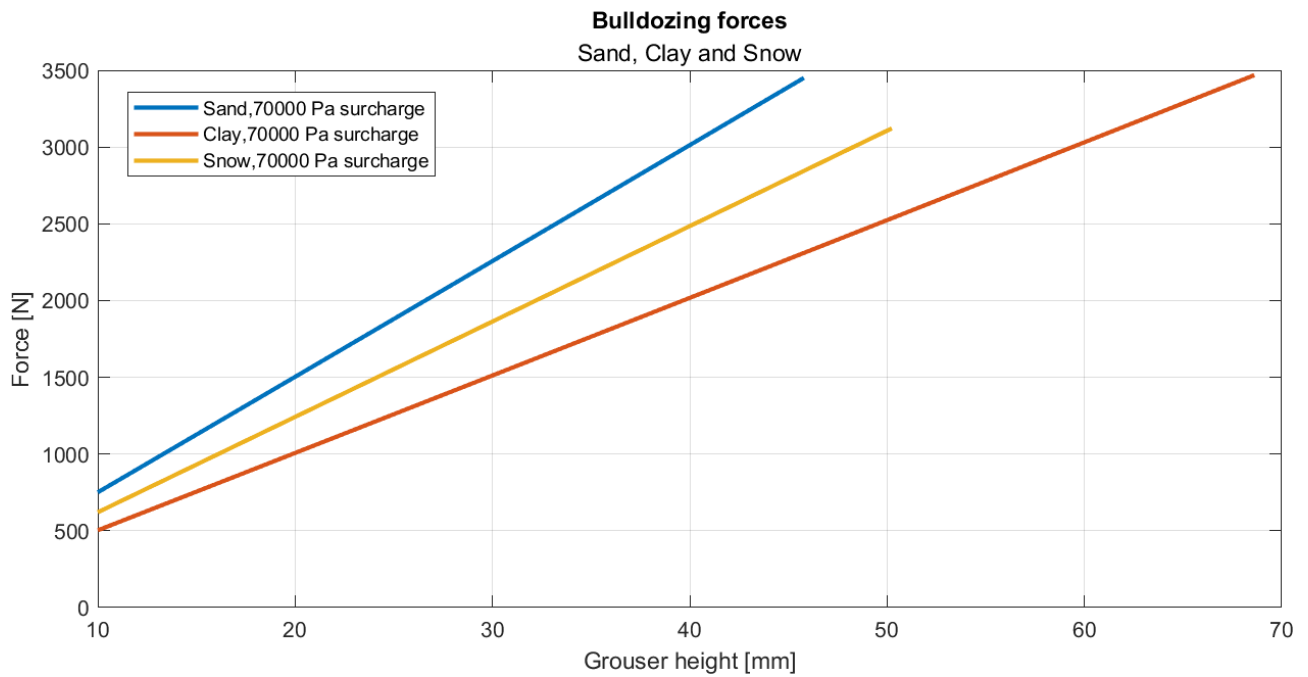


Figure 1.2.14 – Bulldozing forces with 70kPa surcharge

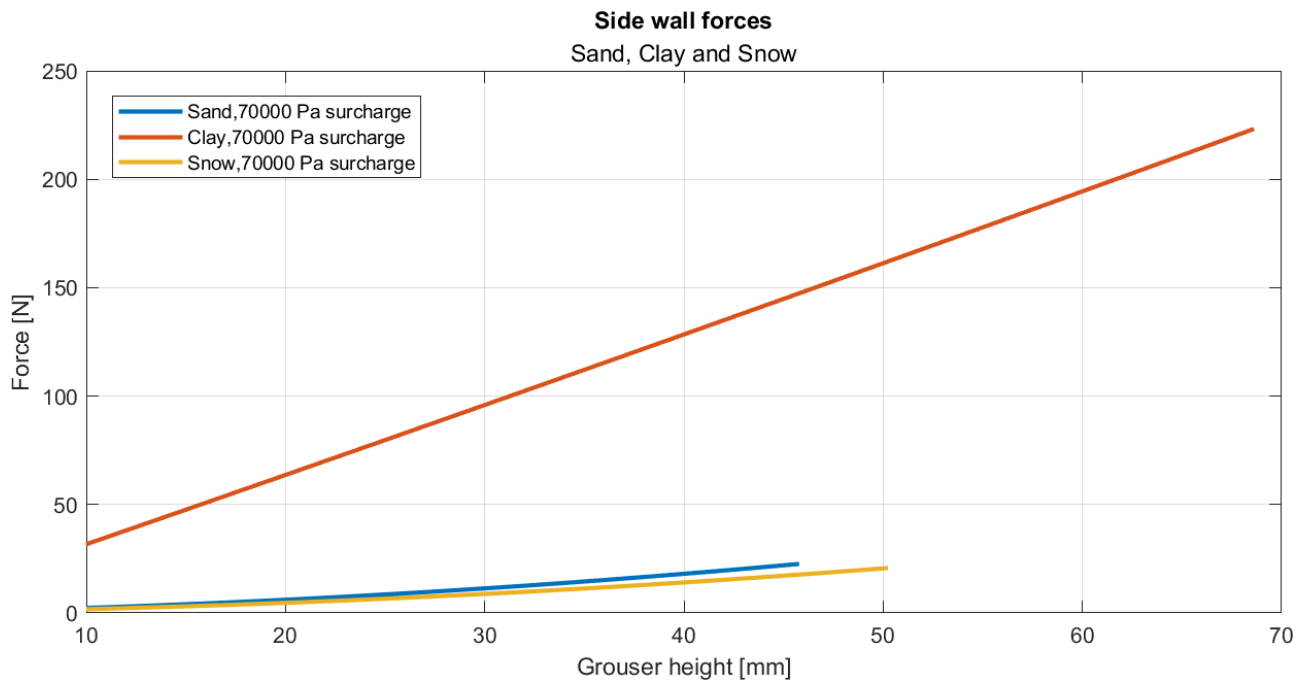


Figure 1.2.15 – Side wall forces with 70kPa surcharge

As these graphs show, the surcharge has a really big impact on the bulldozing forces, especially for sand and snow, due to the friction angle being higher for those soils.

To further show the influence of surcharge on bulldozing force a few tests were made on a single track segment, imposing a movement in the x direction and a certain sinkage at segment surface, so grouser attachment, translating to a different surcharge. Here are the results:

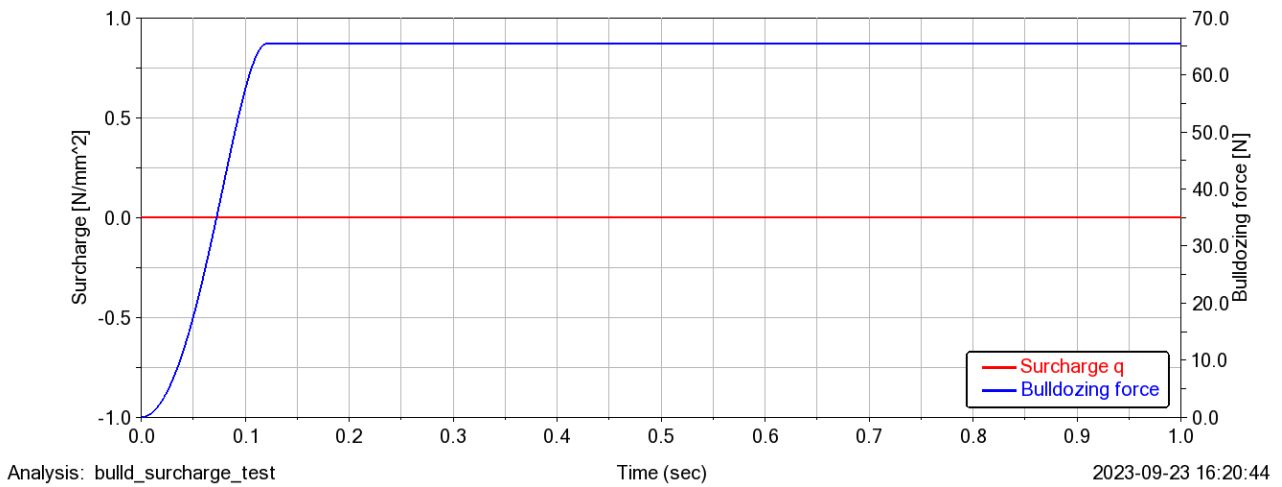


Figure 1.2.16 – Bulldozing force with 0 surcharge

As a first test the sinkage was set to 0 mm at grouser attachment, to fully sink the grouser without surcharge. The force is around 65 N, consistent with the one seen in figure 1.2.12 since our default grouser is 40 mm high.

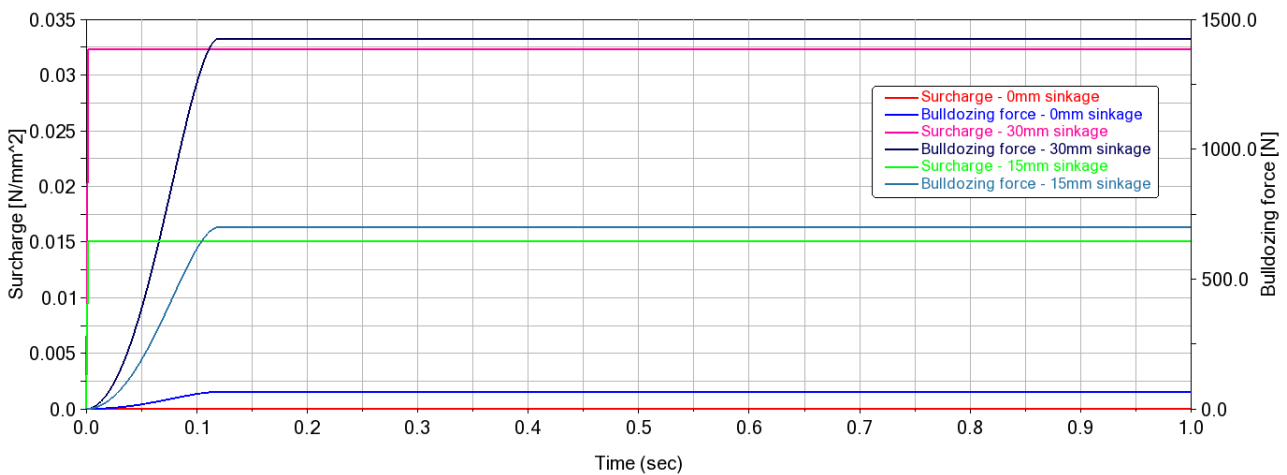


Figure 1.2.17 – Surcharge effect

Again, this clearly shows the big heavy effect surcharge has on the forces generated by the single segments.

In conclusion, sand and snow bulldozing forces can peak at higher values for the same grouser height, but only when the segment passes under wheels, so the points where the pressure peaks. This means at any time stamp there will be some segments exerting high forces and some exerting forces around 2 orders of magnitude lower.

Clay instead as seen before has a much more consistent pressure trend under the track, so every segment should contribute to the total force exerted by the track.

The grouser height could also be further increased by making it slimmer, but in that case there needs to be careful design since we can see how high in magnitude forces are, meaning making the grouser too slim could lead to creaks and failure of the blade itself.

1.2.3 Optimal grouser number and spacing analysis

The previous section could point to the fact that there's an optimal number of grousers that could fit in a track length. To evaluate this, an iterative process was used, calculating the maximum height of the grouser for each case, and using that height on realistic situations for our assembly.

The assumptions made is that the grousers can be spaced freely between each other, although consistently, which isn't really the case for a non-rubber track (a steel track is composed of segments meaning the grousers can only have a set distance between each other, barring cases in which different segments could be used, some with grousers and some without), and the thickness and width of the blade, so grouser length in the x direction and width in the y direction, were kept default, so 76.2 mm and 380 mm respectively.

To get reasonable results, analyses were run for the 3 soils, and an average segment pressure was extrapolated, so as to set the surcharge values q for the equation 1.2.7. This assumption is made because of the linear relationship the grouser force has with surcharge q , so setting an average value shouldn't compromise the end result.

The last hypothesis consists in calculating how many grousers are on average in contact with the ground, exerting bulldozing/side wall force, again extrapolated from data sets.

Here is some useful data:

- Track length (common to all tests): 11.125 m.
- Clay track length in contact with ground: 3.22 m, so 28.94% of the total length.
- Snow track length in contact with ground: 4.96 m, so 44.58% of the total length.
- Sand track length in contact with ground: 3.56 m, so 32% of the total length.
- Clay average segment pressure while in contact: 0.38 bar.
- Snow average segment pressure while in contact: 0.294 bar.
- Sand average segment pressure while in contact: 0.349 bar.

A set of numbers of total grousers was chosen, then the maximum height was calculated, then forces generated from such grouser, which were then multiplied by the average number of grousers inside the ground, calculated using the percentage of track length in contact with the ground shown above.

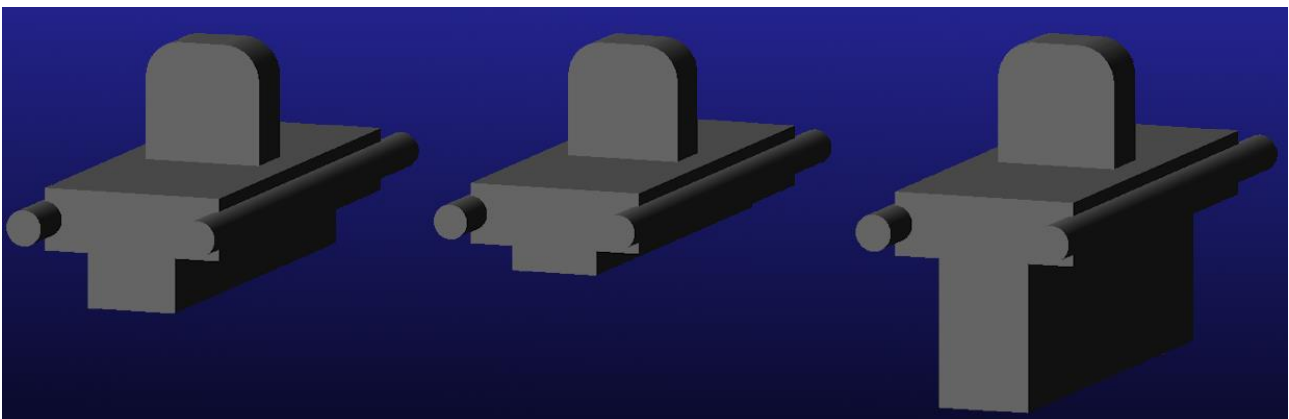
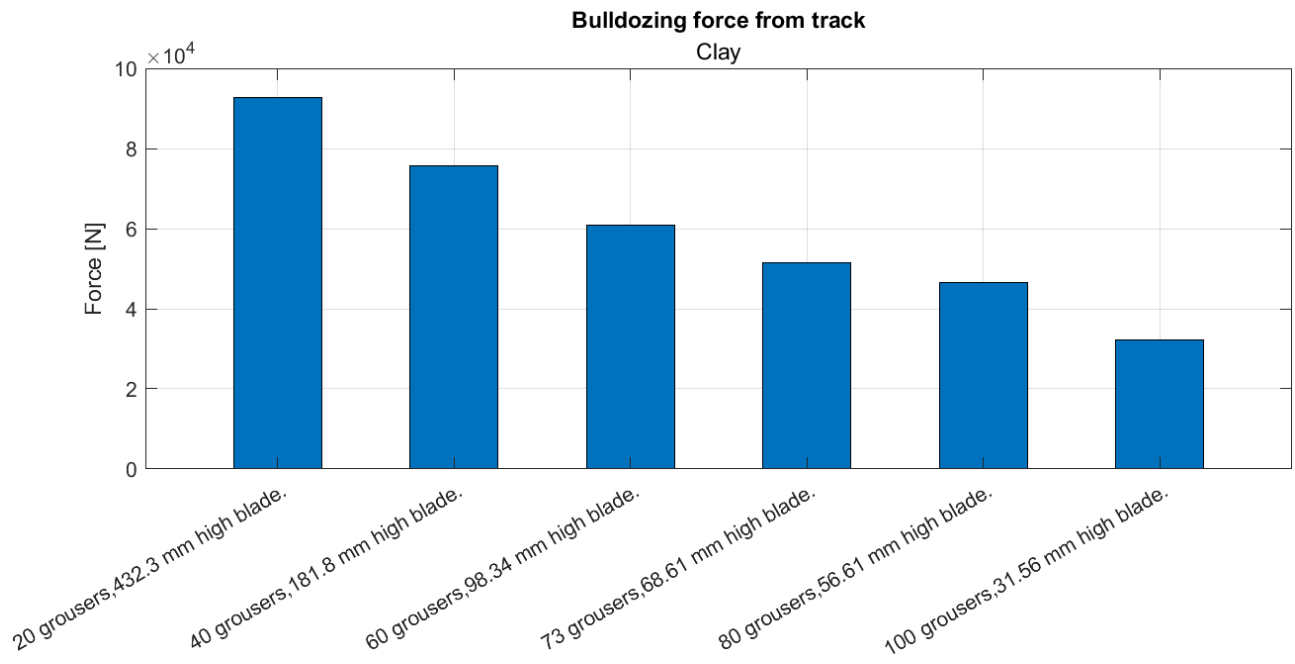
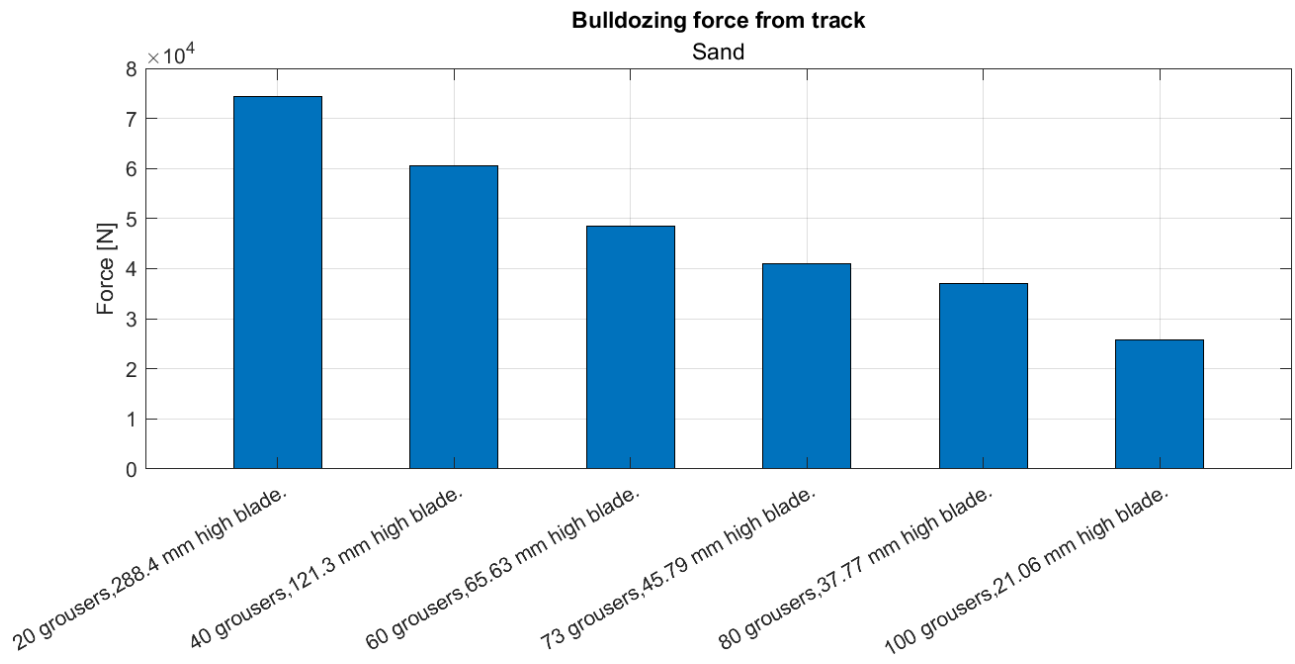
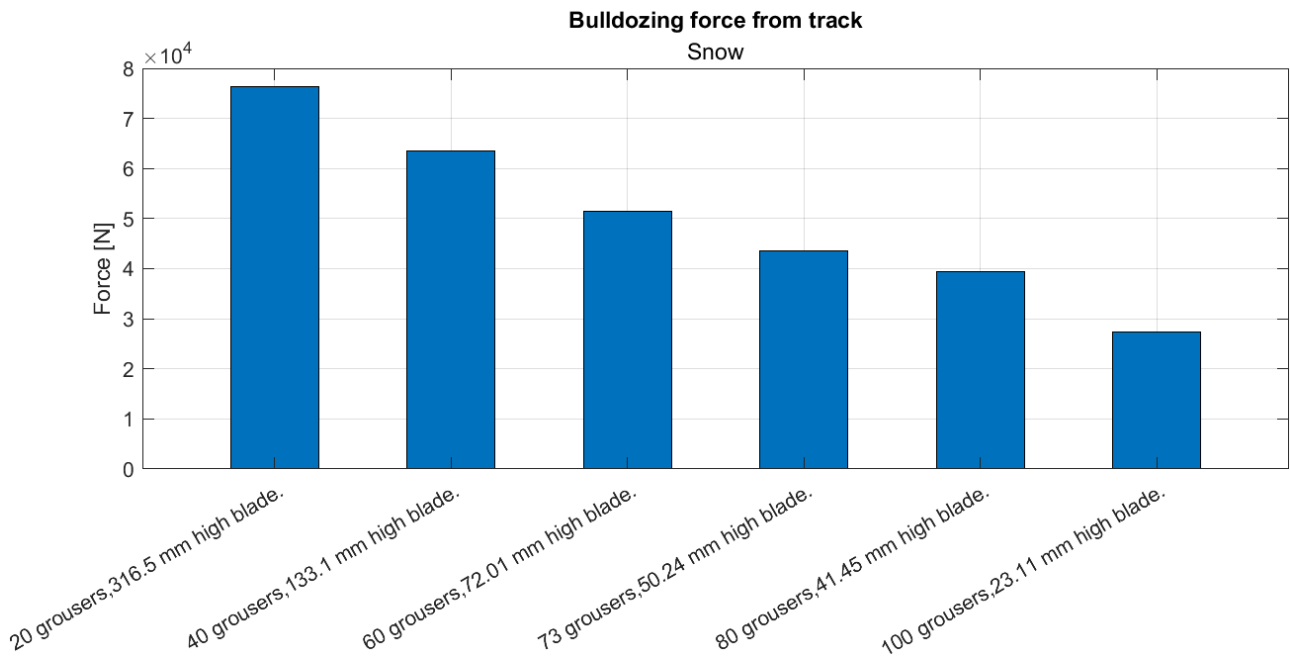


Figure 1.2.18 – Different blade heights (left 45.79 mm, centre 21.06 mm, right 121.3 mm)
 Having stated all assumptions, here are the results:



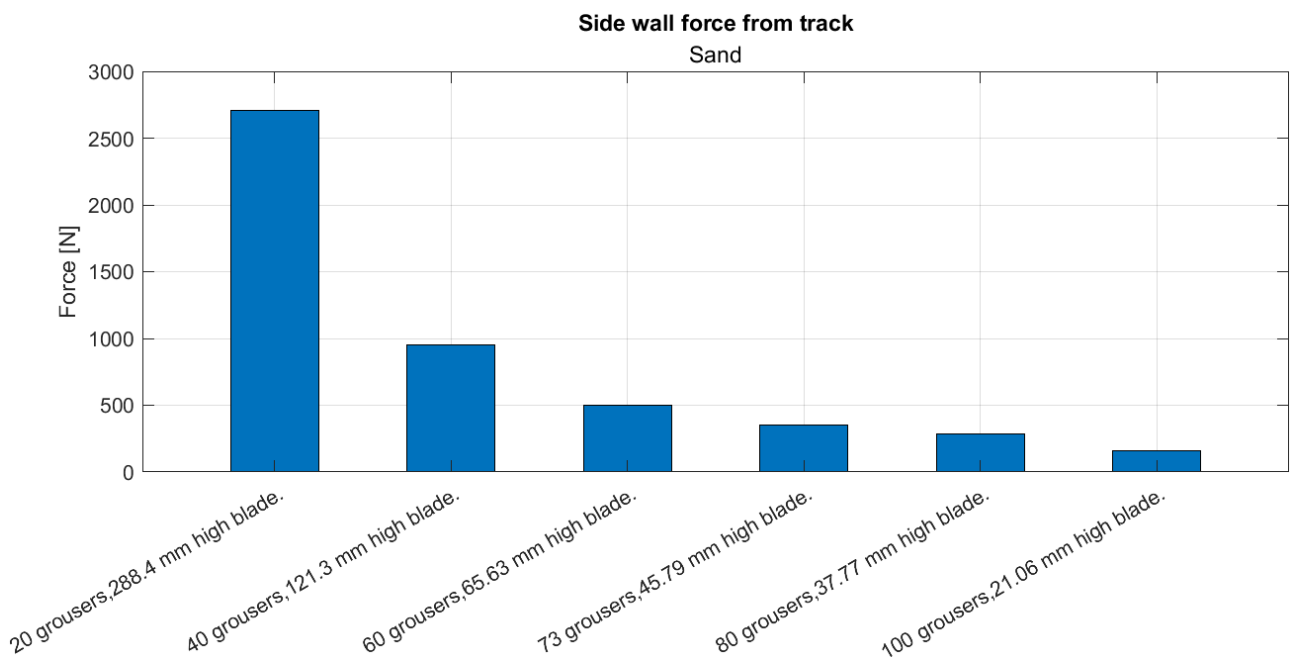


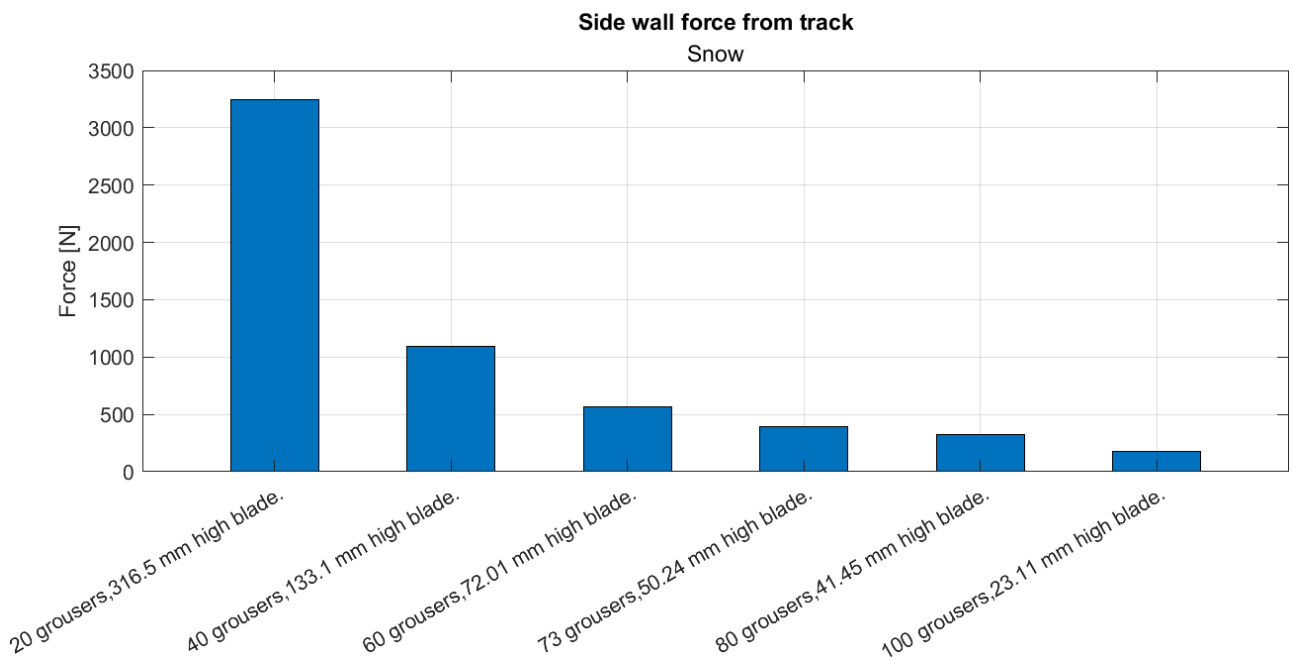
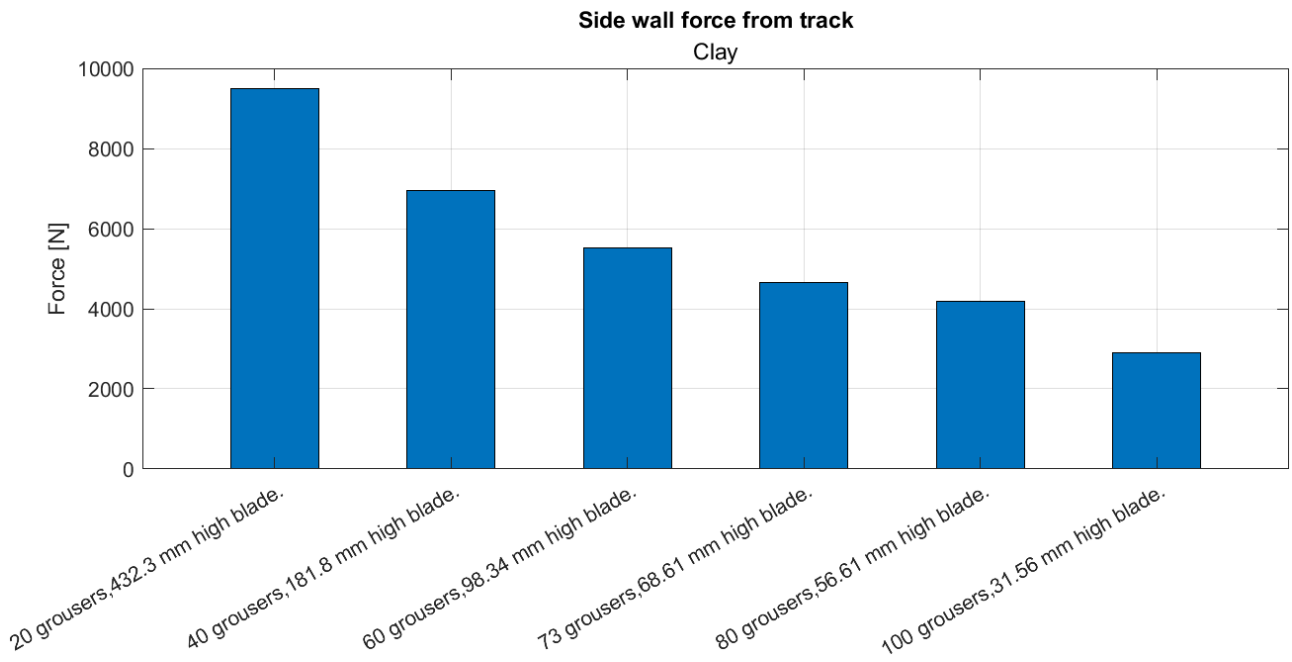
Figures 1.2.19-21 – Bulldozing forces generated from track

As the graphs show, the trend is that having fewer and taller grousers generally is better from the point of view of generating bulldozing forces, for all soils. Though it needs to be said that having, for example, 43 cm grousers in clay's case, would be unpractical for many reasons, such as clearance between the track and the hull, or structural integrity of the segment, that could be subject to very high forces. Lastly, grousers of those dimensions cannot satisfy the assumption that grouser height is much lower than its width, which is 380 mm.

For that reason, it seems that a reasonable value could be 60 grousers, being more capable than the default 73 but not creating the other issues stated.

Now the side wall forces:





Figures 1.2.22-24 – Side wall forces generated from track

Here the effect is even more prominent, especially for sand and snow, but as said for the bulldozing, the first 2 sets are unpractical, still the 60 grouser case still seems like a viable option.

...

1.2.4 Longitudinal force calculation

The shear force is calculated by looking at the displacement of the track segment from when it first enters the soil to where it's currently located. Then this displacement is split into longitudinal and lateral part, each used to calculate the shear force in the given direction [2].

Both shear and bulldozing forces are dependent on the vertical pressure acting on the track segment, hence a mean pressure is calculated from all the segment areas showed above, which are currently in contact with the soil, then this value is used to calculate the shear and bulldozing forces for each grouser and corresponding track segment [2].

Finally, if the vehicle is heavy enough or the soil doesn't exert much resistance, the hull could come in contact with the ground. The soft soil theory for hull contact is the same, with the hull having a lower static friction due to its large contact area [2].

1.3 Segment forces

After all this, the way forces are computed is known. The ATV software though doesn't handle all forces in the same reference frame. The individual segment forces are in fact calculated in the segment's reference frame, while the total forces are then transferred to the global reference frame.

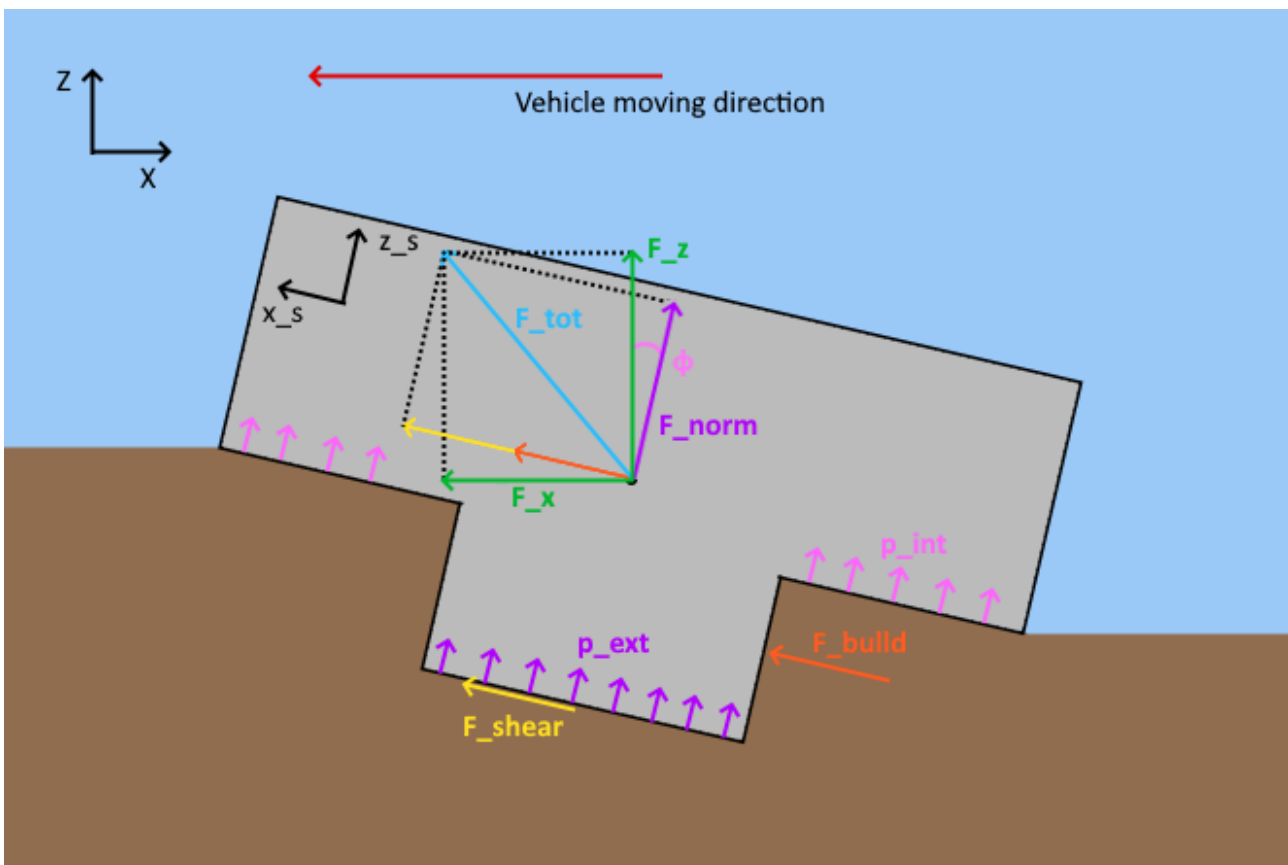


Figure 1.3.1 – Segment forces

This means F_x and F_z are calculated with contribution of all forces combined, and not only the tangential or normal ones respectively.

Chapter 2 Tracked vehicle analyses

Now that we have a decent grip on how the forces depend on different parameters we can see some results and try to compare them between each other and between the plotted ones constructed earlier.

2.1 Assembly description and soil-controller setup

The vehicle on which the analyses were run is a simplified model of a tank. The assembly is composed by the following elements:

- The hull, which is the body of the tank.
- The track, which is composed of 73 track segments, connected to each other via pins at the front and rear end of each, which is then wrapped around the different wheels.
- The sprocket wheel, moved by the powertrain via the driveshaft. The sprocket wheel's teeth are connected to the track segments' pins and impose movement through contact.
- The road wheels, connected via torsion bars and rotational dampers as suspensions, that come in contact with the track by rolling on it and supporting the hull's weight.
- The tensioner wheel, connected to the tensioner, that has the purpose of setting a force to adapt the track tension to the specific needs of the tracked vehicle mission.
- The idler wheel, which has a supporting function on the upper part of the track, not in contact with the ground.

The following image shows where these components lie in the assembly:

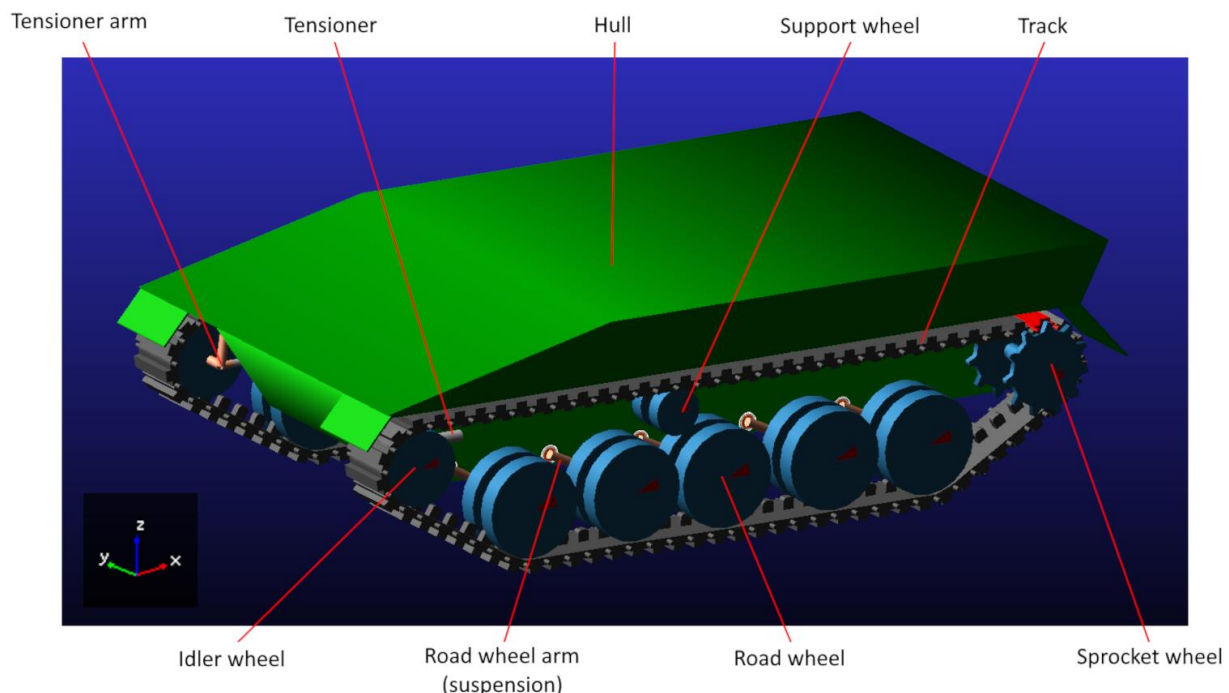


Figure 2.1.1 – Assembly model

Once all components forming the assembly are known, we can proceed to calculate the total mass of the vehicle, which could then be used in rough estimates of forces evaluation:

	Mass	
Hull	12000	[kg]
Track	2190	[kg]
Sprockets	100	[kg]
Road wheels	350	[kg]
Idler wheels	100	[kg]
Support wheels	60	[kg]
Tensioners	10	[kg]
Tensioner arms	60	[kg]
Road wheel arms	300	[kg]
Driveshaft	60	[kg]
Shelf	776	[kg]
TOTAL	16006	[kg]

Table 2.1.1 – Assembly mass in components

Here are instead the dimensions of the assembly parts:

Geometry	Length (X)	Width (Y)	Height (Z)	
Upper Hull	5.35	3	0.4	[m]
Lower Hull	5	1.8	0.7	[m]
Track segment plate	152.4	480	52	[mm]
Segment grouser	76.2	380	40	[mm]
Segment guide	80	50	80	[mm]
	Thickness	Width		
Shelf	15	560	[mm]	
	Radius	Width		
Sprocket	255	480	[mm]	
Road wheel	330	355	[mm]	
Support roll	158	300	[mm]	
Idler wheel	250	355	[mm]	

Table 2.1.2 – Assembly dimensions

To better explain this table, upper hull, lower hull and shelf are part of the hull subsystem, shown here:

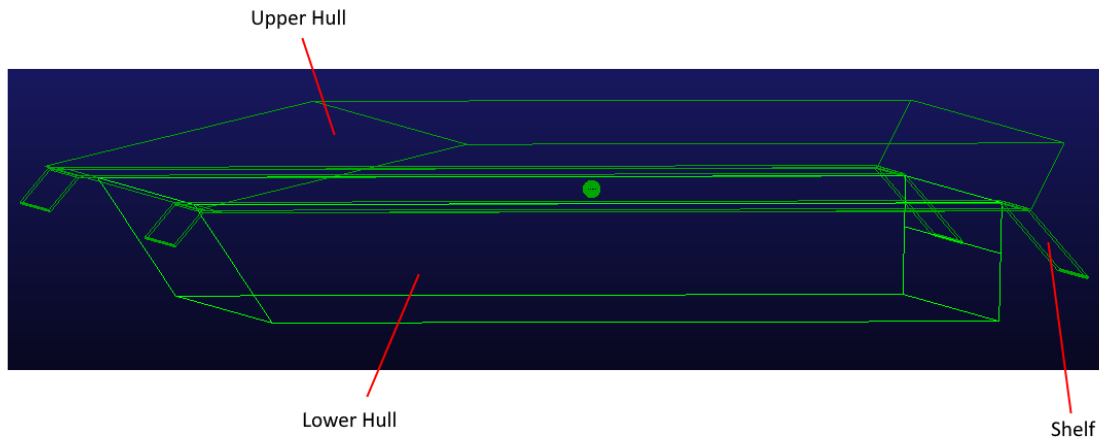


Figure 2.1.2 – Hull parts

And the segment subdivisions:

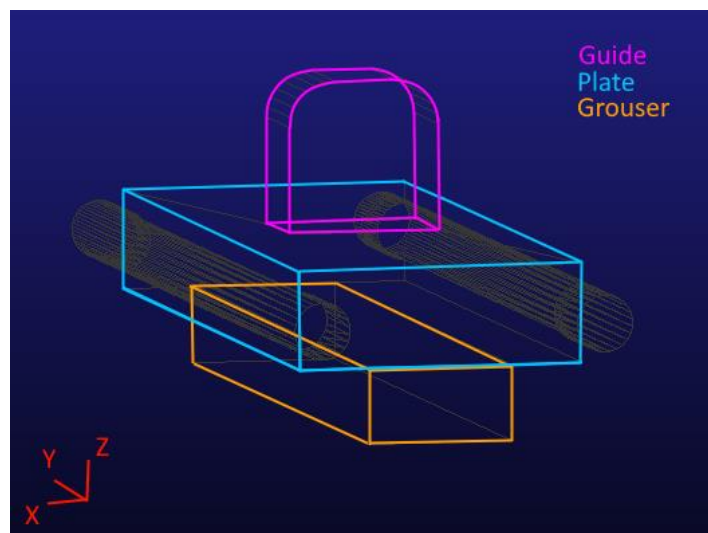


Figure 2.1.3 – Segment parts

Another information that can be given on the assembly is about the powertrain. The modelling of the powertrain consists in simply a shaft having weight and that connects to the sprocket wheel. The engine is not modelled and there is no complexity in shaft geometry. It mostly serves as a device that can either be fixed to a rotational speed or can be controlled through a PI controller, modulating the speed at which the assembly moves. This is the component that requires the setup shown subsequently.

...

Lastly, the tensioner model can be shown. The tensioner is the tool that regulates the tension of the track, meaning how loosely or tightly it is wrapped around the road and sprocket wheels.

It is composed, in our modelled assembly, of an extendible arm hinged to the hull on one end and fixed to it on the other, connected to the idler wheel through the wheel's axle.

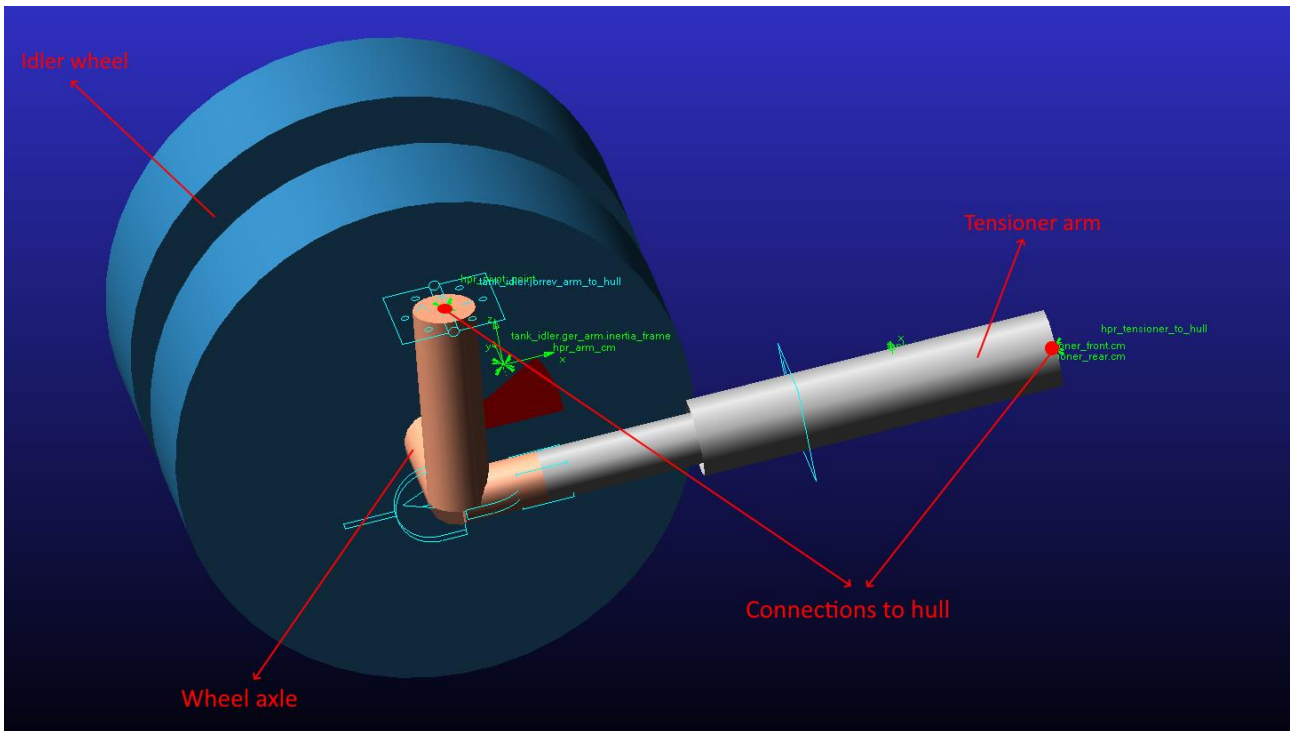


Figure 2.1.4 – Tensioner components

In the figure we can see the hinge on the upper part of the arm (blue hinge icon) and the hardpoint (green) on the right end of the extendible arm, representing it being fixed to the hull.

The tensioner arm has inside a spring, which is preloaded, and has therefore a design length. As the preload raises, the spring shortens and the arm extends. The user can control the tensioner force in various ways:

- Adjusting the characteristic of the spring. The spring can have a linear force-length characteristic or a non linear one, and the user can edit both.
- Adjusting the length of the tensioner; the tensioner will then be controlled to always maintain this length, varying the force accordingly.
- Adjusting the force of the tensioner; the control will instead act on the force, keeping the value steady throughout the simulation.

Adjusting length and force may seem redundant, and, for the same soil, it is. Setting a control on the force or setting a control on the length is the same thing, if all analyses are run on the same soil, but the force at fixed length and vice versa depend also on the terrain the vehicle is cruising on, as analyses will show in the following chapters.

Once the components of the assembly have been established, the user needs to tune certain parameters regarding road discretization or control variables.

The first few analyses done in this section has been run with the same parameters, so as to ensure any big variation is due to the different soils.

The manoeuvre is a simple straight-line acceleration from an initial velocity of 1 m/s to a final velocity of 4 m/s, so from 3.6 km/h to 14.4 km/h, over the course of 1.5 seconds. This is done through the velocity controller setup, which is a PI controller in charge of sustaining an input constant velocity or a function of one over the manoeuvre time.

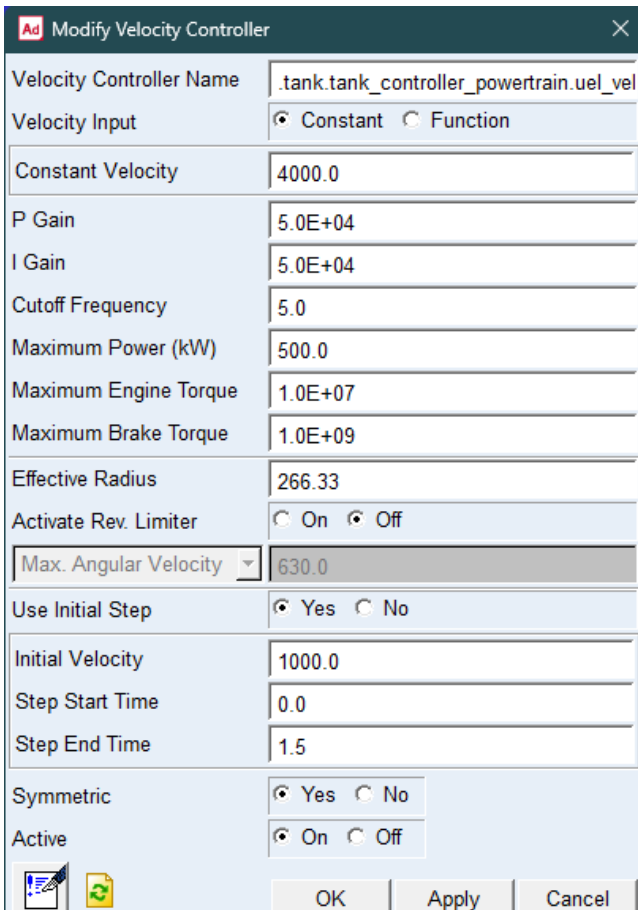


Figure 2.1.4 – Velocity controller setup

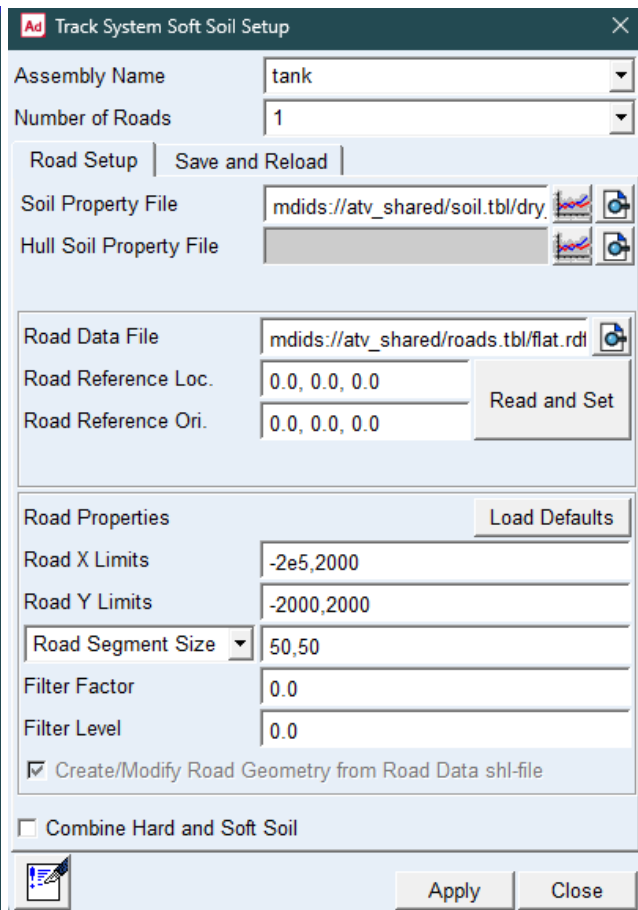


Figure 2.1.5 – Soil setup

The parameters shown in the screenshot have been extrapolated from a series of analyses and seem to be the ones that stabilize our controller the most in the test runs. After doing this, we need to wrap the track segments around the supporting wheels, also choosing for this case a half-vehicle symmetry, since we're only doing straight line operations.

The following step is the soil setup; As seen in the screenshot, this is based upon defining a certain soil property file to be used for both track contact and hull contact, and then setting up the road dimensions appropriately to the manoeuvre we're doing. In this case it's a simple straight-line acceleration, so we set up a road long enough to cover the tank movement and wide enough to fit it. Lastly road segment size is important for the track segment split described in chapter 1.3.1. This symmetric dimension setup may not be optimal but it's sufficient to prevent big errors from happening during the calculation. This road setup was only used for these starting simulations comparing different soils.

After the soil setup, the only thing missing is the analysis setup, which is the step defining how long will the manoeuvre last and how many iterations of calculations need to be performed. We also set an initial velocity, in this case congruent with the one set in the controller, to enhance stability.

Ad Tracked Vehicle Analysis

Tracked Vehicle Assembly: tank

Variant: default

Analysis Name: dry_loose_sand

End Time: 6 [Sec]

Number of Steps: 1500 [-]

Mode of Simulation: interactive

Initial Velocity: 1000.0 mm/sec

Setup Tensioners:
 .tank.tank_idler.uel_idler_tensioner

Set DEBUG/EPRINT

Reload Static Positions

Start at Equilibrium Set Equilibrium Parameters

	Error	Maxit	Stability	Imbalance	Tensioner Set
<input checked="" type="checkbox"/> 1:	100.0	250	100.0	100.0	<input type="checkbox"/>
<input checked="" type="checkbox"/> 2:	10.0	250	10.0	10.0	<input checked="" type="checkbox"/>
<input type="checkbox"/> 3:	0.1	250	0.1	0.1	<input checked="" type="checkbox"/>

Load Results after Simulation

Create Analysis Log File

Figure 2.1.6 – Simulation setup

2.2 First analyses

Having run a different analysis for every soil present in the database, we can see how the tank and its components behave under varying conditions.

The first thing we can notice is how there's 2 different classes of behaviours of the velocity controller: The control has in any case an oscillatory behaviour, but for some soils the oscillations are very noticeable, while for some other they act more as a slight ripple, with a much higher frequency and much lower amplitude of oscillation. Here are a couple examples, showing the velocity behaviour on the soils "dry_loose_sand" and "dry_sand_LLL":

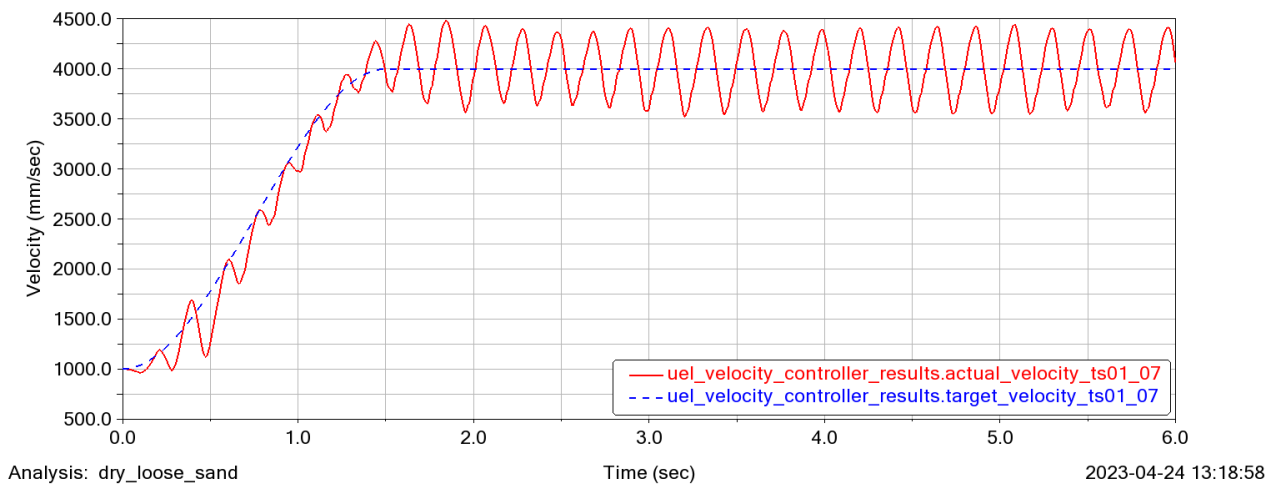


Figure 2.2.1 – Dry loose sand velocity results

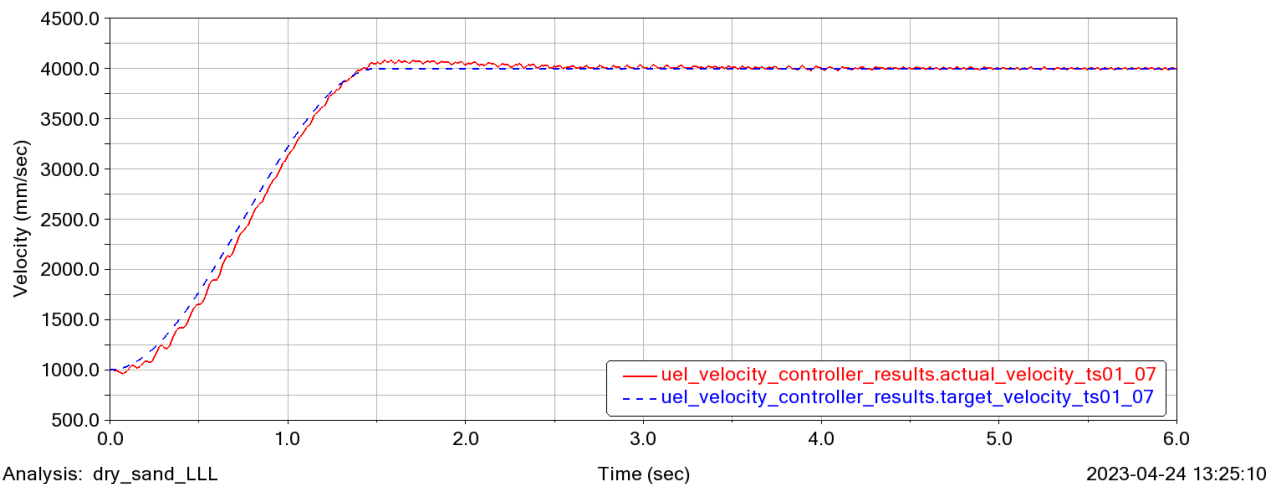


Figure 2.2.2 – Dry sand LLL velocity results

We can see there still are oscillations, but the control is way more accurate.

The terrains that give the first type of result are:

- Dry compact sand
- Dry loose sand
- LETE sand

While the terrains giving the second one:

- Dry LLL sand
- Heavy clay WES 40
- Lean clay WES 32
- LETE sand 2nd
- Sandy loam
- Soft snow

In terms of velocity, all results in the same category are comparable, with the exception of soft snow, which experiences a much higher sinkage and pitch variation resulting in a much different behaviour:

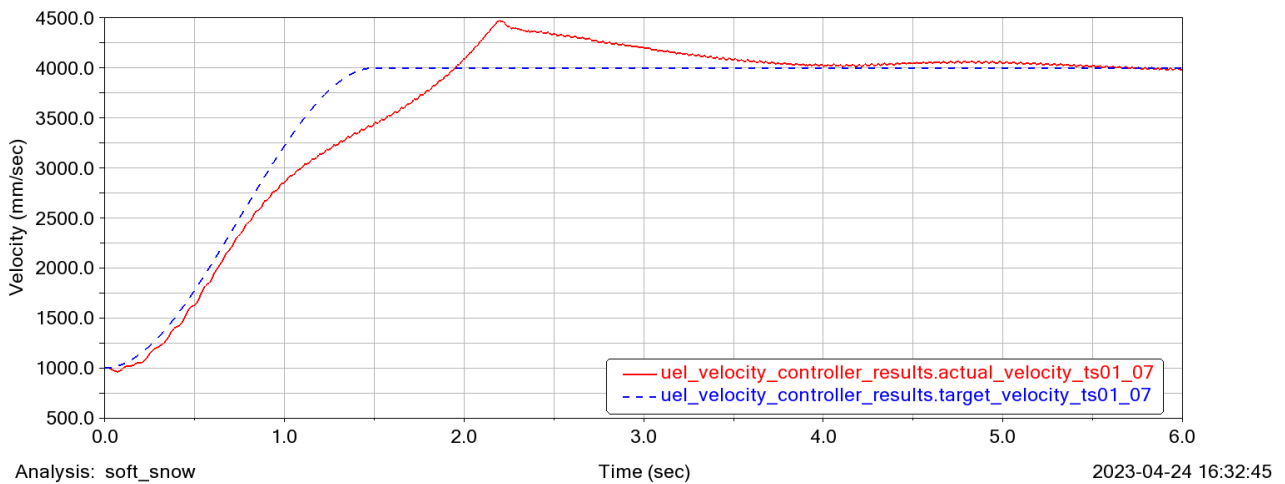


Figure 2.2.3 – Soft snow velocity results

2.2.1 Soil parameters and behaviour

As said before, the parameters of every soil were compared, checking whether or not to use bulldozing instead of shearing and to see if there were any visible effects of different parameters, for the soils demonstrating a behaviour of type 1 (oscillating) or type 2 (stable)

Here is a table comparing all parameters:

	Dry loose sand	Dry compact sand	Dry sand LLL	Heavy clay WES 40	Lean clay WES 32	LETE sand	LETE sand 2nd	sandy loam	soft snow	
spec weight	1.525E+04	1.525E+04	1.525E+04	1.726E+04	1.697E+04	1.525E+04	1.525E+04	1.256E+04	3.000E+03	N/m ³
Kc	0.000E+00	9.570E+04	9.900E+02	1.840E+03	1.520E+03	1.020E+05	6.940E+03	1.198E+04	6.160E+03	N/m ²
Kphi	1.585E+06	3.277E+06	1.528E+06	1.033E+05	1.196E+05	5.301E+06	5.058E+05	6.744E+05	1.493E+05	N/m ³
n	1.010E+00	1.150E+00	1.100E+00	1.100E-01	1.500E-01	7.900E-01	7.100E-01	8.153E-01	1.530E+00	\
K0	0.000E+00	0.000E+00	0.000E+00	0.000E+00	0.000E+00	0.000E+00	0.000E+00	0.000E+00	0.000E+00	N/m ³
Au	5.030E+08	5.030E+08	5.030E+08	1.033E+06	1.196E+06	5.030E+08	5.030E+08	5.000E+08	4.000E+07	N/m ⁴
Cdamp	5.000E-04	5.000E-04	5.000E-04	1.000E-05	1.000E-05	1.000E-05	1.000E-05	1.000E-03	1.000E-05	Ns/m
Cr	1.570E+03	1.370E+03	1.040E+03	2.069E+04	1.379E+04	1.300E+03	9.600E+02	3.000E+03	1.200E+02	N/m ²
Phir	6.466E-01	5.418E-01	4.887E-01	1.047E-01	1.920E-01	4.765E-01	4.765E-01	3.910E-01	2.860E-01	rad
Kr	7.400E-02	4.700E-02	1.000E-02	5.000E-02	5.000E-02	2.000E-02	1.140E-02	3.600E-02	3.900E-03	m
Ci	1.570E+03	1.370E+03	1.040E+03	2.069E+04	1.379E+04	1.300E+03	1.150E+03	2.500E+03	7.600E+02	N/m ²
Phii	6.466E-01	5.418E-01	4.887E-01	1.047E-01	1.920E-01	5.428E-01	5.498E-01	4.922E-01	4.050E-01	rad
Ki	7.400E-02	4.700E-02	1.000E-02	5.000E-02	5.000E-02	2.000E-02	1.150E-02	4.100E-02	4.240E-02	m
hb	40	40	40	40	40	40	40	40	40	mm
ls	80.31085267	70.7614914	66.5717681	44.42361816	48.52456146	70.84415438	71.42692251	66.83643047	60.66870306	mm
grous distance	76.2	76.2	76.2	76.2	76.2	76.2	76.2	76.2	76.2	mm
shear/bulldoz	shear	bulldoz	bulldoz	bulldoz	bulldoz	bulldoz	bulldoz	bulldoz	bulldoz	

Table 2.3.1 – Soft soil parameters

In the table the soils displaying a behaviour type 1 were highlighted in green, and the ones with a type 2 behaviour were highlighted in blue. Also, for each row, so each parameter, the maximum value was highlighted in yellow and the minimum in red.

The parameters are the ones described in chapter 1, so the ones used to calculate both horizontal and vertical forces generated by ground contact with the track segments.

The addition of “r” and “i” to the longitudinal parameters addresses the difference between the internal and external shearing surfaces.

We can see that the most “extreme” soils are snow, dry loose sand, and heavy clay, displaying a lot of min/max parameters. Another thing we can evaluate is that contrary to expectations, the damping value has basically no effect on the oscillating behaviour of the assembly, with both type 1 and type 2 soils displaying the minimum damping out of all (e.g. LETE sand and LETE sand 2nd) and 2 different type 2 soils having either the maximum value or the minimum (sandy loam, max, and soft snow, min). The exact same can be said for Au. The hypothesis of the behaviour being due to a combination of different parameters rather than to a single one becomes hence very likely.

As for the shear/bulldozing discussion, the default configuration of the tracks was compared: Knowing the track pitch is 152.4 mm, and the grouser length is 76.2 mm, we can calculate the distance between grousers and then, using equation (1.2.7), calculate the minimum distance between grouser l_s necessary to be able to use the bulldozing force instead of the shearing one. The only soil that is not able to use the bulldozing force with default segment geometry is dry loose sand.

Having said that type 1 soils show unsatisfying results, the analyses will focus on 3 different soils from the type 2 chart, those being dry sand, heavy clay and snow.

2.3 Vehicle parameters on different soils

The simulations run on sand, clay and snow show interesting variations in vehicle displacement and forces generated, which will be shown here.

These simulations are setup with a constant velocity of 2 m/s or 7.2 km/h without acceleration for better consistency.

Starting with velocity:

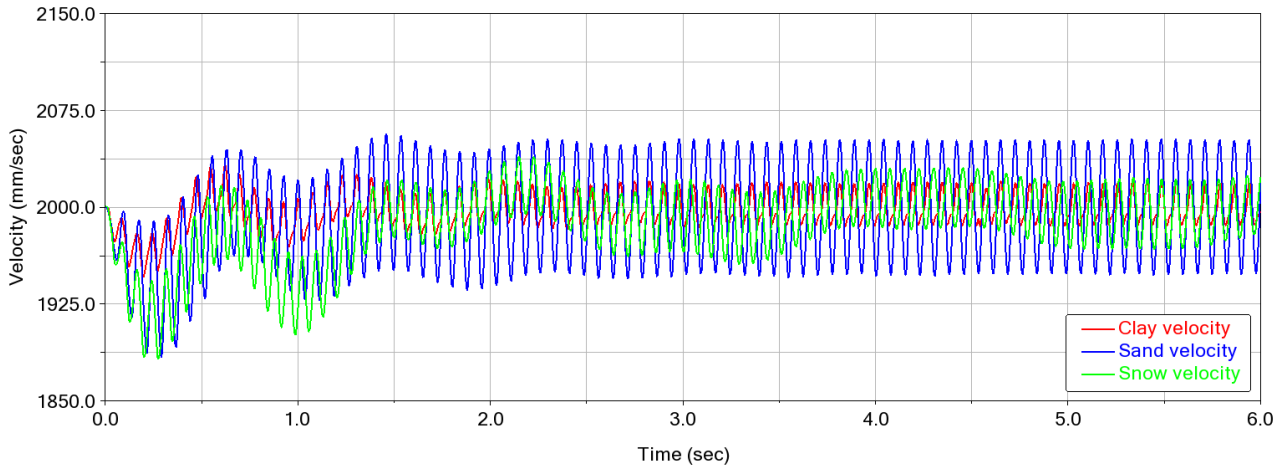


Figure 2.3.1 – Velocity on different soils

The most stable velocity is kept on clay, but also sand, while having higher gaps between peaks and valleys, is stably averaging 2 m/s. Snow instead also has fluctuations in the average value, but it still is very close to the control requirement.

Now comparing vertical displacement of the hull centre of gravity:

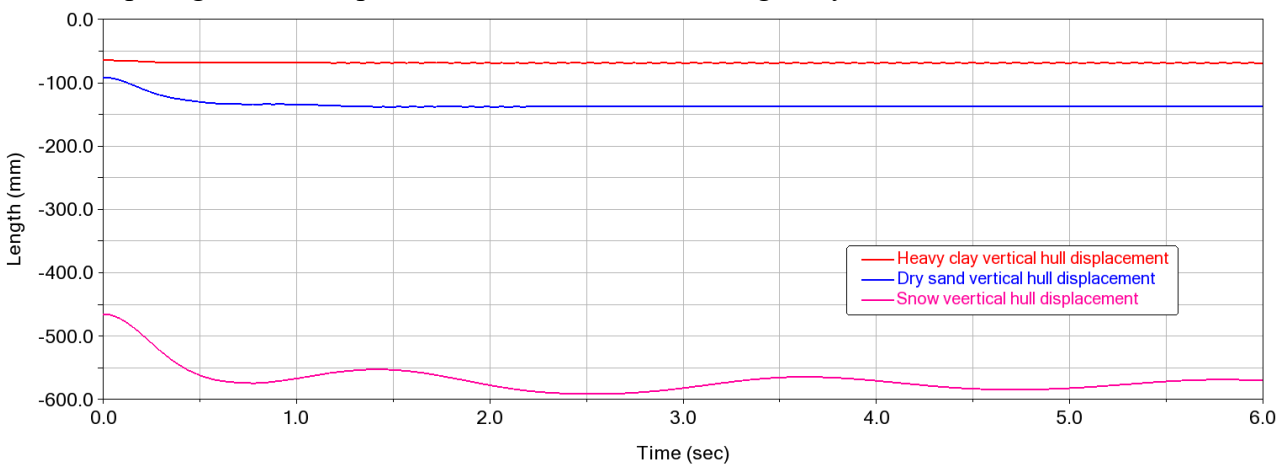
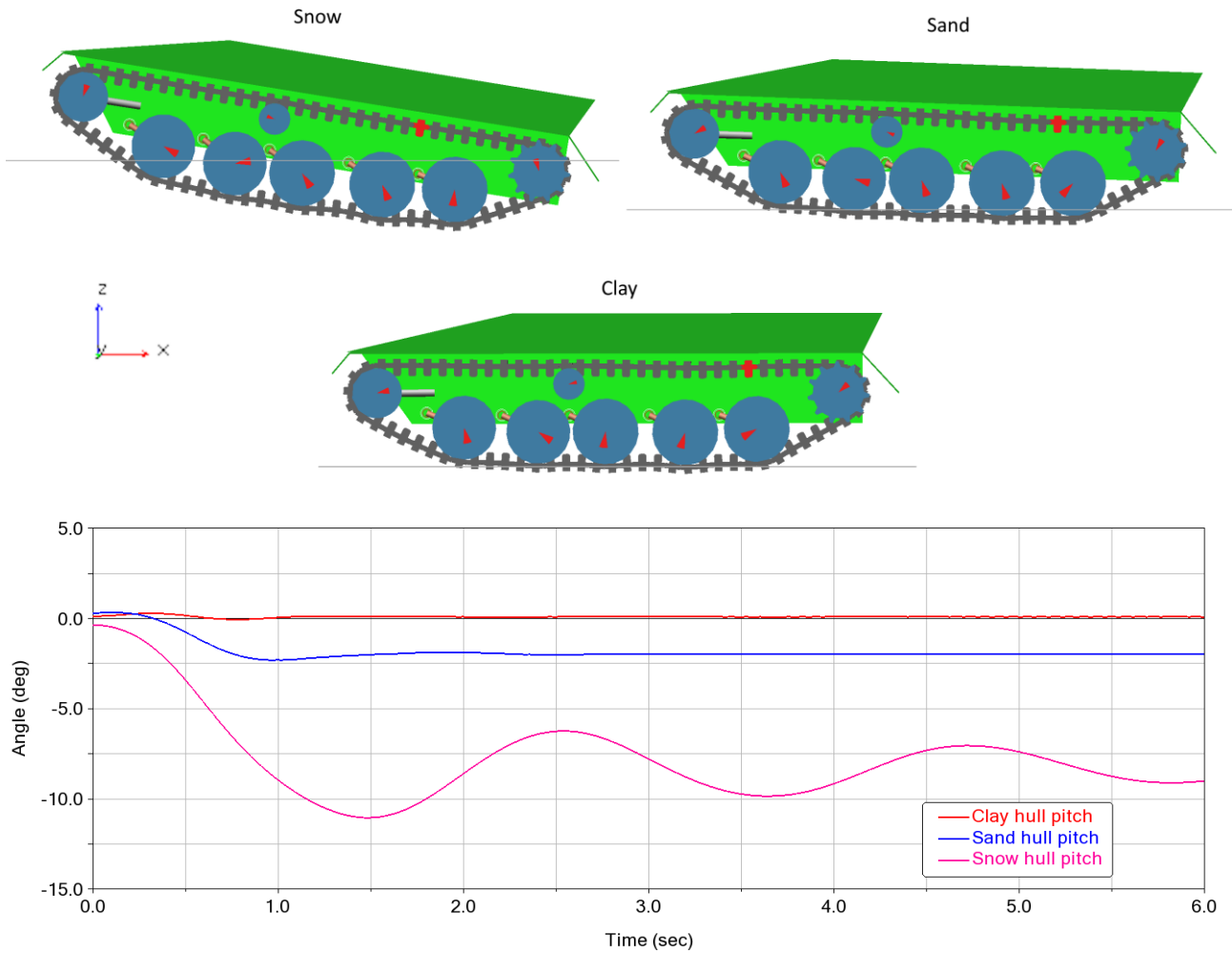


Figure 2.3.2 – Vertical hull displacement values for different soils

Since the measurement is done at the hull, the motion is the result of both suspension and soil deformation. Comparing the three trends a lower frequency of the oscillation can be seen passing from clay to sand to snow, i.e. from harder to softer terrains, together with an increase of the settling time. Also, obviously, snow has by far the most significant displacement, while for clay it is only around 60 mm.

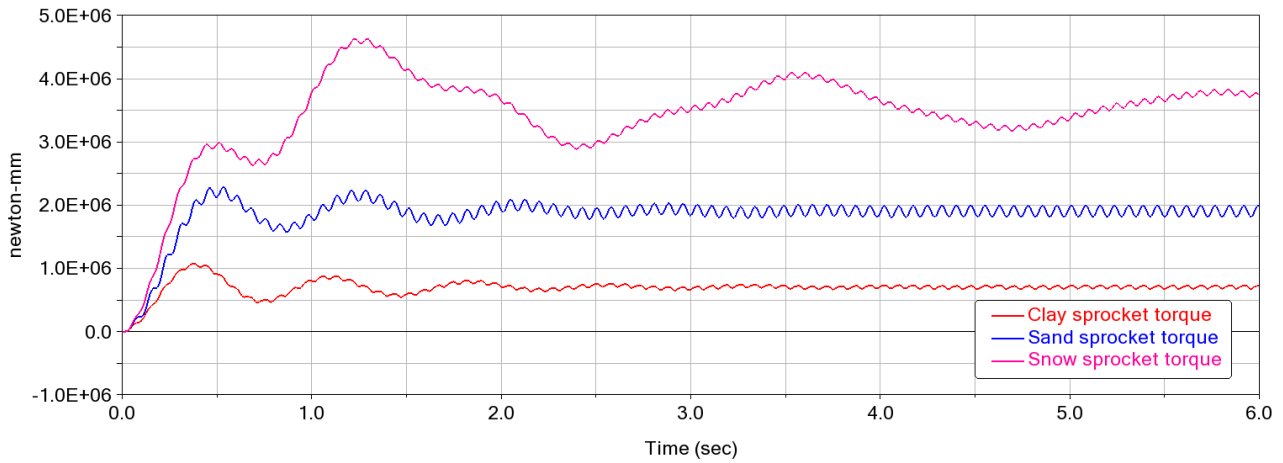
Now let's compare pitch:



Figures 2.3.3-4 – Pitch values for different soils

The thing we can see from the pitch is how the harder the soil, the lower it is. The hardest soil in fact, like clay, shows a steady state pitch value very close to 0, meaning the vehicle is stable in the horizontal position, while softer sand or snow stabilizes at higher in module negative values after more pronounced oscillations. In the first picture we can visualize the pitch of the vehicle on the 3 soils, and understand the minus sign, which is due to the vehicle moving in the negative X direction.

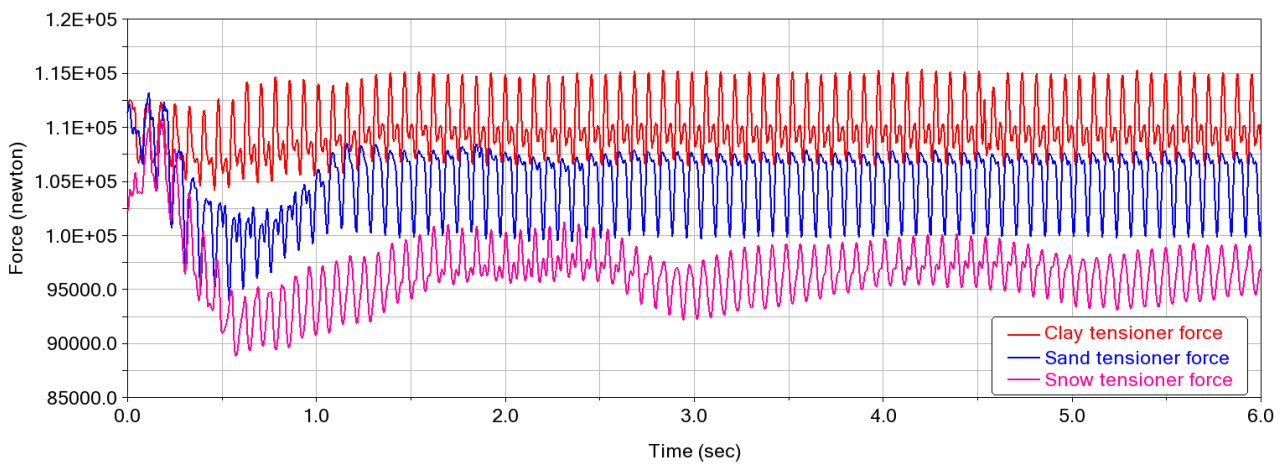
Now let's compare Sprocket torque:



Figures 2.3.5 – Sprocket torque values

The torque input is higher for softer soils, due to the terrain being more subject to deformation, and hence absorbing more force and power to keep moving. Also, like most values, the oscillations due to heavy sinkage on snow don't allow the parameter to fully stabilize after 6 seconds.

Lastly, let's compare tensioner force:

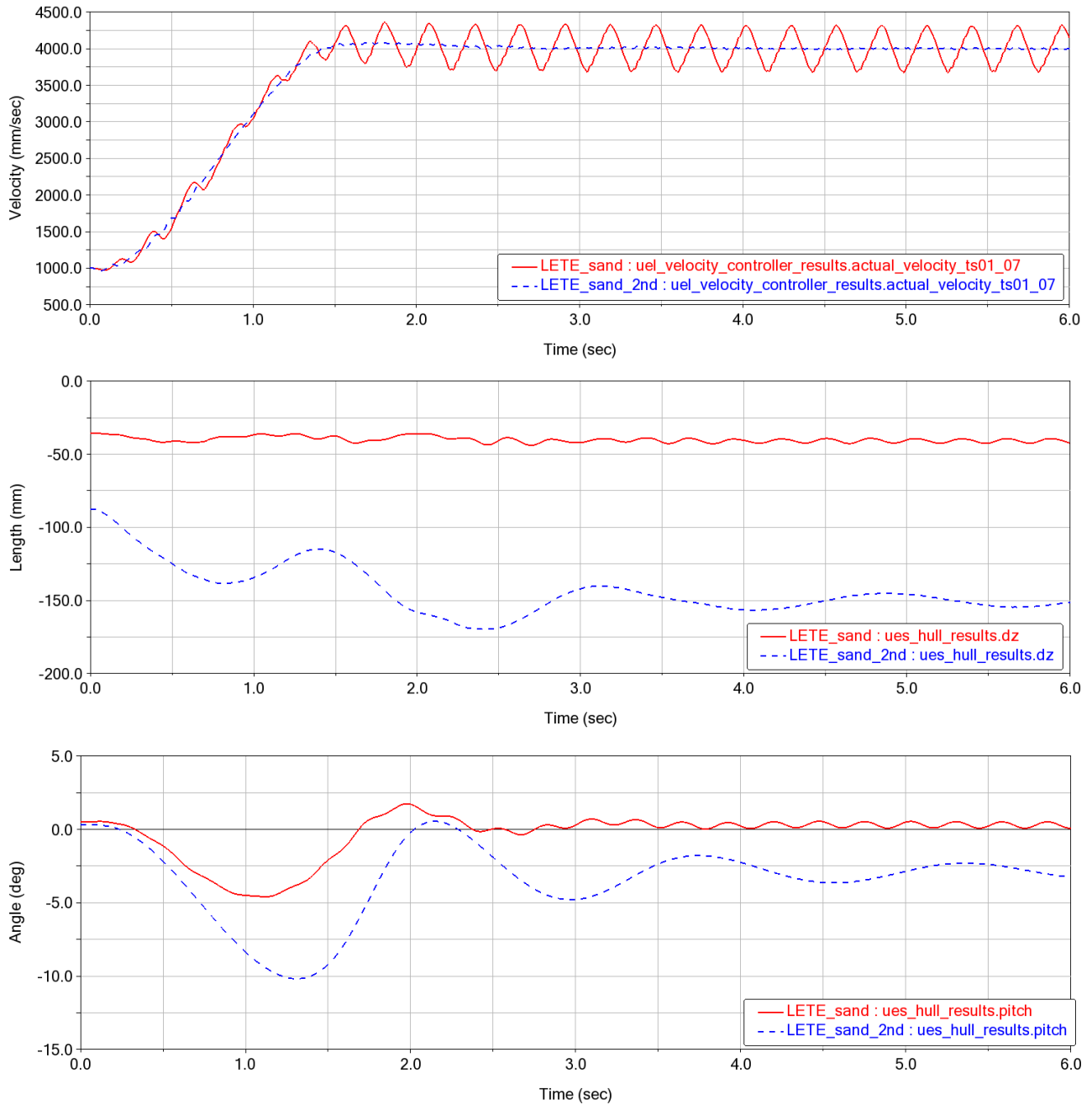


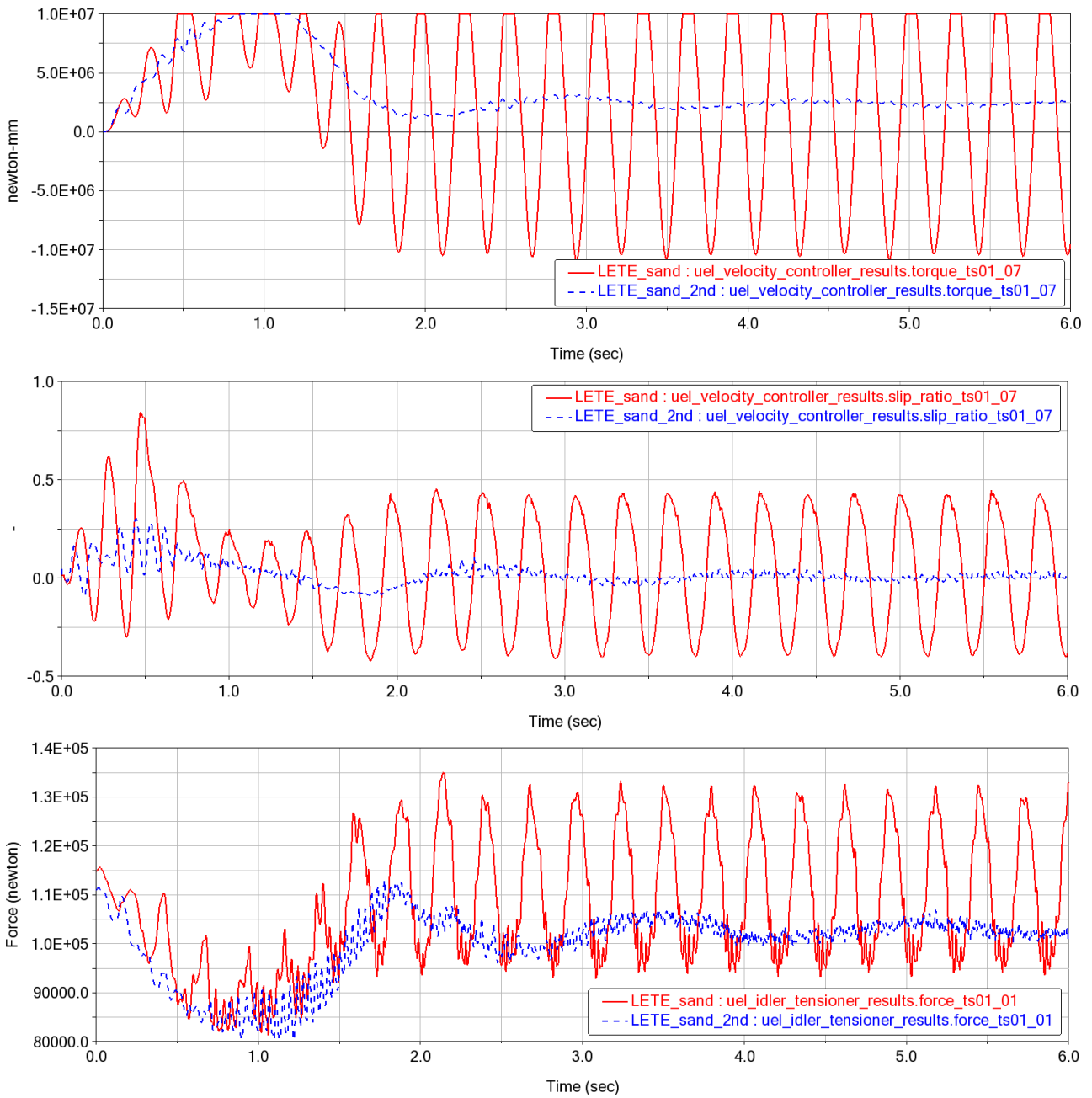
Figures 2.3.6 – Tensioner force values

The tensioner is setup in the same way for all analyses, imposing its design length. As shown here, softer soils put less stress on the tensioner to maintain the same length. Oscillations are in this case pretty significant for all soils, the vibration is underdamped with a main frequency of around 15Hz.

2.3.1 Similar soils from the 2 types

A direct comparison between 2 similar soils of different types (LETE sand and LETE sand 2nd, as seen in table 3.3.1, are very similar barring the “K” parameters, which has a significant difference) is shown, for all the variables shown in the other analyses:





Figures 2.3.7-12 – LETE sand and LETE sand 2nd comparison

Interesting to see how even though most parameters are similar, there are significant discrepancies in a lot of values, even averaging out the huge oscillations of the type 1 soil.

2.3.2 Segment forces analysis

One more analysis was run at lower speed and without the controller to have a better grasp at how the forces and displacements are linked. For this analysis we set a fixed angular velocity of 225 deg/s for our sprocket wheel, and ran the analysis on dry sand LLL. First thing we see is how even at a completely constant angular velocity of our sprocket, the terrain response is not perfectly stable and has some fluctuations in the longitudinal velocity.

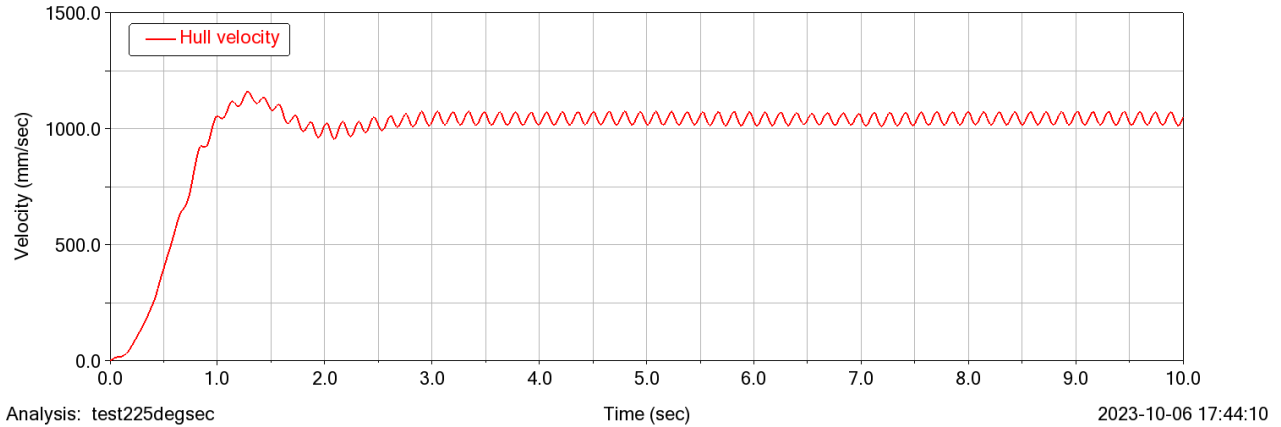


Figure 2.3.13 – Longitudinal velocity in sand

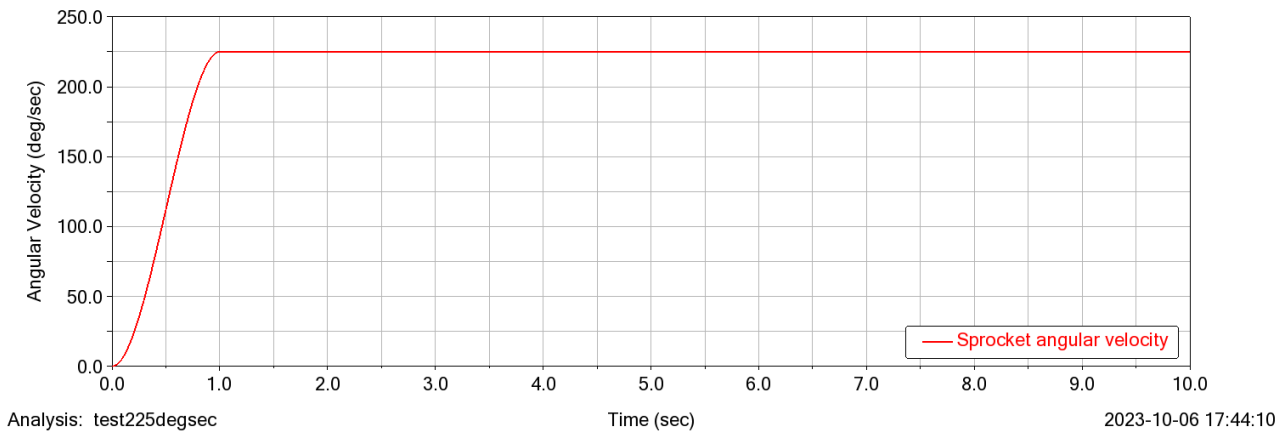


Figure 2.3.14 – Angular velocity of the sprocket wheel

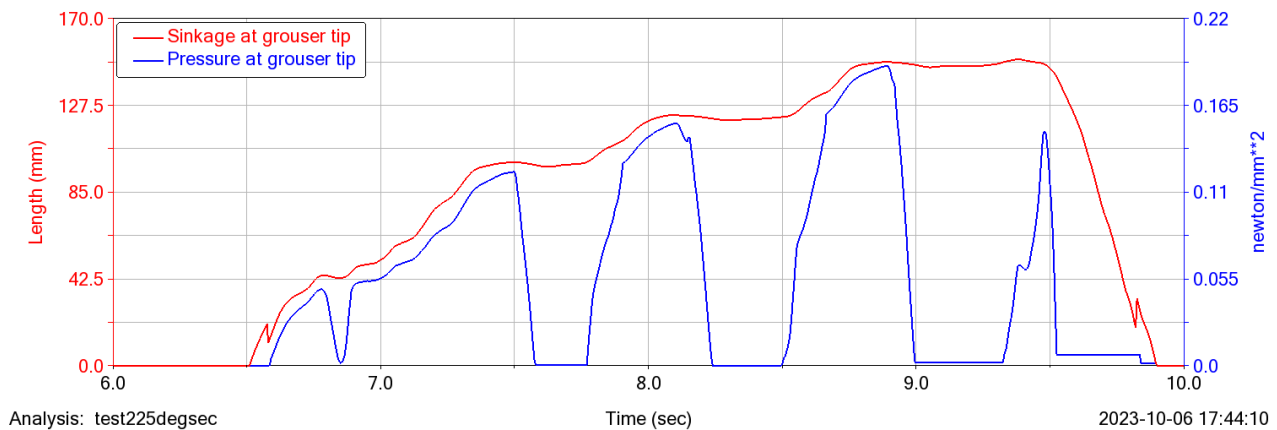


Figure 2.3.15 – Pressure-sinkage trend vs time

The next interesting thing to note is how sinkage and pressure are linked. Like analysed in chapter 1.1, here we can see how during loading the pressure and sinkage follow a very similar trend, while in unloading, we can see how pressure (blue line) has huge decreases and how the sinkage (red line) has instead really small ones. This could also represent, since we're in a pretty stable regime, a trend of pressure close to the static one, since here we can see the segment passing under all 5 road wheels, and how between each one, the segment is close to being unloaded.

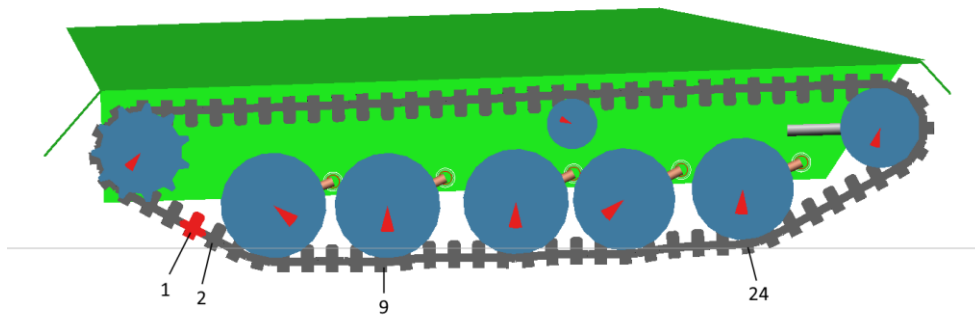
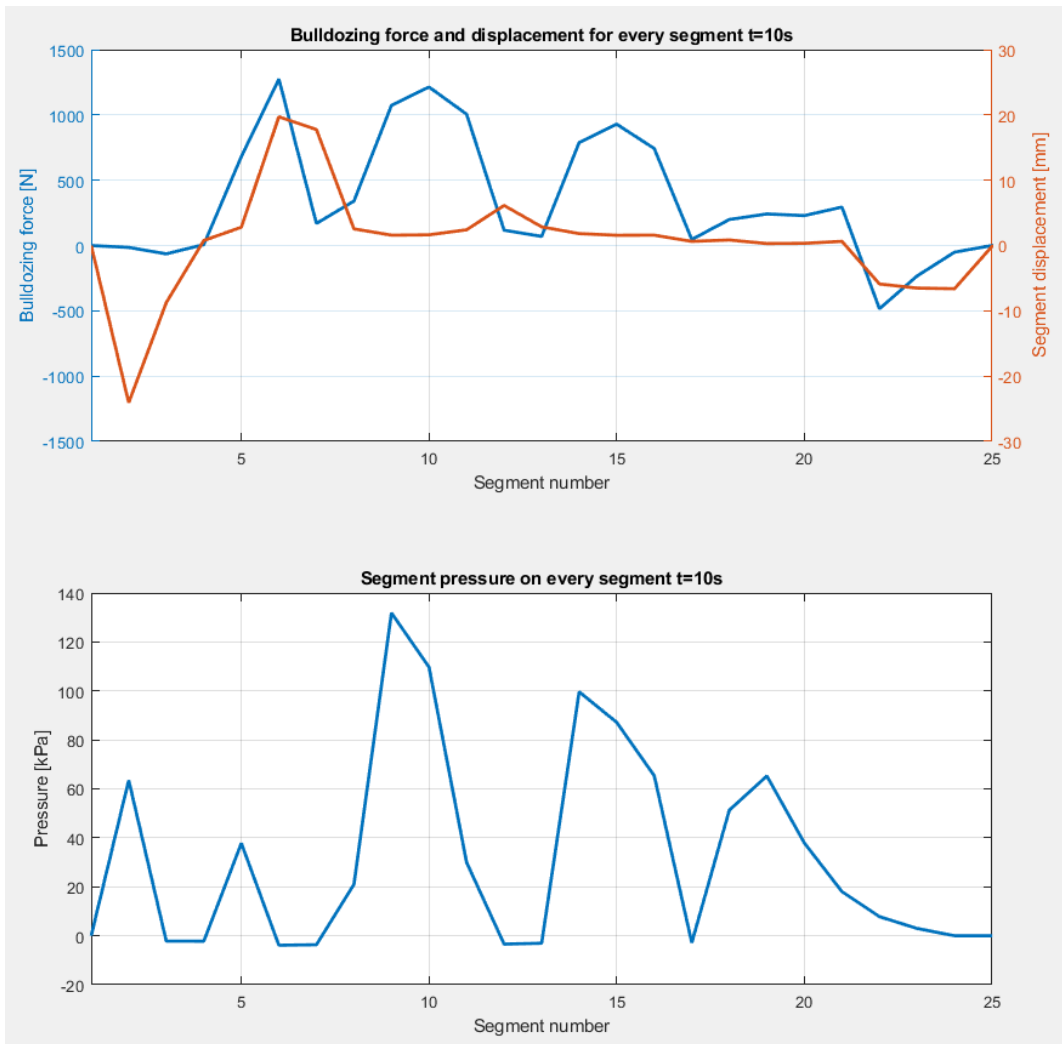


Figure 2.3.16 – Segment numeration

The segments are numbered starting from the red segment, which is segment number 1, in the counter-clockwise direction.

Using this information it's possible to analyse the force variables of each segment at a certain time step:



Figures 2.3.17 – Displacement relationship with forces

Regarding longitudinal forces, here in these graphs we can see the connection between longitudinal displacement J (red) and bulldozing force. It's clear how the sign of j is the decider of the sign of the forces generated by each segment, and magnitude depends by both displacement and surcharge. At this instant in time, the track develops a positive force, barring the few segments in the front of the track.

Lastly we have a visual representation of how the road is left after the tracked vehicle has passed. We can see a bit of ripple caused by the oscillations mentioned beforehand.

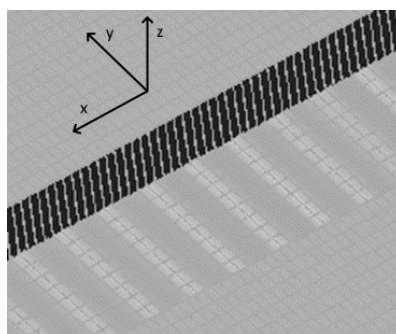


Figure 2.3.18 – Soil shape after track solicitations

2.4 Issue with total track forces

A brief comment should be made on how the absence of realistic damping in the terrain simulations regarding longitudinal forces leads to a very oscillatory behaviour when no load is applied.

A simple analysis was run with these settings:

- Vehicle speed: 1.5 m/s or 5.4 km/h.
- Flat road, with sand soil.
- Default segment geometry
- Default tensioner setup

The longitudinal forces coming from all track segments are then extracted:

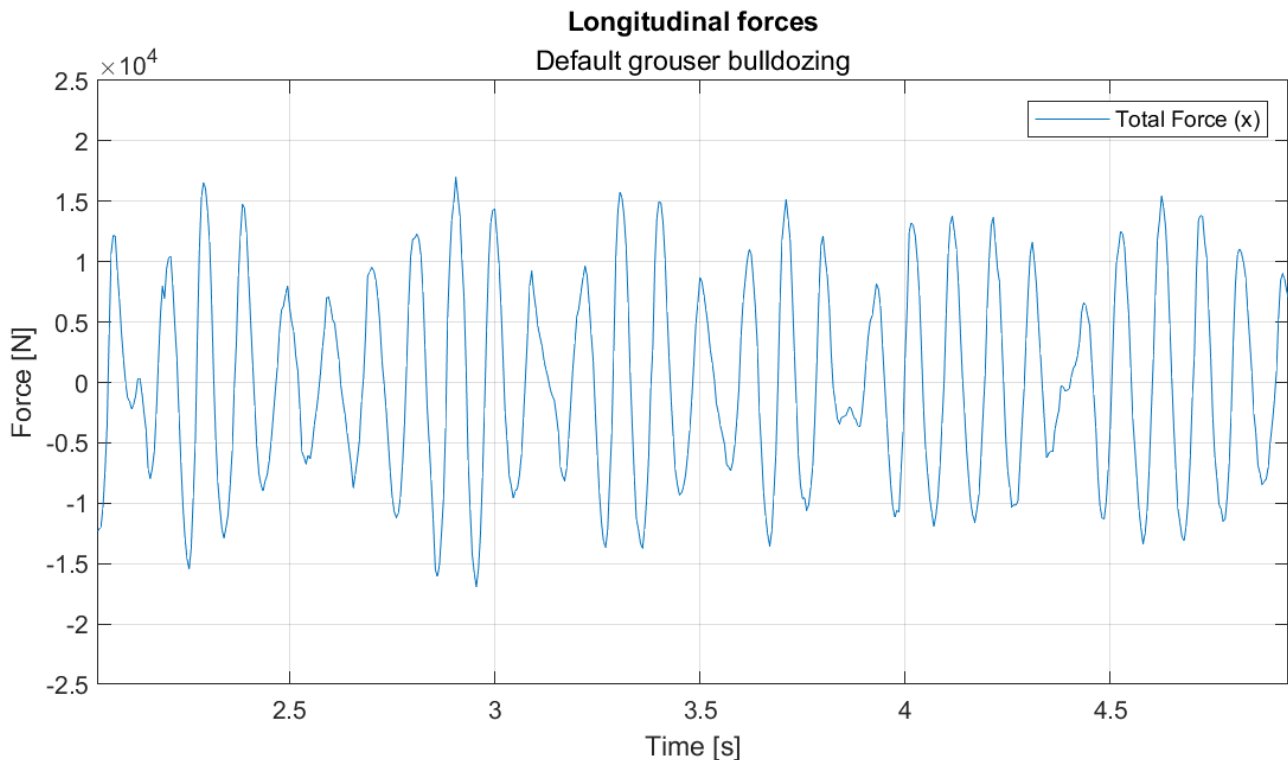


Figure 2.4.1 – Total force along the global X direction

The force is heavily oscillating and it's impossible to extrapolate results from such a trend. The problem lies in the fact that longitudinal forces are modelled without any damping, so the track experiences micro-oscillations, and when slip varies from negative to positive values, the forces change sign without damping, causing these big oscillations. Because of this, the results discussing the whole assembly will have to rely on stable parameters like torque and power outputs from the sprocket, or drawbar pull values, that better reflect the real performance of the vehicle.

2.5 ATV pressure-sinkage analysis over time

To show the behaviour described in the previous section with data support, a simulation was run with the following settings:

- Vehicle speed: 2 m/s or 7.2 km/h.
- Vehicle mass: 16006 kg.
- Track width: 480 mm.
- Track length: circa 3.22 m on average (clay), or 21.16 segments in contact with the ground.
- Flat and uniform terrain, clay soil.
- Simulation time: 6 s.

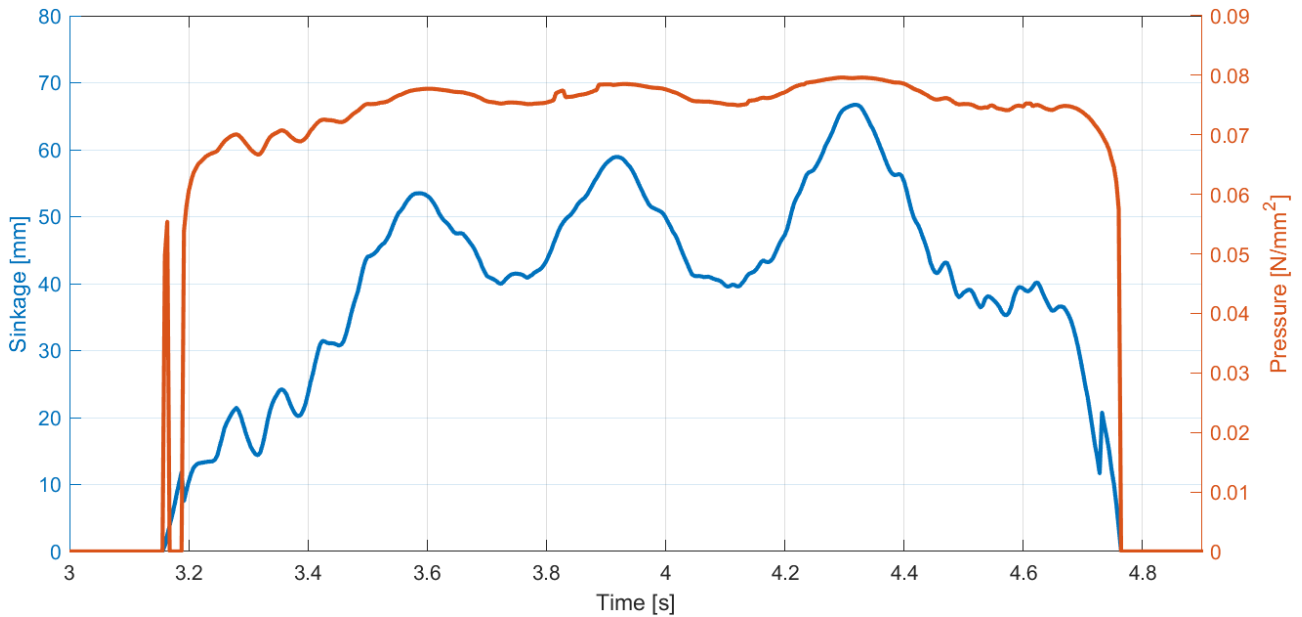


Figure 2.5.1 – Pressure (red) and sinkage (blue) in a clay simulation

There's a simulation error before 3.2 seconds, but it's irrelevant to our deductions: unlike the other soils, here the segment has much higher sinkage variations and much lower pressure ones, meaning the whole track acts to support the tank weight and not only the segments passing under the road wheels.

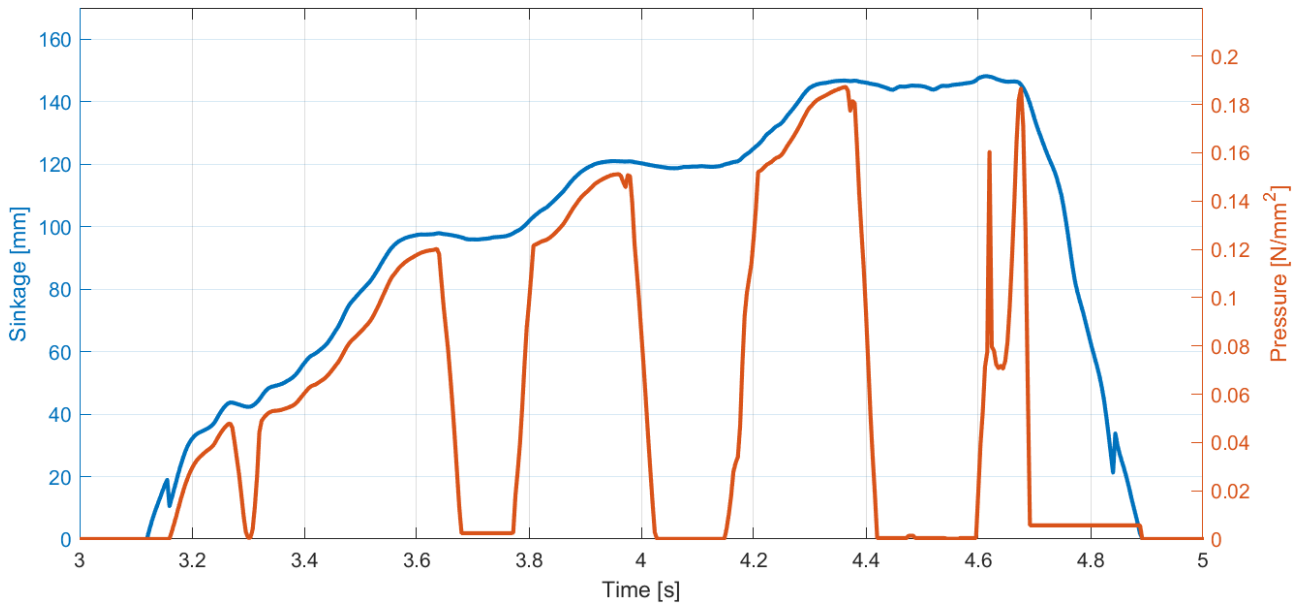


Figure 2.5.2 – Pressure (red) and sinkage (blue) in a sand simulation

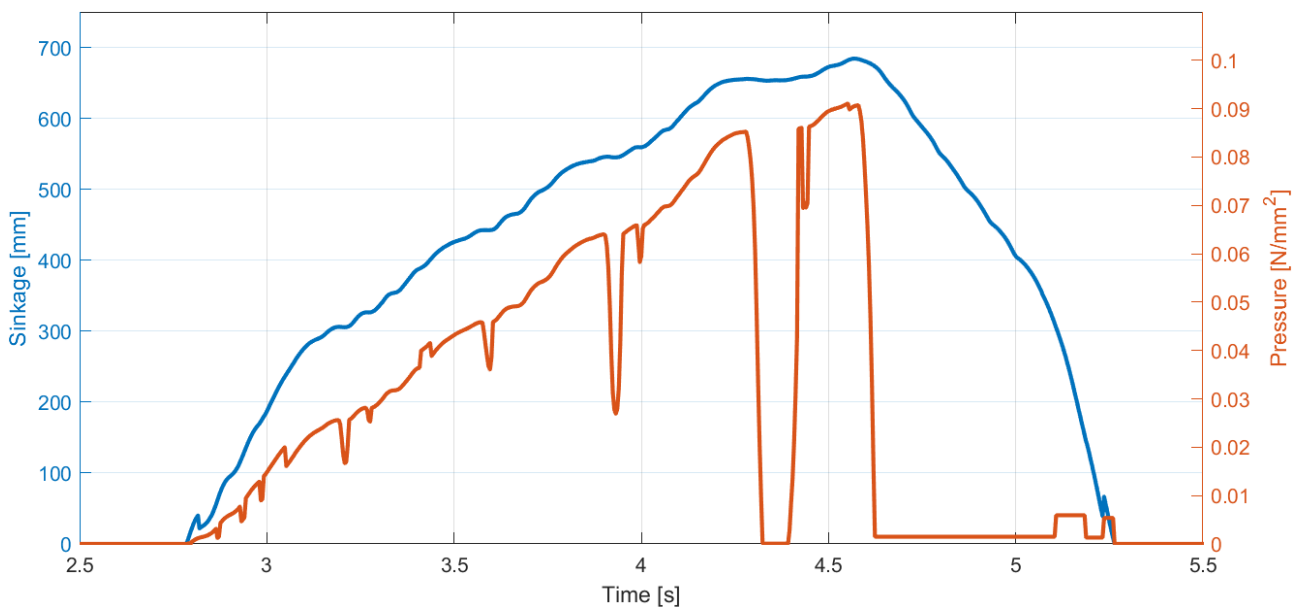


Figure 2.5.3 – Pressure (red) and sinkage (blue) in a snow simulation

As it can be seen, the pressure waves in a sand simulation represent quite clearly the segment passing under the wheels, with zero pressure in between, because the slightest difference in sinkage makes pressure fall until a new point is reached. This is also true for snow, but it's less noticeable because being snow really soft and sinkage values really high, the segment is constantly sinking up until 4.3 seconds, and hence pressure never really dips too much, even though for slight sinkage variations almost unnoticeable at this scale, the discrepancy in pressure is huge.

2.6 Drawbar pull testing

In a tracked vehicle analysis, one of the most important parameters is the drawbar pull; this is the tractive force that is applied to the vehicle in the direction of movement, so how much load it is able to sustain while maintaining a certain cruise speed.

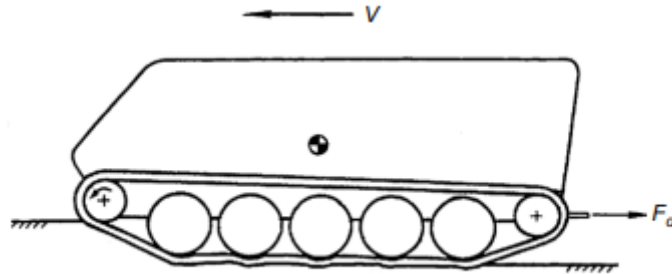


Figure 2.6.1 – Drawbar pull application [1]

Once the force is applied, it's interesting to calculate the power absorbed by the drawbar and the tractive efficiency, which is the ratio between drawbar power and sprocket power.

$$W_d = F_d \cdot V \quad (2.6.1)$$

$$\eta_{do} = \frac{W_d}{W_s} \quad (2.6.2)$$

Furthermore, to develop a thrust, the vehicle needs to generate slip. This value is calculated as such:

$$i = 1 - \frac{V}{V_t} = 1 - \frac{V}{r\omega} \quad (2.6.3)$$

Where:

- V is the forward speed of the vehicle.
- V_t Is the track speed, which is the product of the sprocket rotational speed ω and its radius r .

For the first analysis, the objective was to generate a drawbar pull-slip characteristic and a tractive efficiency-drawbar pull characteristic, to be able to see how our assembly performs.

The tool to measure this force and the other parameters involved in such an analysis was provided by the ATV technical support. This tool enables the user to apply a force to the rear of the assembly, pulling it backwards and calculating the power developed by such force.

This tool is modelled through linear viscous damping; This means that it applies a force to our vehicle that is directly proportional to the speed it is cruising at. This limitation prevents us from applying a constant force that is very large, as that would prevent the vehicle to move at a sustainable speed and hence would result in a smaller force.

2.6.1 Drawbar characteristics

As said, the aim of the analyses is to construct with simulation data the drawbar pull, slip and tractive efficiency characteristics. Two sets of analyses were run, each using a different track segment, one with the default grouser and one without a grouser at all, to also see the influence the grouser has in the force generation and in the tractive prowess of the vehicle.

To do so, the analyses had to be consistent, and a few parameters were chosen in advance:

- The vehicle is moving in a straight line, on the terrain `dry_sand_LLL`, at 4 m/s.
- The first set uses the default grouser geometry, described in table 2.1.2 and shown in figure 2.1.3, and is ran using the bulldozing calculation.
- The second set uses a solid segment with no grouser, and, since no bulldozing forces are in play, is ran using the shearing calculation.

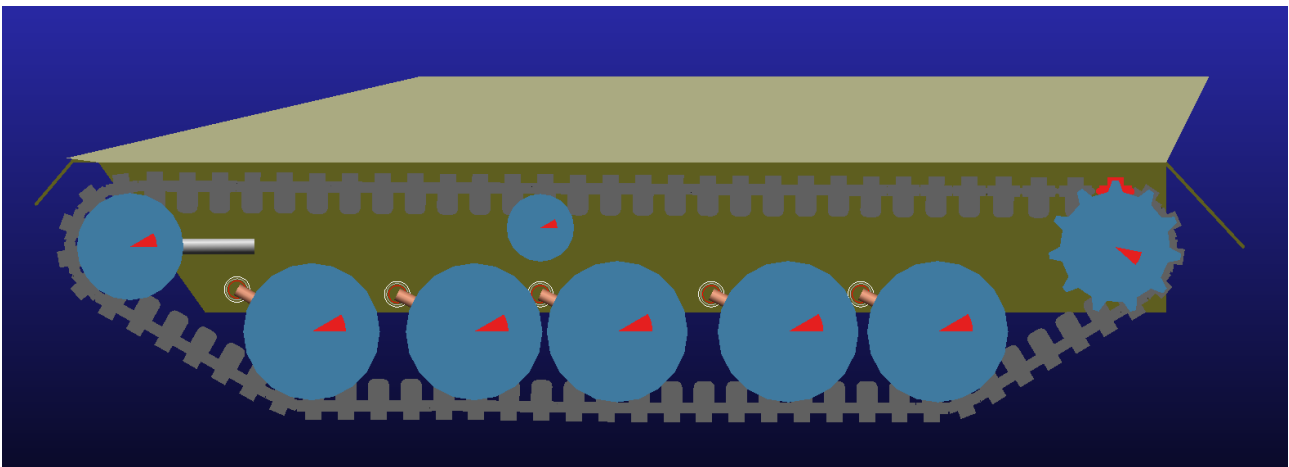


Figure 2.6.2 – Tank with default track segments

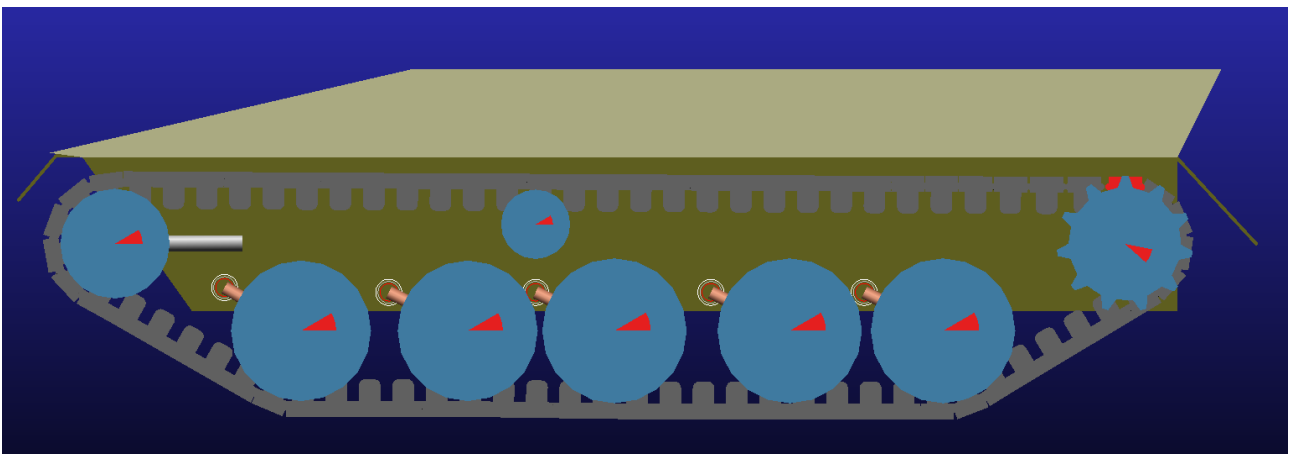


Figure 2.6.3 – Tank with no grousers

Each set of analyses was then run with different drawbar parameters, and hence force applied, until the assembly was not able to maintain the imposed speed of 4 m/s. The drawbar parameters were then extracted from simulation data and the characteristics were drawn.

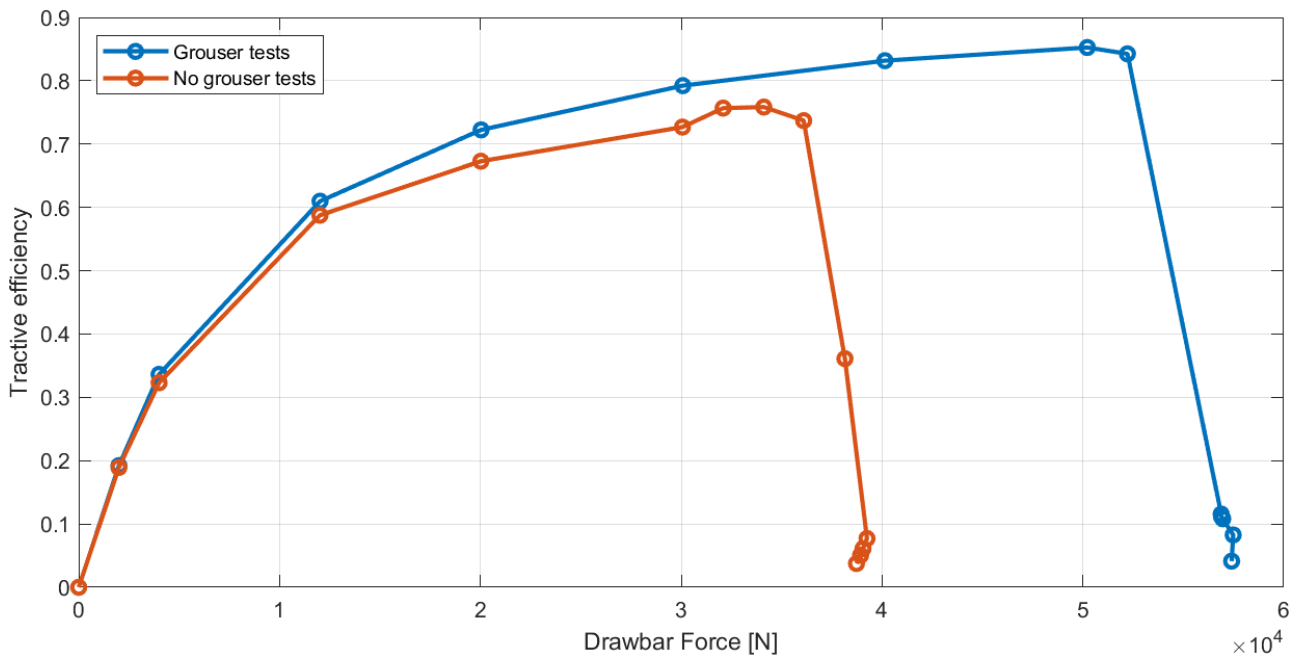


Figure 2.6.4 – Efficiency-force characteristics

The tractive efficiency is higher for higher drawbar pull forces, until it reaches values that are too high and cause too much slip, resulting in higher power drawn from the sprocket wheel and hence lower efficiency. It's easy to also see how the grouser vehicle is capable of sustaining higher pull, and even at the same pull forces is more efficient.

Efficiency	Grouser	No grouser	Variation
F=12000 N	60.97%	58.75%	3.78%
F=20000 N	72.24%	67.29%	7.36%
F=30000 N	79.23%	72.68%	9.01%

Table 2.6.1 – Efficiency variation

For these 3 forces as an example, the % variation in efficiency is small, but gets higher with higher forces.

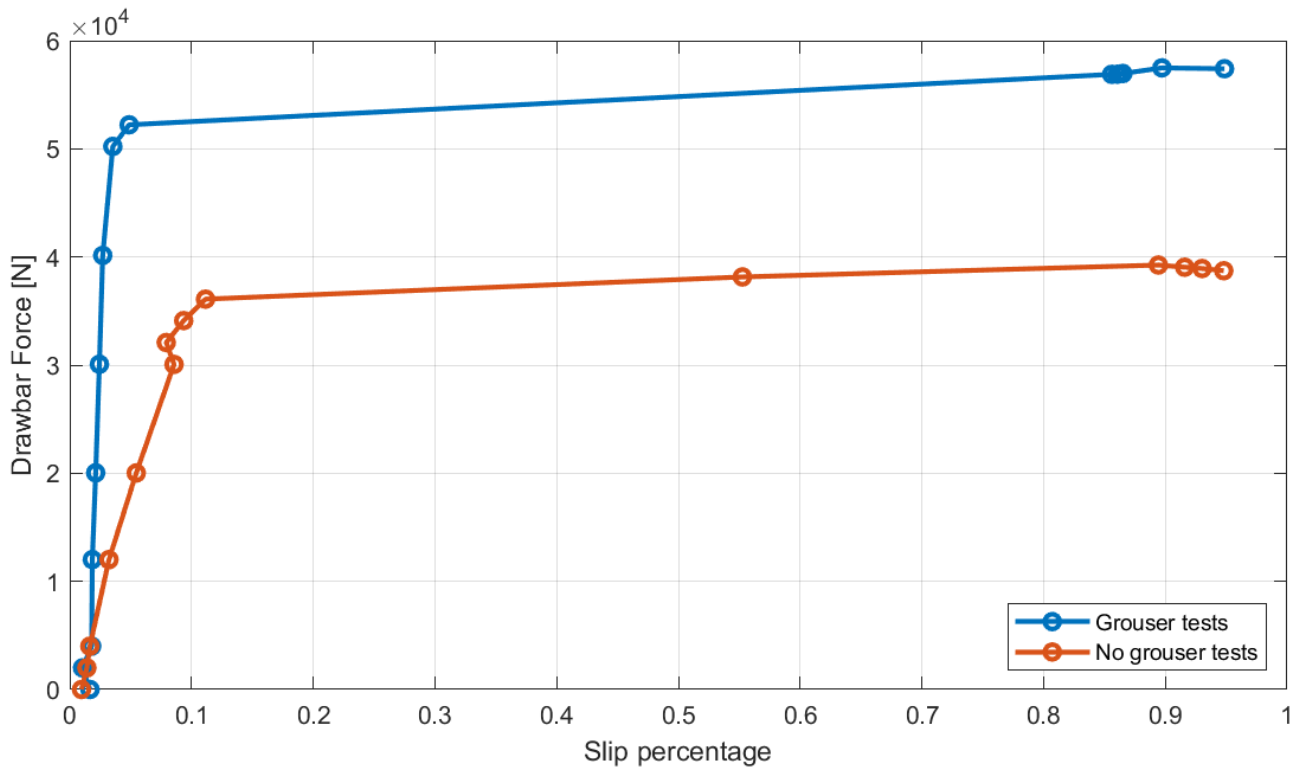


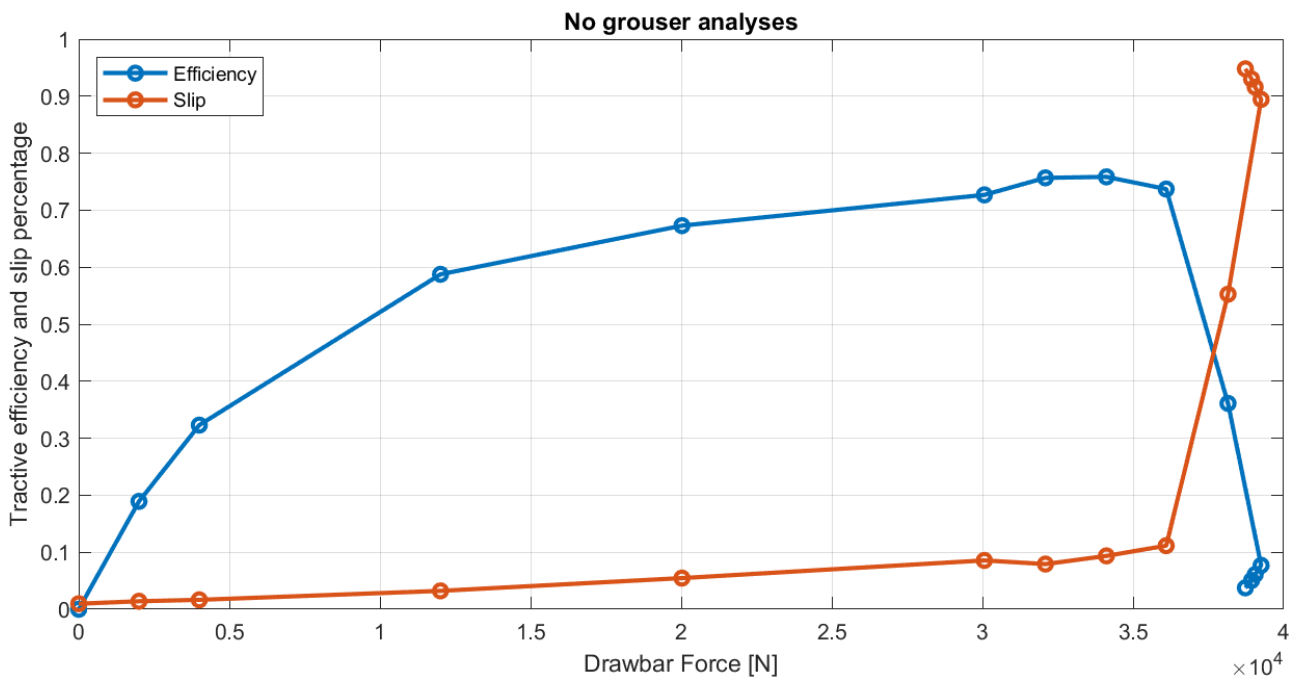
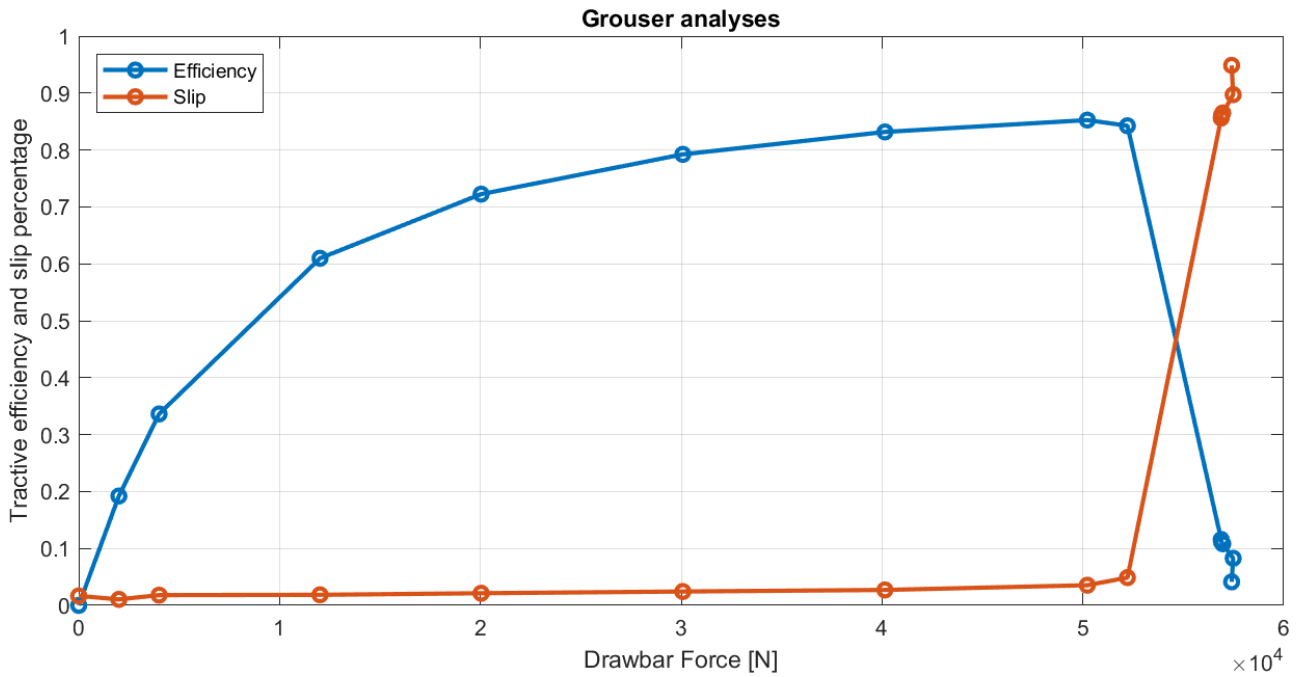
Figure 2.6.5 – Force-Slip characteristics

The slip characteristic shows much of the same things said before. Higher slips happen at lower forces for the no grouser vehicle, also showing the slip itself is much higher at lower forces.

Slip	Grouser	No grouser	Variation
F=12000 N	1.85%	3.22%	-42.55%
F=20000 N	2.13%	5.47%	-61.06%
F=30000 N	2.44%	8.57%	-71.53%

Table 2.6.2 – Slip variation

The percentage variation is much higher in this case, as the slip is 70% lower in the grouser case than in the no grouser case.



Figures 2.6.6-7 – Slip and efficiency over drawbar pull

These last plots highlight how efficiency and slip are related, as, for high forces, higher slip percentages result in lower efficiencies, and the force required to get the track to reach almost full slip for both cases. In the literature, these plots are computed for a wheeled tractor moving on clay, but in any case the trends are very similar, with the literature plots showing higher slip, due to the nature of wheels when opposed to a tracked vehicle.

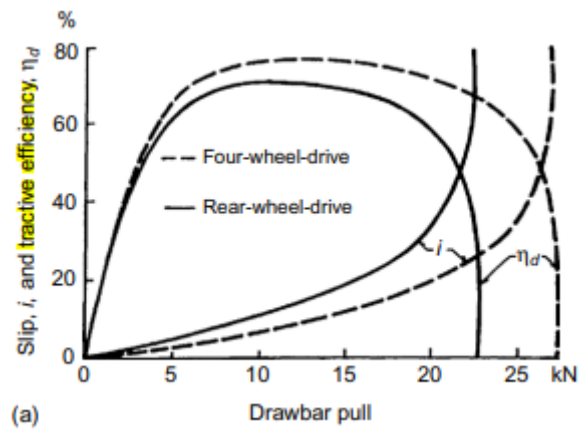


Figure 2.6.8 – Efficiency and slip over drawbar pull for a wheeled tractor [1]

2.6.2 Grouser height tuning

The following study was conducted to check the influence of grouser dimensions in the drawbar pull tests. To do this, a few changes were made to the default segment geometry.

The aim was to run analyses at different grouser heights, from 20 mm to 70 mm. Since the analyses were run on sand, equation 1.2.10 was used in order to evaluate the minimum spacing between two consecutive grousers that are 70 mm high.

Grouser height [mm]	Spacing [mm]	Length [mm]
70	116.50	35.90

Table 2.6.3 – Grouser length calculation

These are the analysis parameters for this study:

- Vehicle speed: 3 m/s on sand.
- Grouser length: 35.86 mm (this was chosen to have a small percentage headroom for the bulldozing activation).
- Drawbar pull force: 24 kN.

The calculations regarded the tractive efficiency trend and the slip trend. Here are the results:

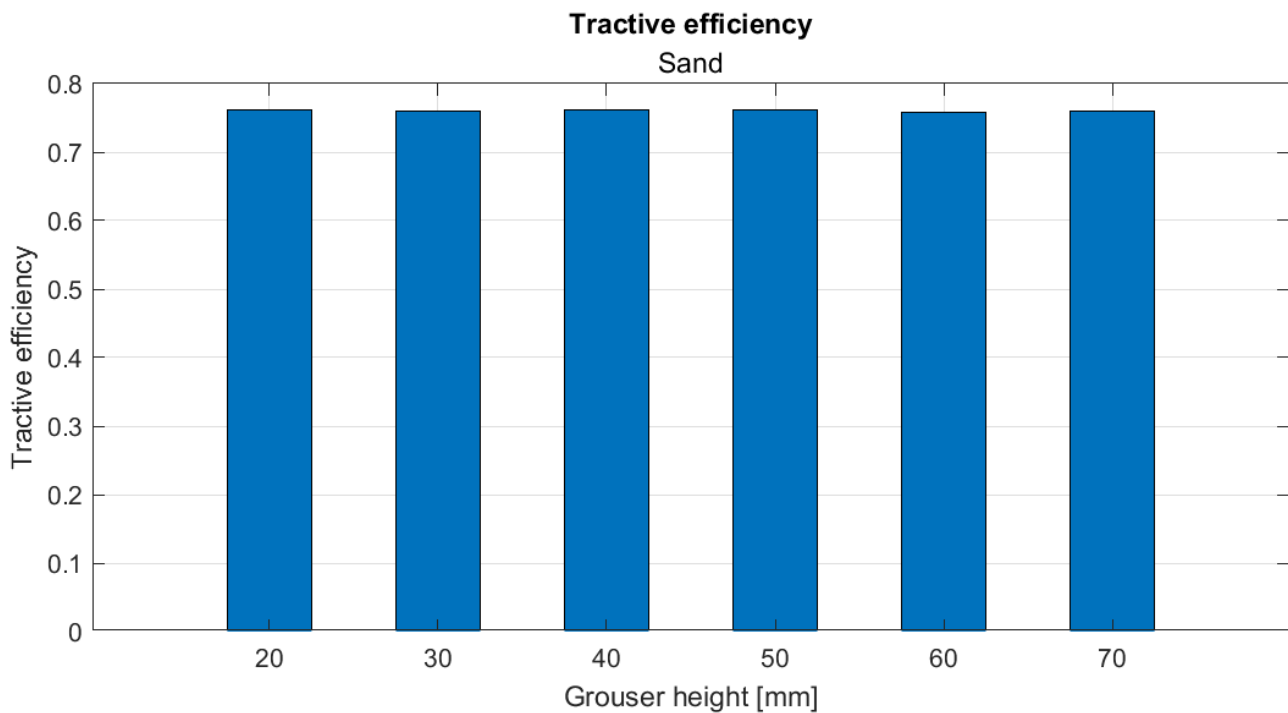


Figure 2.6.9 – Tractive efficiency with different grouser height

As shown, the tractive efficiency stays at 76% in all tests, meaning that at this force and forward speed the grouser height has no significant effect.

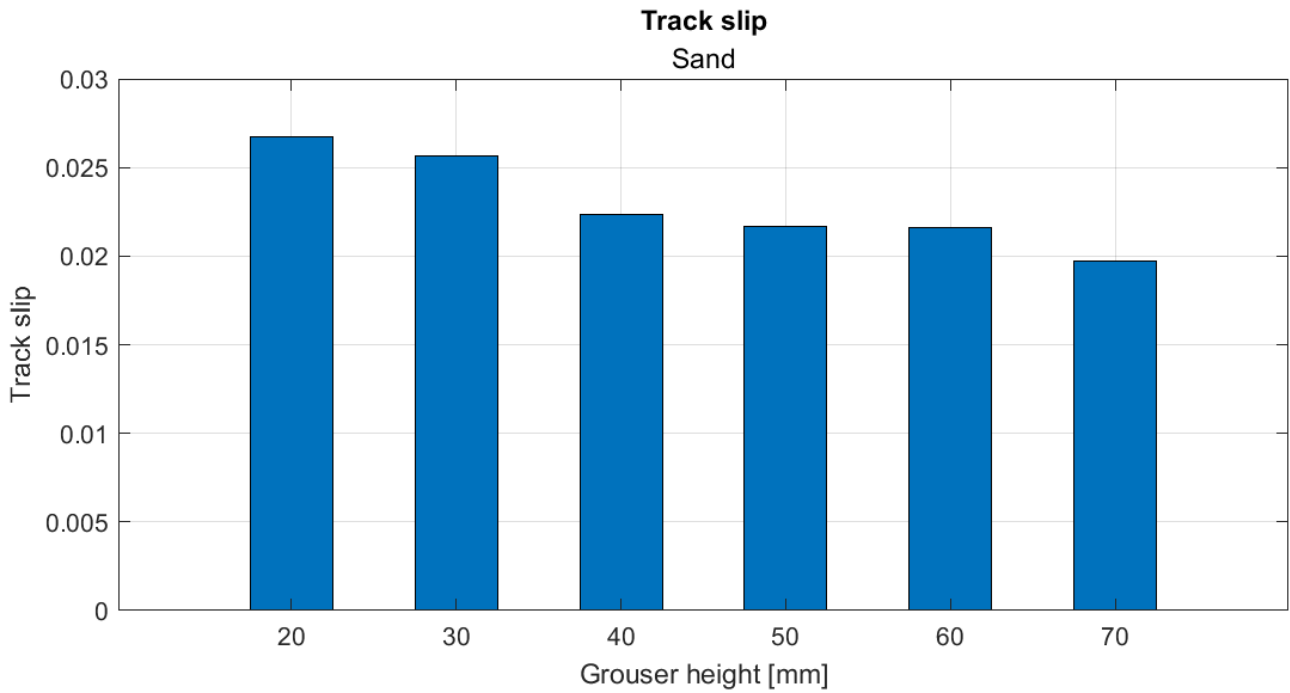


Figure 2.6.10 – Track slip with different grouser height

Here instead the trend is closer to what is expected, with higher grousers generating more tractive forces and hence less slip. The imposed pull is still the same, so the vehicle is able to generate the same tractive force with less slip. It should be noted that it's expected to register a change in efficiency if pairing with slip variation. This is not the case because checking data, even if the rotational speed of the sprocket wheel is higher for higher slip, the torque exerted is higher for higher grousers, due to the bigger resistance and forces generated by segments with taller grousers.

2.7 Tensioner tuning

The ATV software gives us a tool using which we can regulate the tensioner behaviour, being able to modify its average force or average length during the analysis. The tensioner's purpose is to add tension to the track, keeping it from being too loose around the ground wheels. The element has a default design length and therefore force that was used for all analyses discussed up until now.

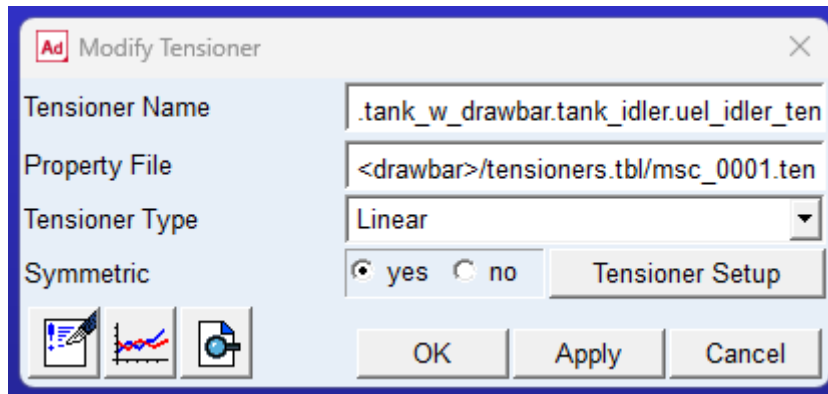


Figure 2.7.1 – Tensioner type and symmetry selection

In this window we're able to select the type of tensioner, between rigid, linear or non linear, and through the property file we can check the curve properties of its behaviour.

Tensioner data	Spring properties	
Damping	30	Ns/mm
Preload	95000	N
Initial length	500	mm
Minimum length	400	mm
Maximum length	600	mm
Stop stiffness	1000	N/mm
Stop exponent	2	/
Stop damping	1	/
Linear Stiffness	10000	N/mm

Table 2.7.1 – Tensioner data

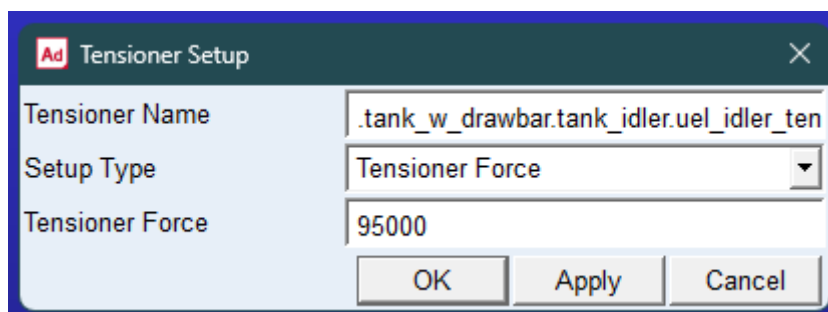


Figure 2.7.2 – Tensioner setup

The tensioner is preloaded with a force of 95000 N, so modifying the tensioner force means that we compress or extend the spring from the default 500 mm according to the linear stiffness, assuming we select the linear tensioner.

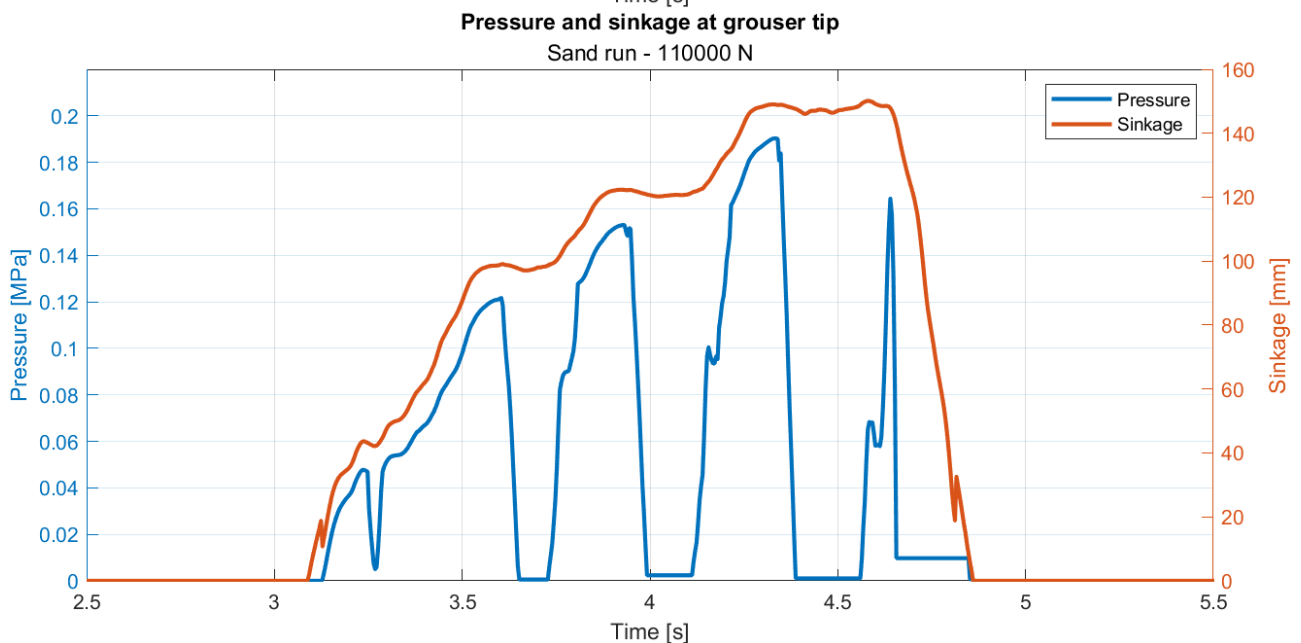
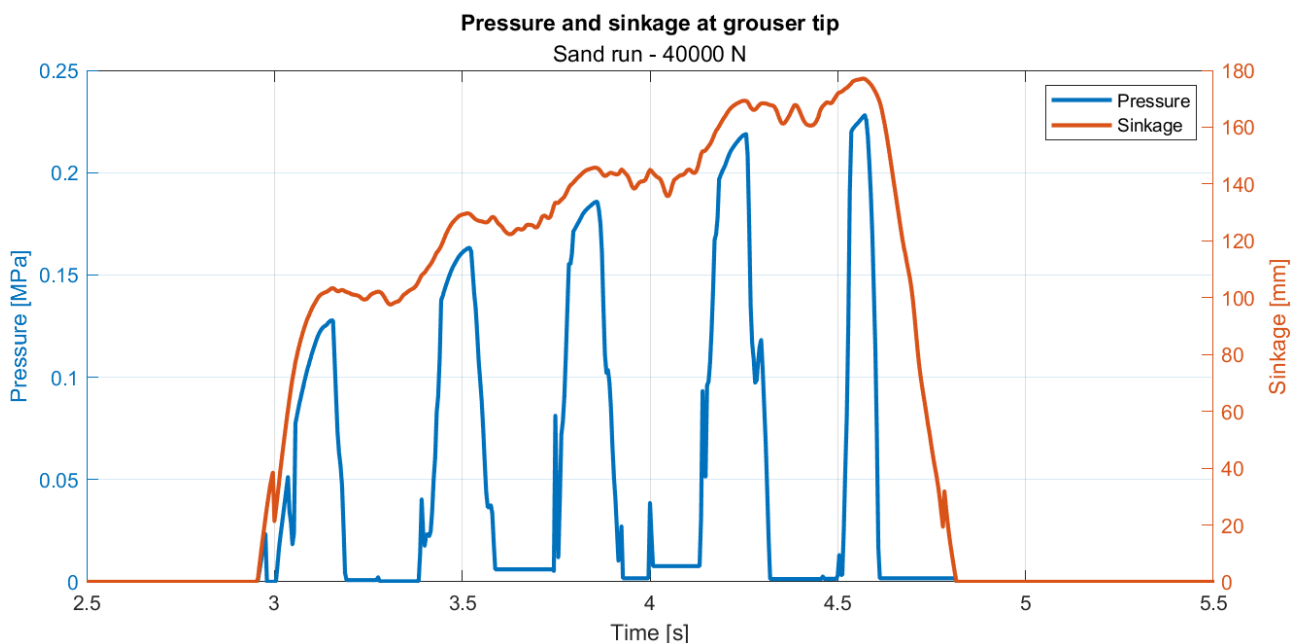
It's important to note that the spring length is not the tensioner length, and a compression of the spring will result in a higher tensioner force and a more extended tensioner.

Having laid out the basis of how the setup works, 3 analyses per soil were performed, having these characteristics:

- Vehicle speed: 2 m/s or 7.2 km/h.
- Simulation time: 6 s.
- 3 different tensioner forces: 40000 N, 110000 N, 500000 N.

A higher tensioner force should result in a more even pressure distribution below the track, so that is what these analyses are going to be focusing on.

Firstly following a single track segment in its passing below the track, on sand:



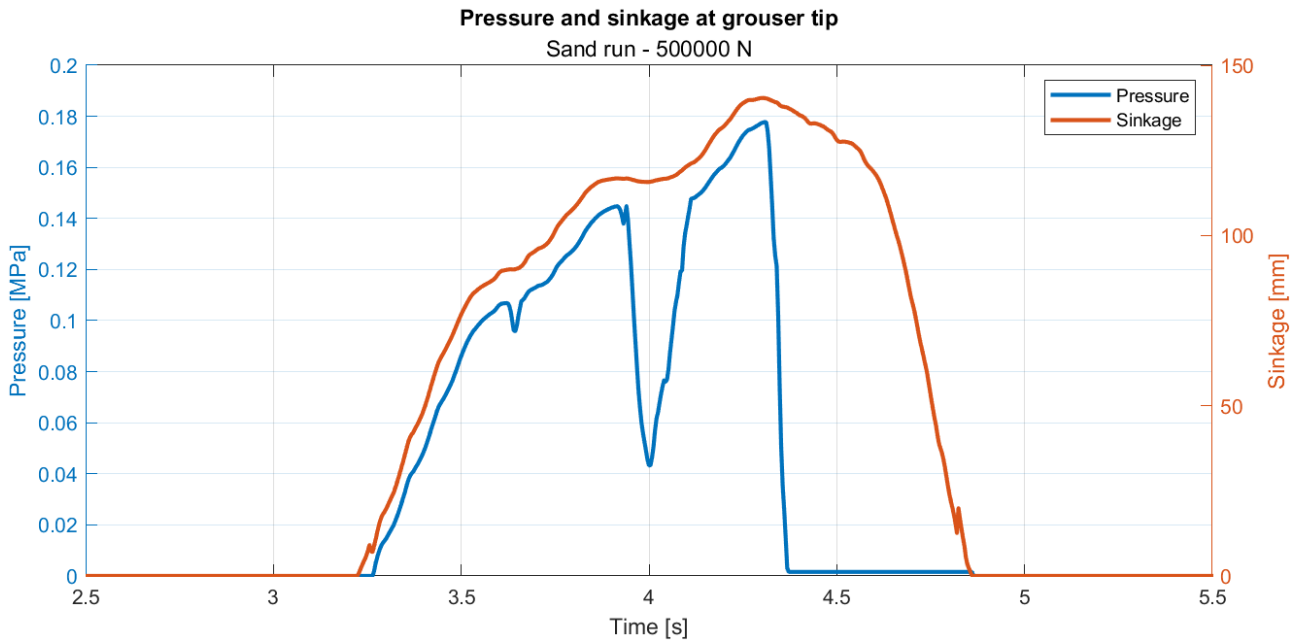
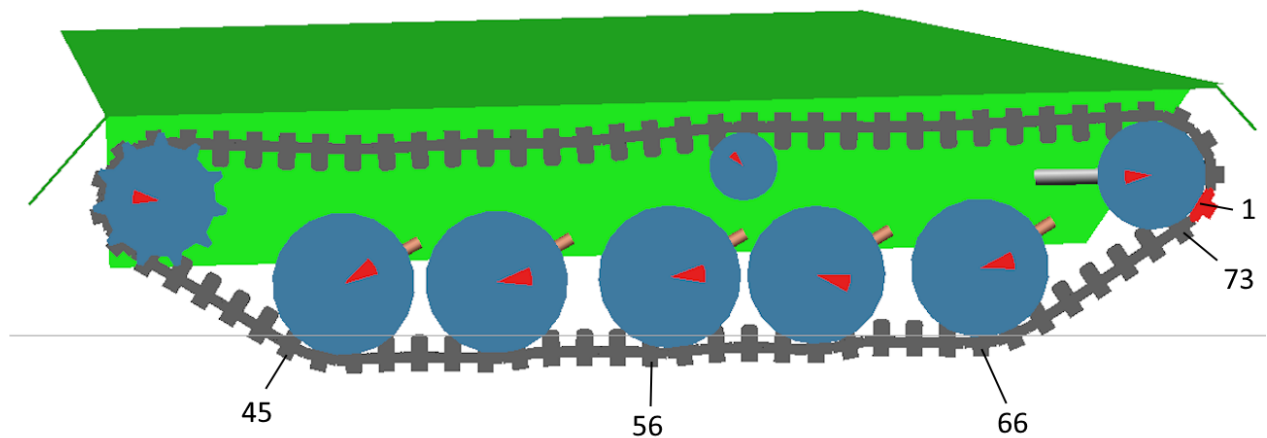


Figure 2.7.3-5 – Pressure and sinkage of a grouser with 3 different tensioner forces

The first plot, with a loose tensioner, clearly highlights the passing of the segment under each road wheel, charging and discharging after each one. As force increases, the track is wrapped tighter around the wheels, and the pressure swings get less significant. Even then, at 110000 N, which is really close to the default force exerted by the tensioner, as seen from figures 2.4.23-25, the passing under the 5 road wheels is pretty clear. This changes with the last test: 500000 N is in fact enough to almost eliminate pressure swings, and to make the passing under the 5th and last wheel ineffective on segment pressure.

There is also a way to plot the variables at an instant in time for every track segment; In this way, with also the aid of a screenshot of the analysis animation, we can see what segments pass under wheels and how the configuration affects pressure on the segments.



Pressure and sinkage for every grouser $t=2.5s$

Sand run - 40000 N

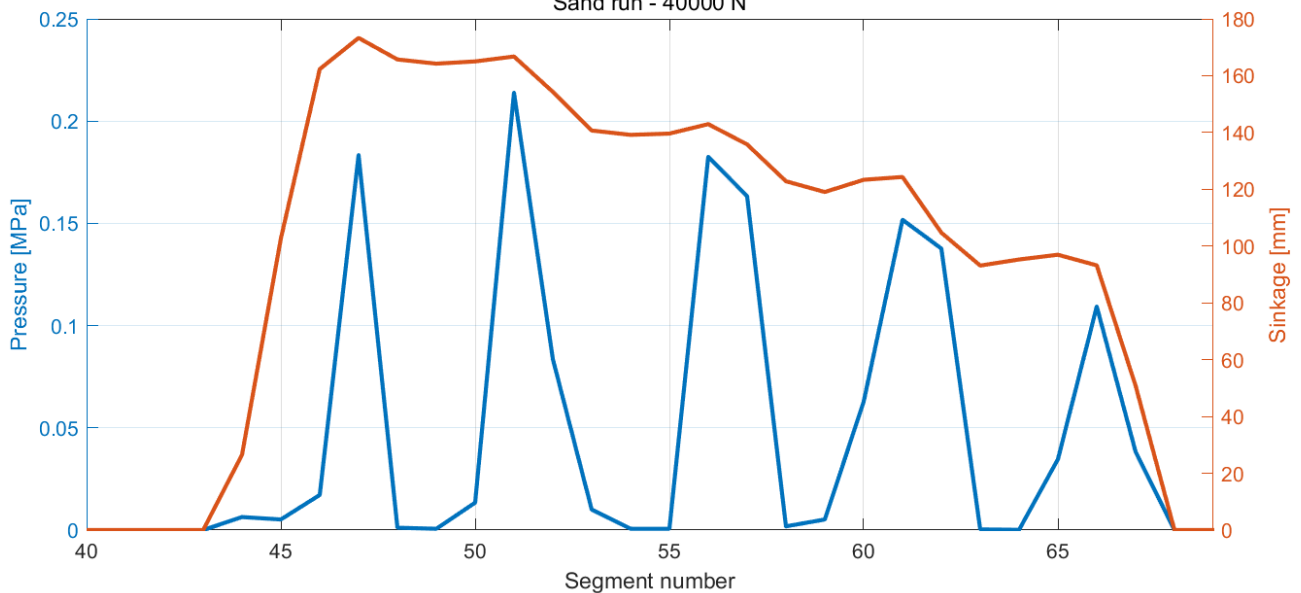


Figure 2.7.6 – Pressure and sinkage of each segment on sand, 40000 N tensioner

The segment in red is segment number 1, and from there 2, 3 etc in the counter clockwise direction. Segment 73 is the last segment of the track, and is therefore the first counting clockwise. Knowing this we can identify each segment in the track.

We can see how this plot is very similar to figure 2.5.3, which is expected since the vehicle moves at constant speed, so the situation is close to being stationary. Pressure peaks under the 4th road wheel at just over 2 bar. In the screenshot instead we can see how the upper track is loose around the support wheel and the tensioner, and how the lower track stays at roughly the same height of the last wheel it passed under.

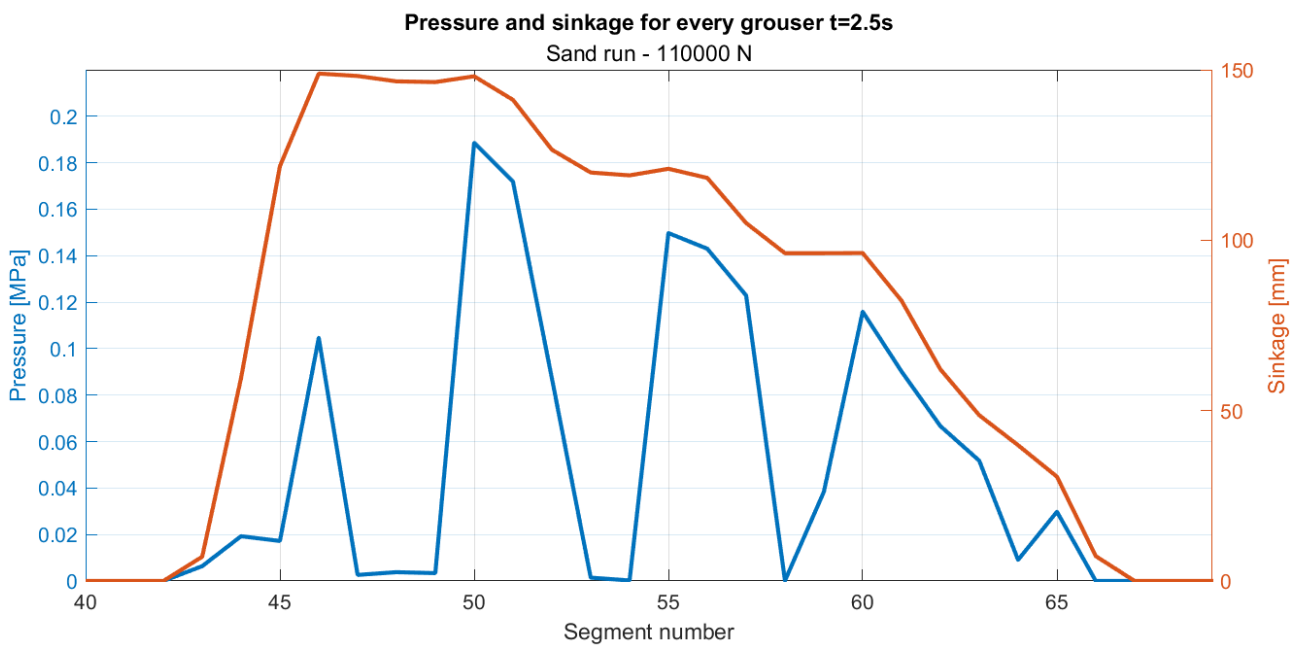
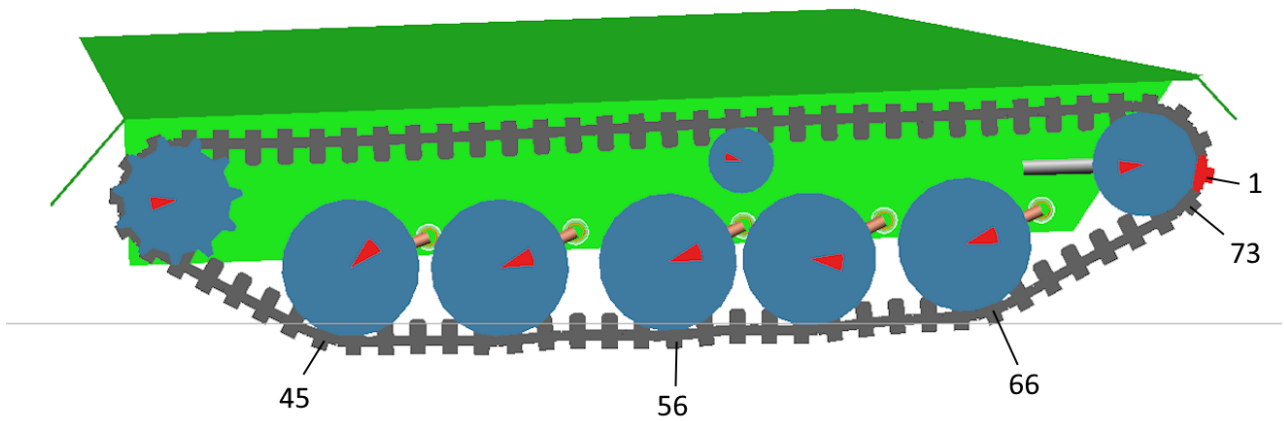


Figure 2.7.7 – Pressure and sinkage of each segment on sand, 110000 N tensioner

Not many differences can be seen here, except for the first 2 wheels, so the last few segments in contact. This setup is close to what the default setting is, and it can be seen how the pressure peaks are lower and more distributed, as pressure peaks again under the 4th road wheel but it's under 2 bar and the segments under the first two wheels have a more distributed pressure trend; this means the tensioner is working and gives us a better load distribution. Another thing to note is the angle of the suspension bars: the first and last road wheels seem to have a more rotated suspension compared to the others, and in general the angles here are tighter.

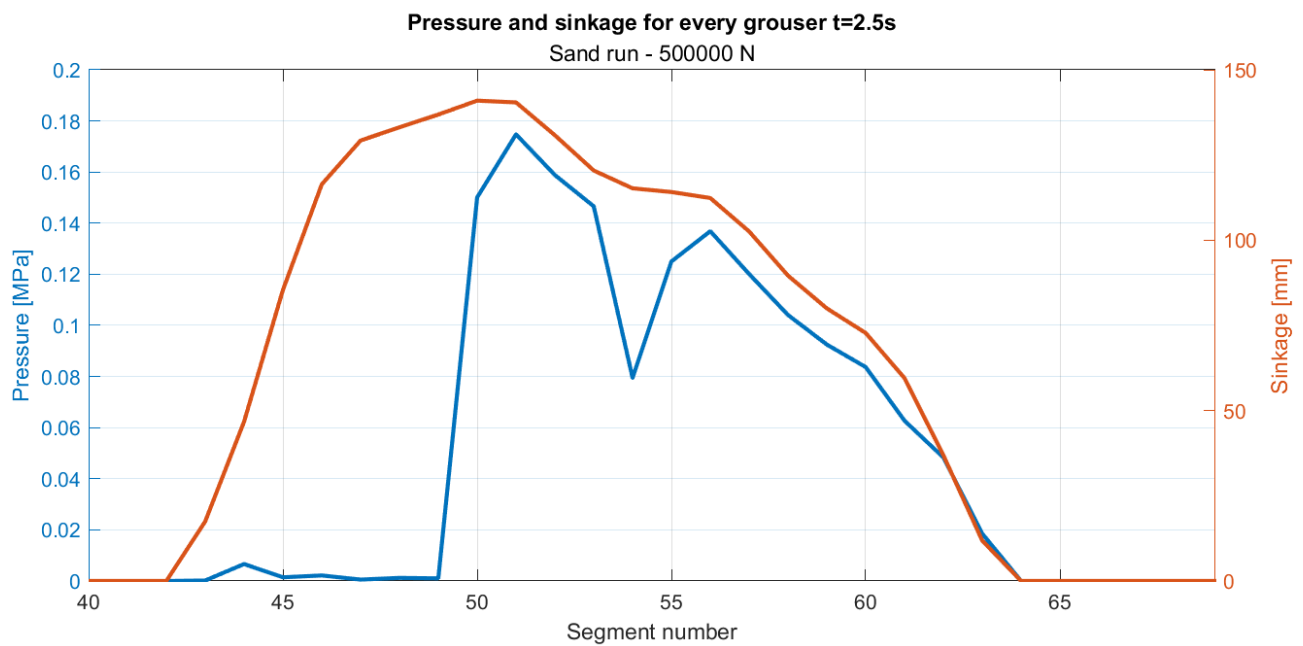
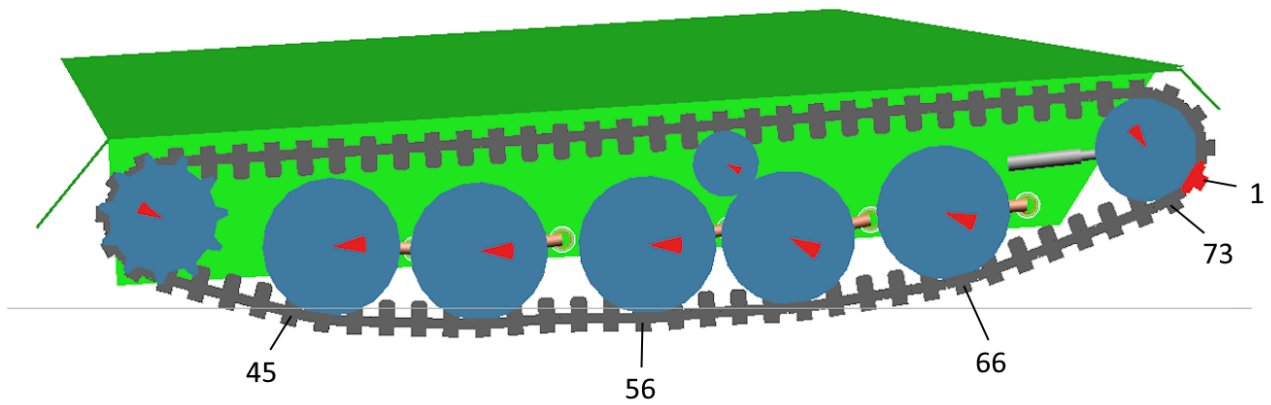


Figure 2.7.8 – Pressure and sinkage of each segment on sand, 500000 N tensioner

In this extreme case the differences are quite noticeable: first of all, less segments are actually in contact with the ground, and the suspension bars are almost parallel to the hull. In general, the whole track is much tighter and the tensioner is extended further than in the last 2 runs. The pressure here peaks once again under the 4th road wheel but at under 1.8 bar, further distributing the pressure. It's also notable though, that the 5th wheel feels no pressure and therefore doesn't generate any significant forces. The suspensions being so stressed is due to the fact that they need to balance both the vehicle weight and the extra track tension, instead of just the vehicle weight.

Looking at clay results:

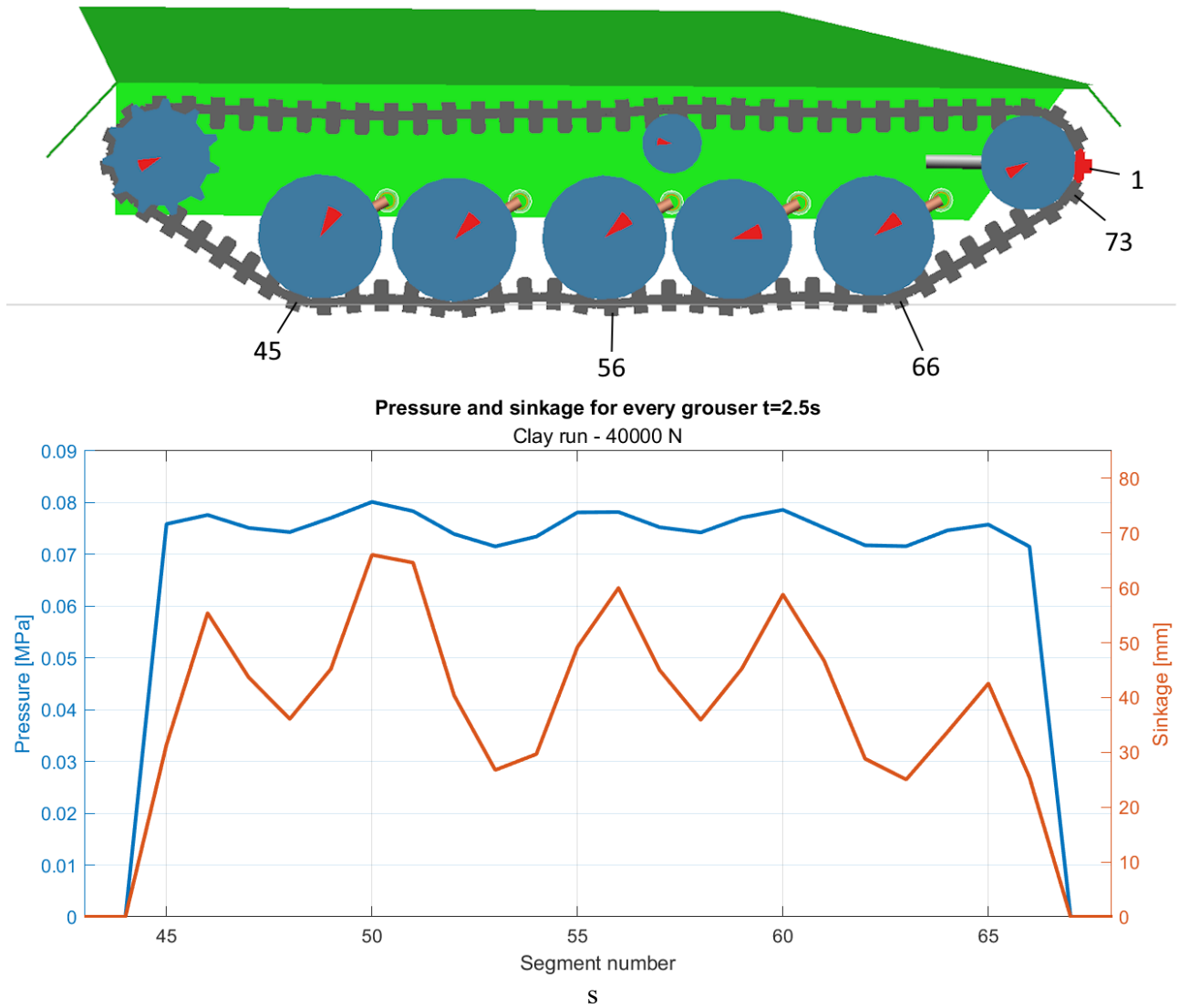


Figure 2.7.9 – Segment pressure and sinkage of each segment on clay, 40000 N tensioner

In the clay test the elastic return of the terrain is very clear under the road wheels, since the segments start to wrap around them with the vertical force coming from the soil. The pressure waves are more prominent than in any other clay simulation, while still being quite stable due to the terrain properties. The peak is just under .8 bar.

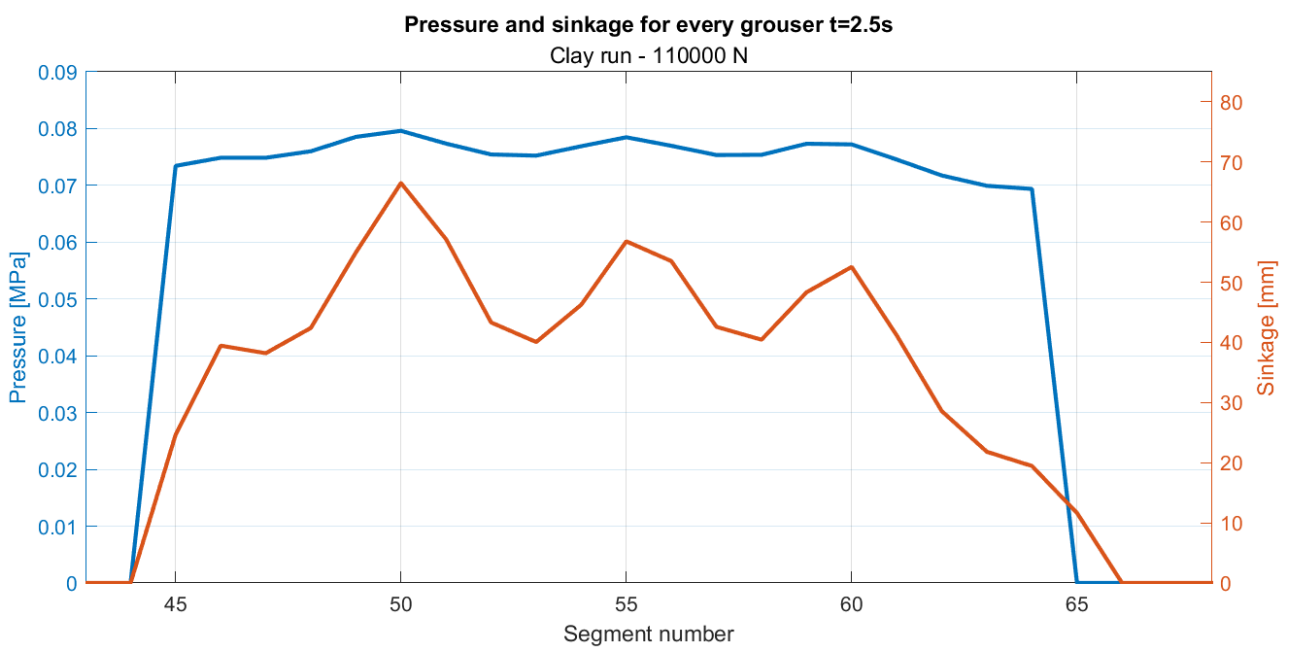
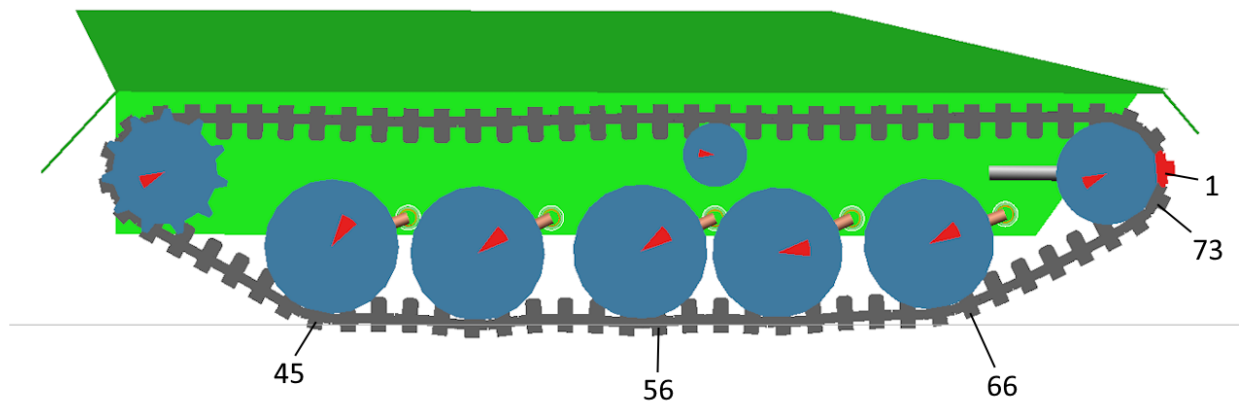


Figure 2.7.10 – Segment pressure and sinkage of each segment on clay, 110000 N tensioner

Again little differences; the segments oscillate less in between roadwheels but the behaviour is really close. The first and last wheels are more compressed, like in the sand case, and their suspension bar is more horizontal. In this case, the tensioner has close to no effect on the pressure peaks, as the value is still roughly the same.

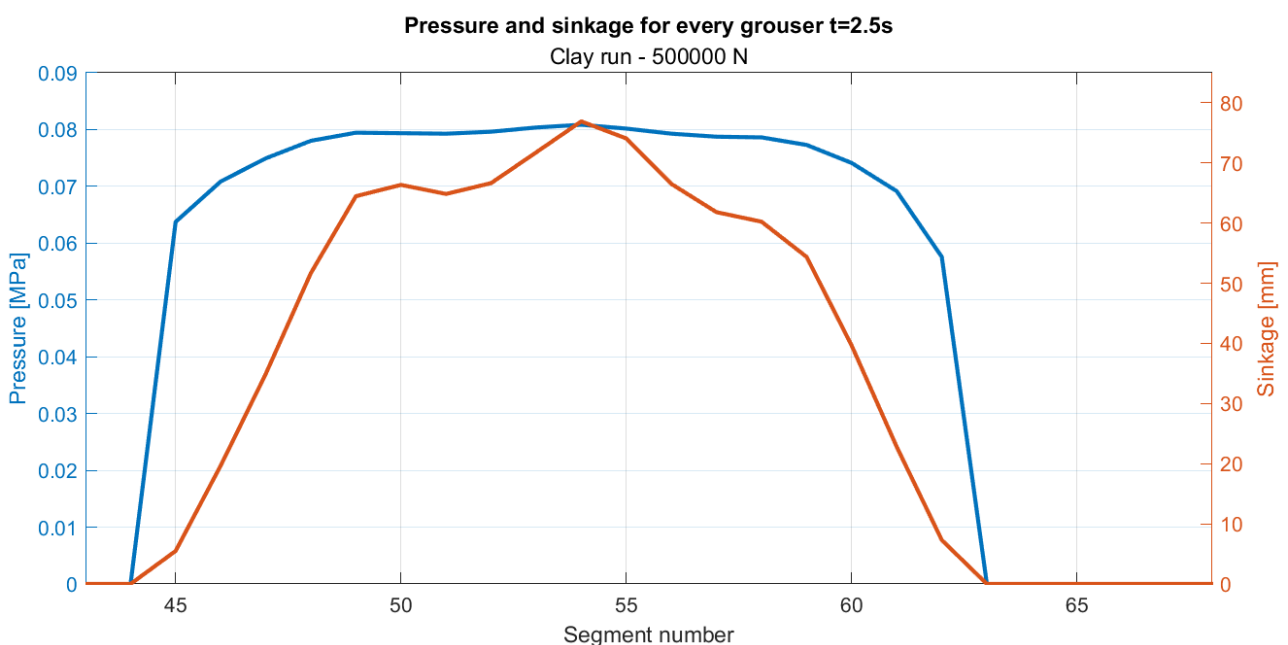
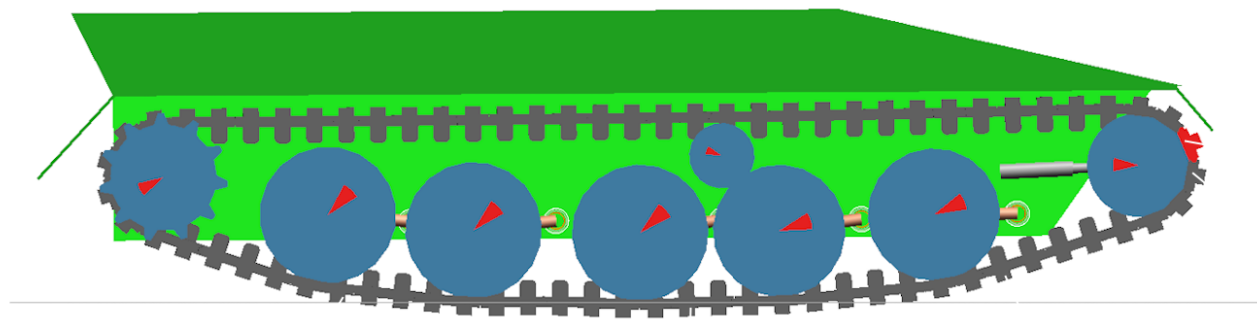


Figure 2.7.10 – Segment pressure and sinkage of each segment on clay, 500000 N tensioner

Again, the suspension bars are almost horizontal, and there is really small oscillation of sinkage, and even less of pressure. The latter is in fact almost equally distributed under the whole track, but it should be noted that less of the track actually does come in contact with the soil. This also means that on clay, the tensioner has the opposite effect, and here pressure is surely more distributed under the part of the track that is in contact with the ground, but since less of it does, the pressure peak here is slightly higher than in the looser tensioner cases, at just over .8 bar.

Now for snow:

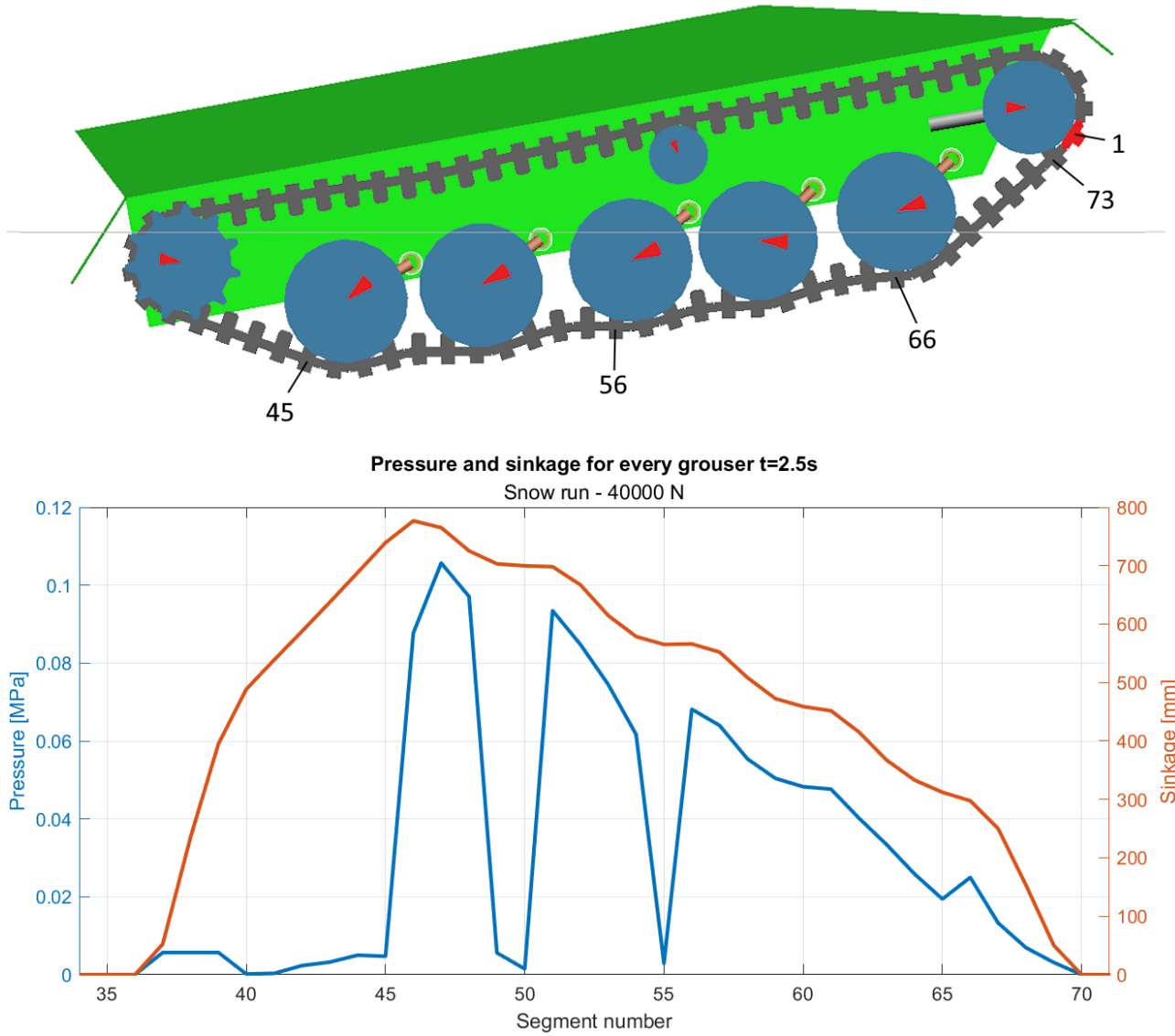


Figure 2.7.11 – Segment pressure and sinkage of each segment on snow, 40000 N tensioner

Sinkage is much higher, and pressure peaks appear more for the latter part of the track than at the beginning, but much of what has been said for the other soils remains true. Pressure peak is under the last road wheel due to the much higher pitch present in the snow simulations, and it's a bit over 1 bar.

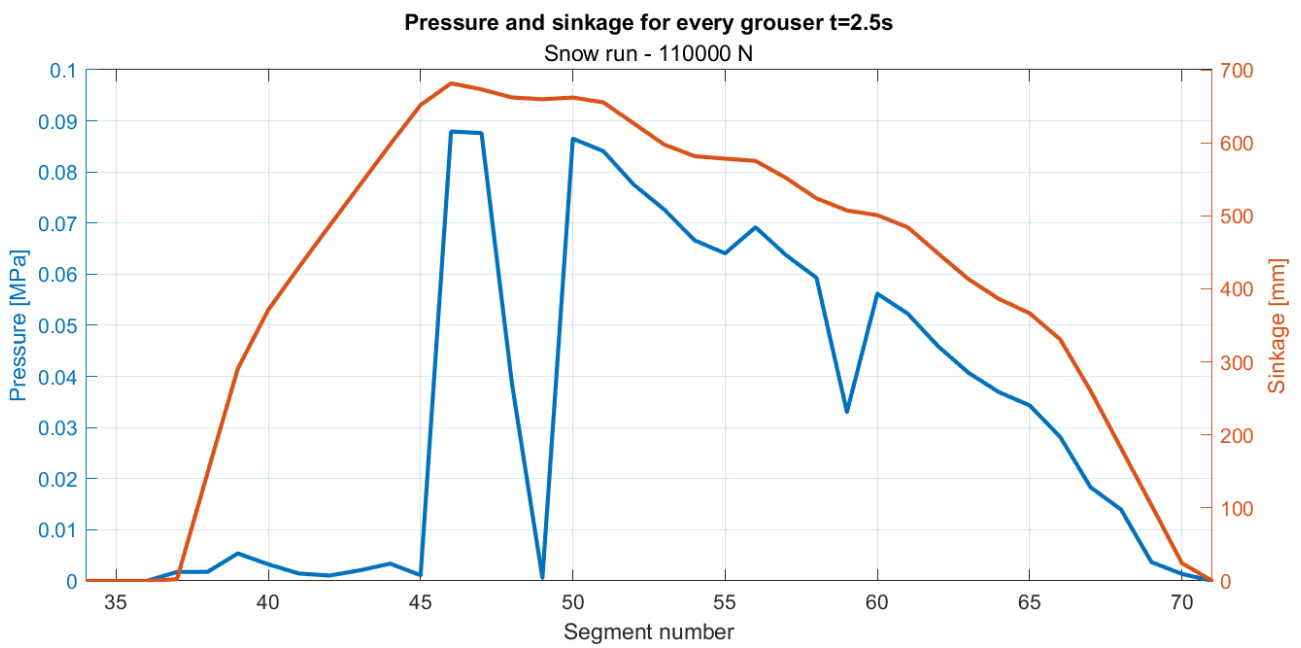
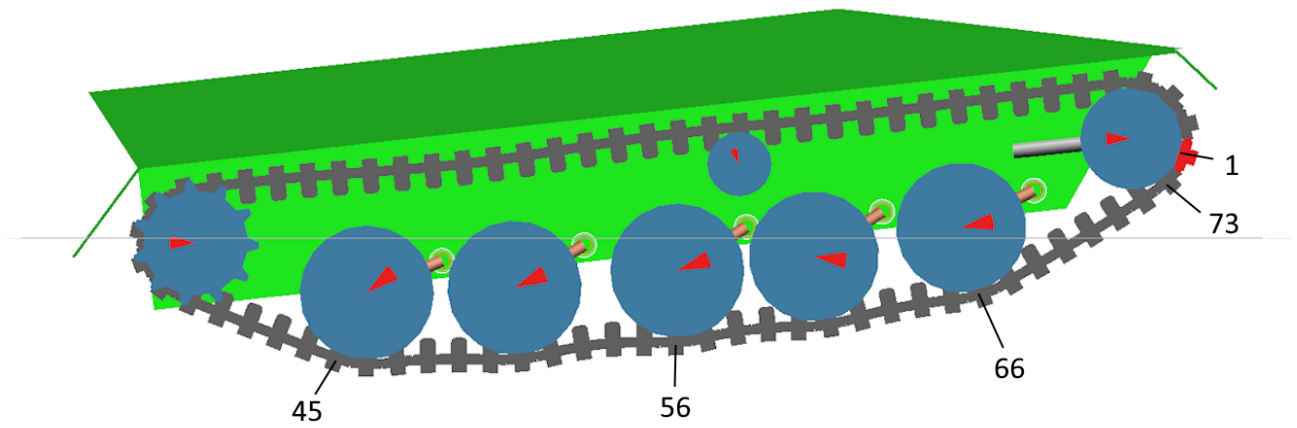


Figure 2.7.12 – Segment pressure and sinkage of each segment on snow, 110000 N tensioner

This eliminates the pressure jump from road wheel 3 (segment 56) to road wheel 4 (segment 50), and makes sinkage more linear. Pressure peak decreases to under .9 bar.

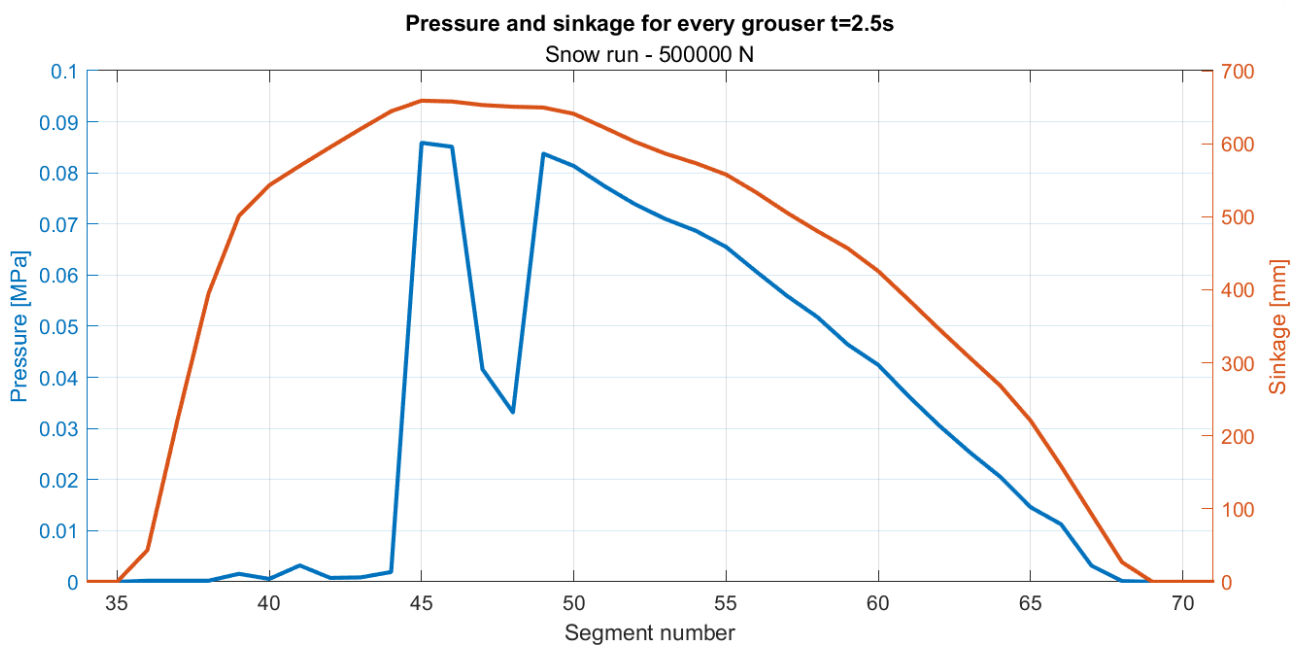
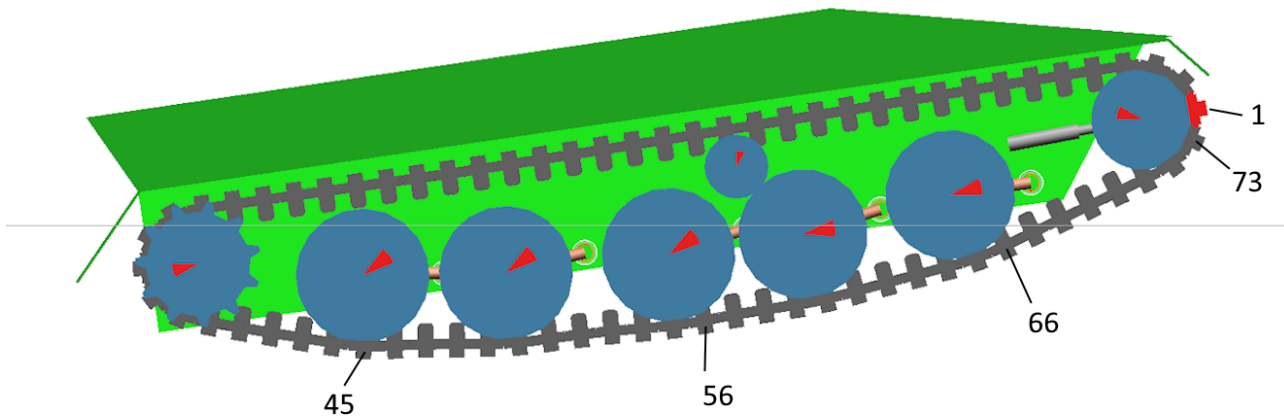


Figure 2.7.13 – Segment pressure and sinkage of each segment on snow, 500000 N tensioner

In this configuration the pressure scales linearly until the 4th road wheel, then there's a dip, and a new peak under the 5th road wheel, which besides a few oscillations is very close to the 110000 N case. Also the pressure peak is slightly lower, at .85 bar.

We can then say that the tensioner is essential to the load distribution for sand and snow, while the tests give close to no variation and even negative effects on clay.

More interesting variables that can be inspected are segment displacement and pressure when linked to the shearing and bulldozing forces generated by it.

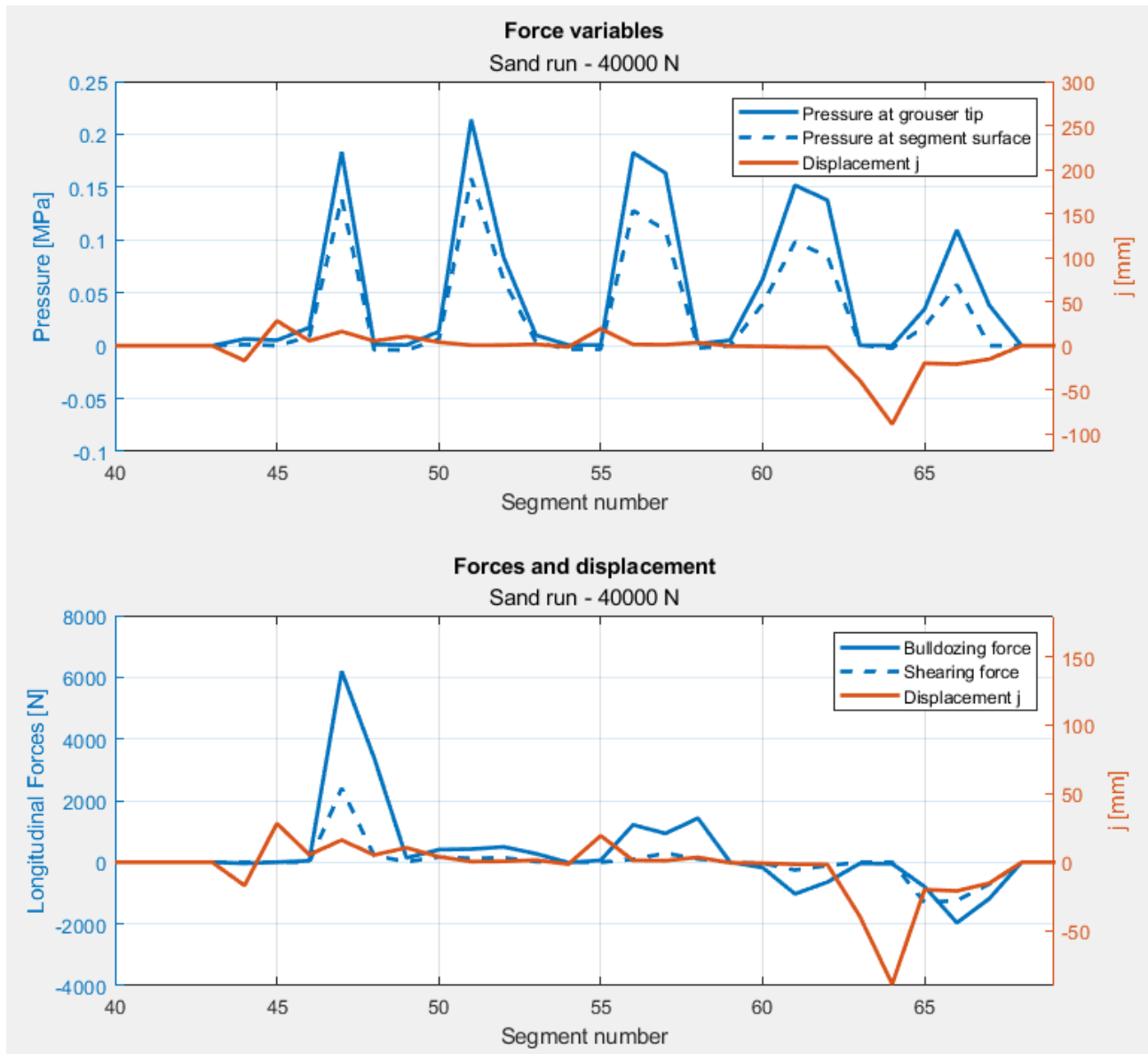


Figure 2.7.14 – Pressure and longitudinal forces with segment displacement j

This plot shows how the longitudinal forces are generated with a combination of displacement and pressure; if one of the 2 variables is close to zero, the resulting force will be close to zero. For example, segment 64 has a very high displacement, but since pressure is very close to 0 for that segment, the resulting force is non significant. Segment 47 instead has a high positive force because it's under a pressure peak and has a relatively high displacement. This shows also the linkage these forces have to the 2 variables: displacement regulates the sign of the force, in fact if displacement is negative, like for segment 66, the resulting forces will be negative. The magnitude of such forces also depends on the displacement, but is more heavily influenced by how much pressure (or surcharge) the segment is under. For this loose tensioner run, the plot shows how the most forces are concentrated in a few segments and the others are instead inert.

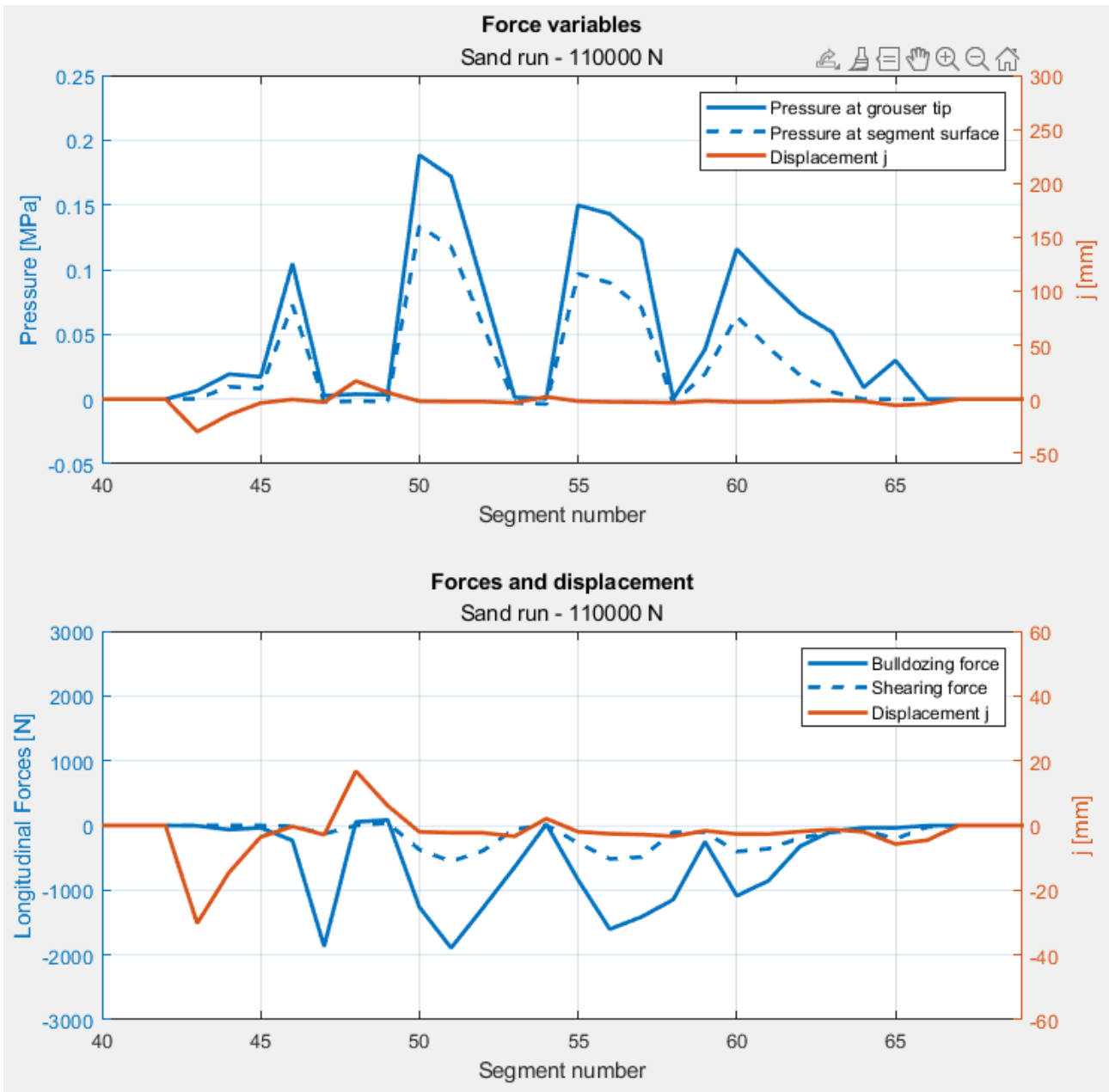


Figure 2.7.15 – Pressure and longitudinal forces with displacement j

With higher tensioner force, more of the segments are involved in the generation of forces. Noticeably, the slips are mostly negative, and hence all forces generated at this instant (again, 2.5 s) are negative.

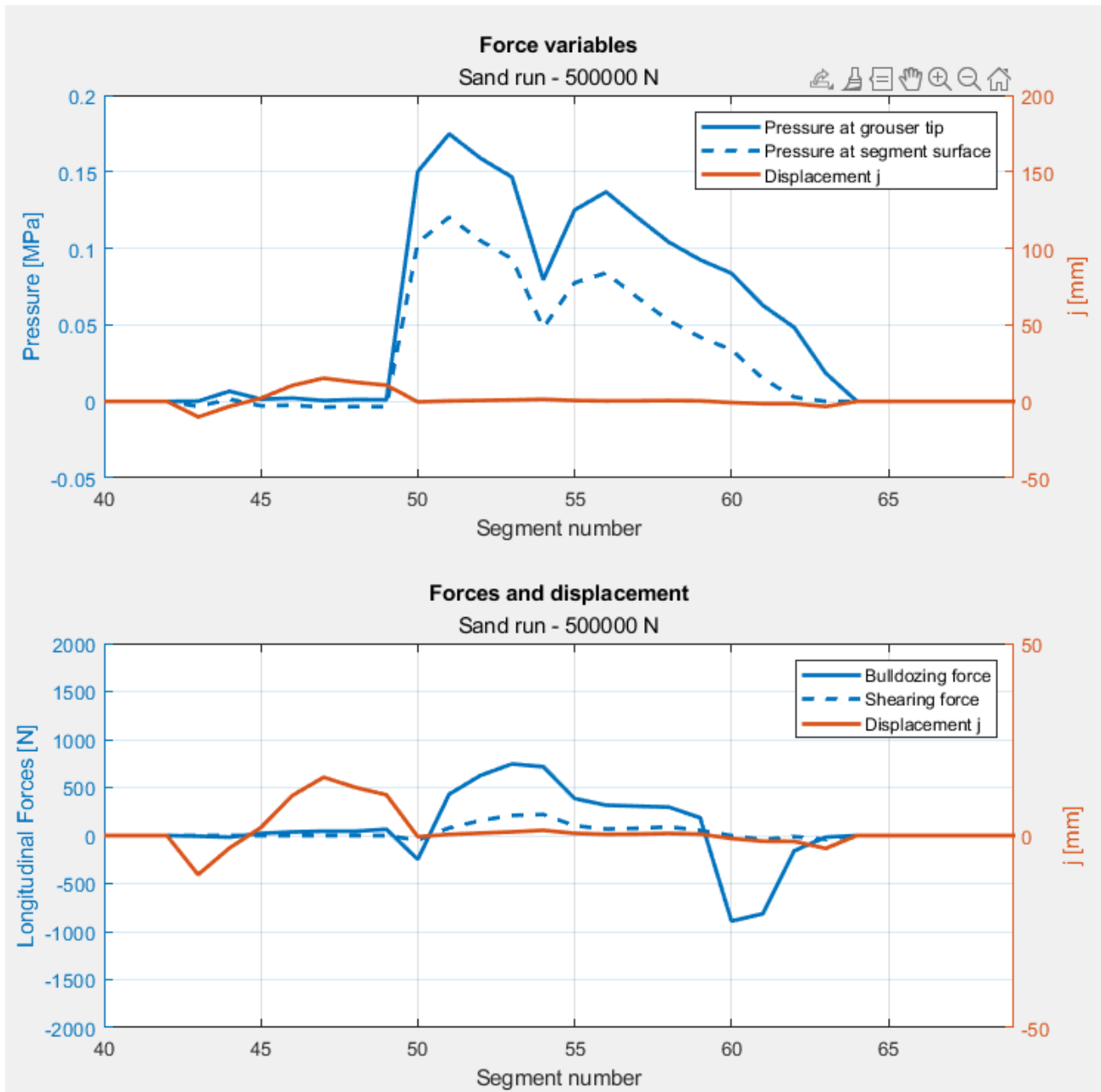


Figure 2.7.16 – Pressure and longitudinal forces with displacement j

A notable thing to note in these plots is how the magnitude of these forces is much lower when compared to the lower tensioner force runs. The forces and pressure are in fact more evenly distributed under the whole track, and more segments are involved in the total force generated.

Looking at clay results:

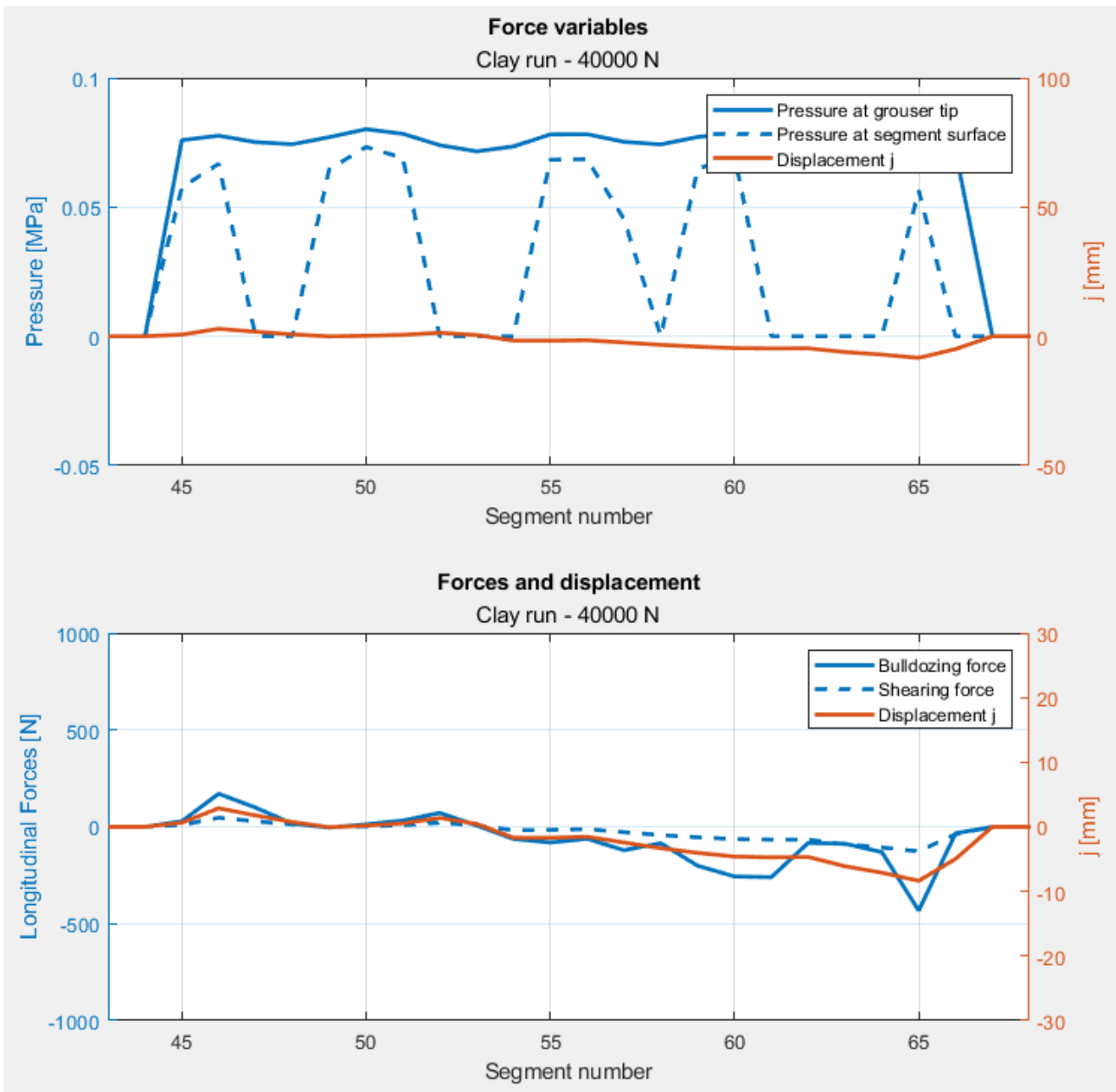


Figure 2.7.17 – Pressure and longitudinal forces with displacement j

For clay, the much lower pressure results in lower overall forces, but more consistent again, even with the loose tensioner. Also here, the forces are mostly negative, again coherently with displacement.

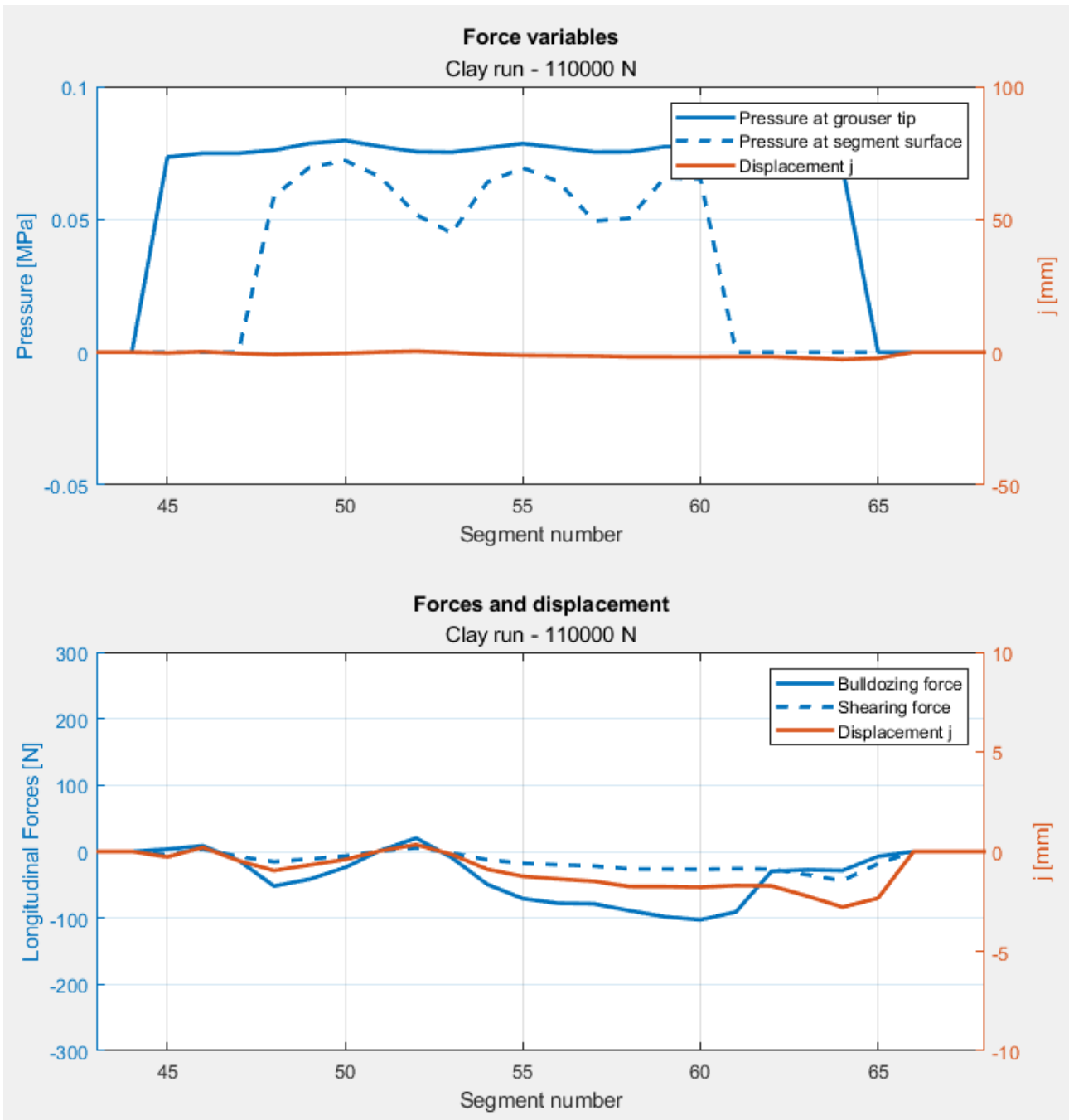


Figure 2.7.18 – Pressure and longitudinal forces with displacement j

This plot here shows how segment pressure heavily influences bulldozing force, seeing as the highest forces are from segments 48-60, the ones where the segment pressure is higher. Again mostly negative forces linked to mostly negative displacements.

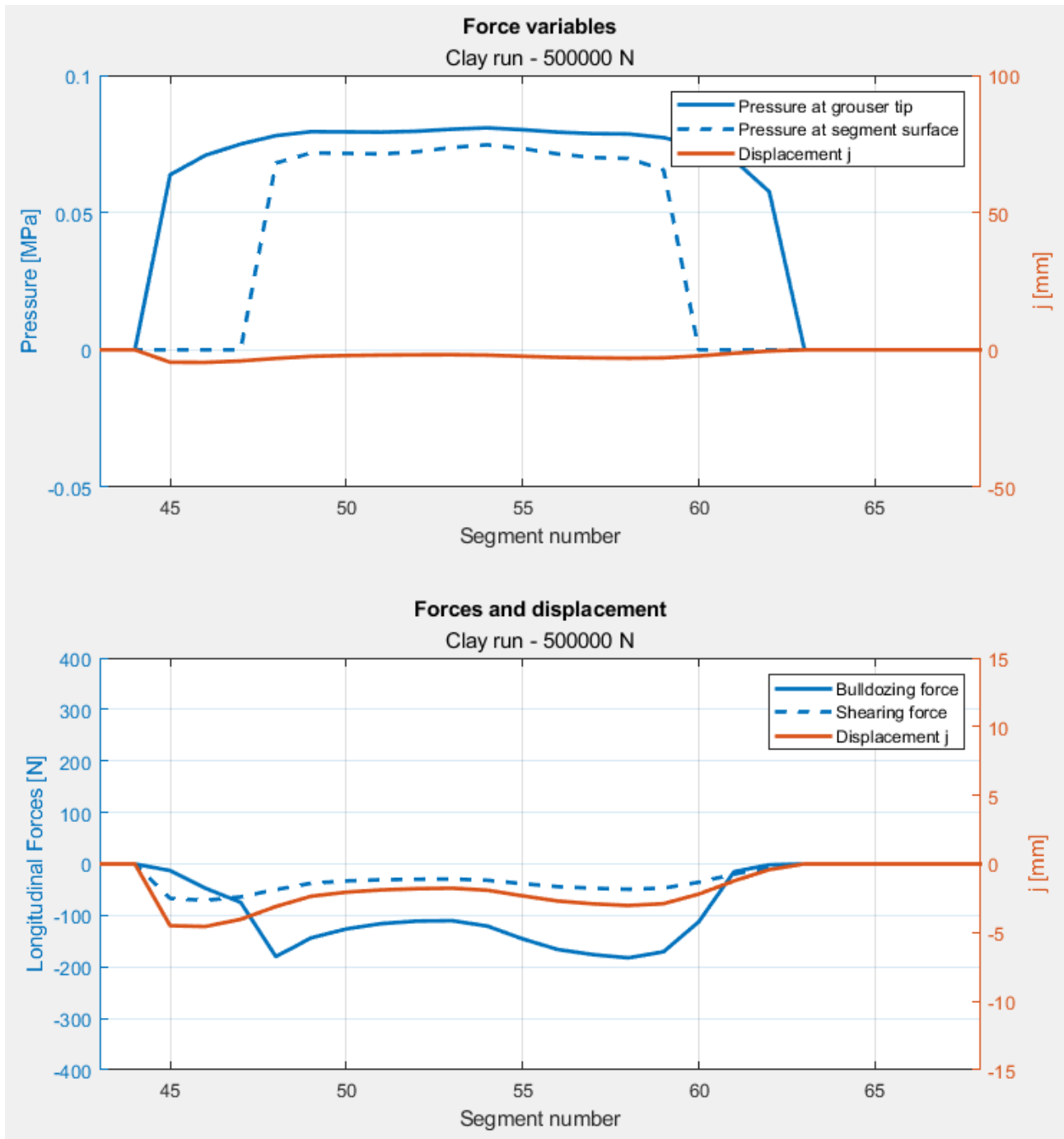


Figure 2.7.19 – Pressure and longitudinal forces with displacement j

Here, all forces are negative. These plots highlight even better the linkage between segment pressure and bulldozing force, and how instead shearing forces are more linked to tip pressure and displacement combined.

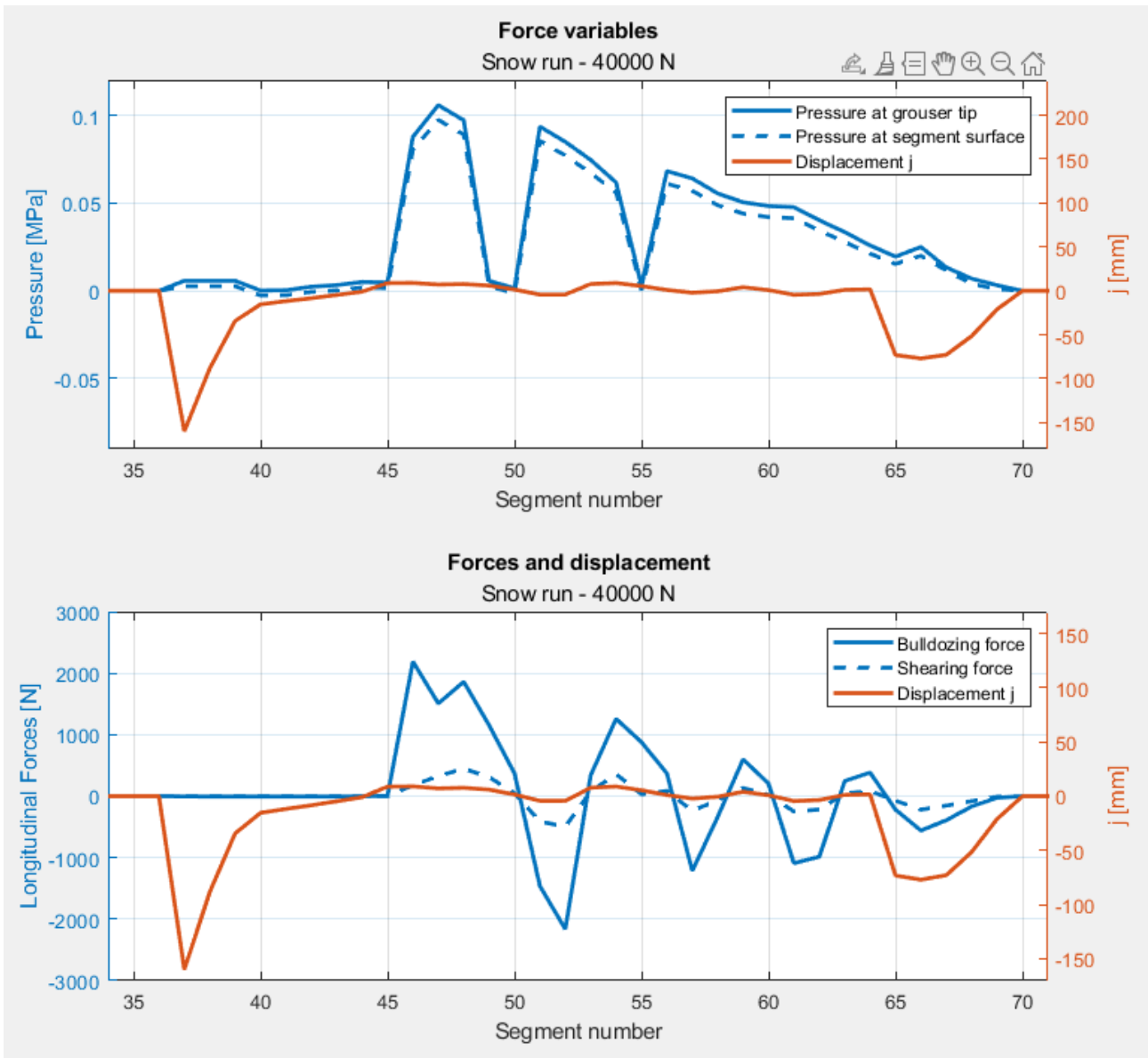


Figure 2.7.20 – Pressure and longitudinal forces with displacement j

The peculiarity of the snow plots is how, due to more of the track being in contact with the ground, even the slanted parts that go from the tensioner wheel to the first road wheel and from the last road wheel to the sprocket, are in contact with the ground. In fact, they have segments that slip way more than the others, but, especially those exiting the contact area, so those in the rear (36-40) aren't subject to pressure and therefore don't generate significant longitudinal forces.

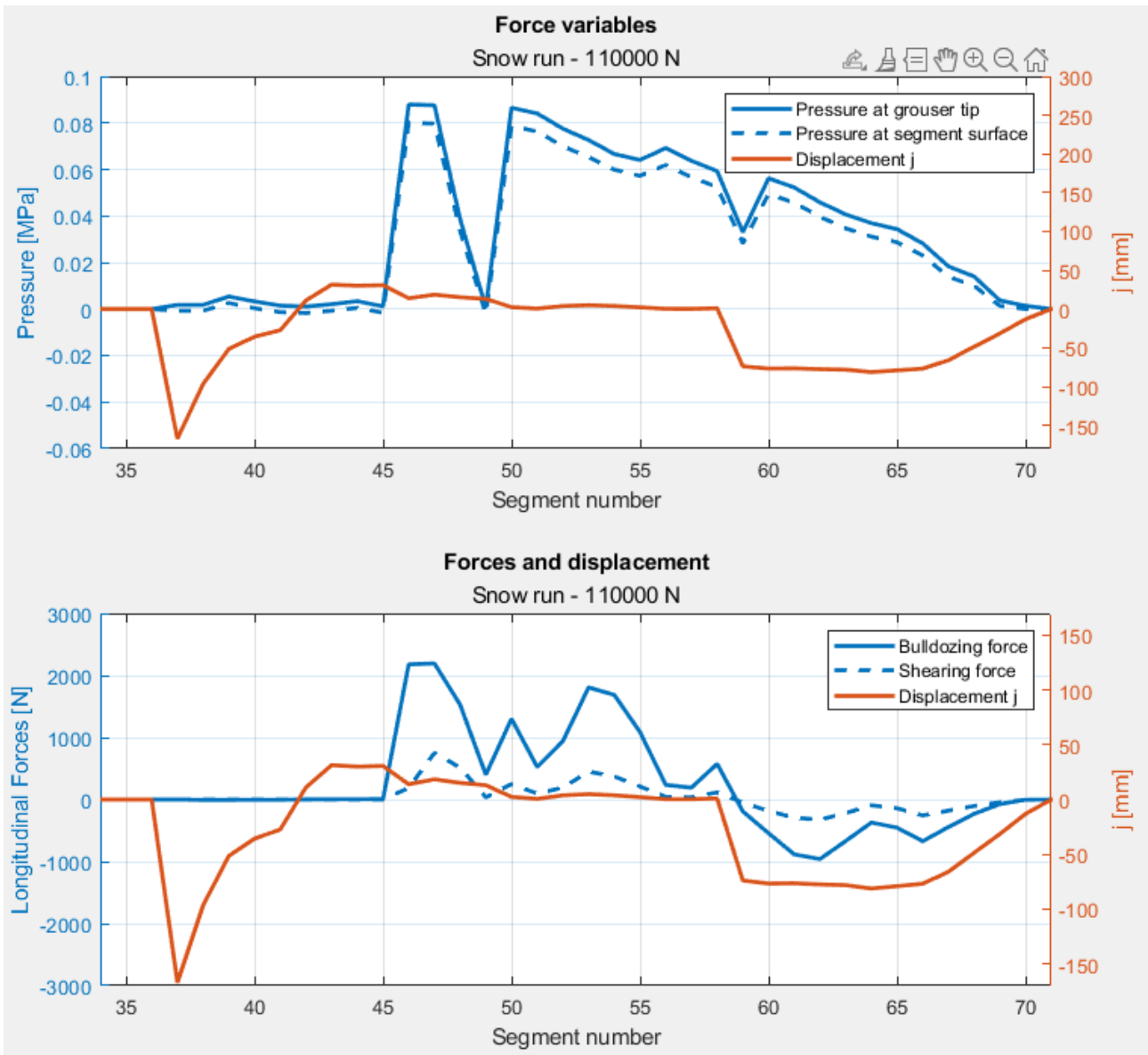


Figure 2.7.21 – Pressure and longitudinal forces with displacement j

Again, high slips in front and rear, but more consistent forces, both in magnitude and sign throughout the track.

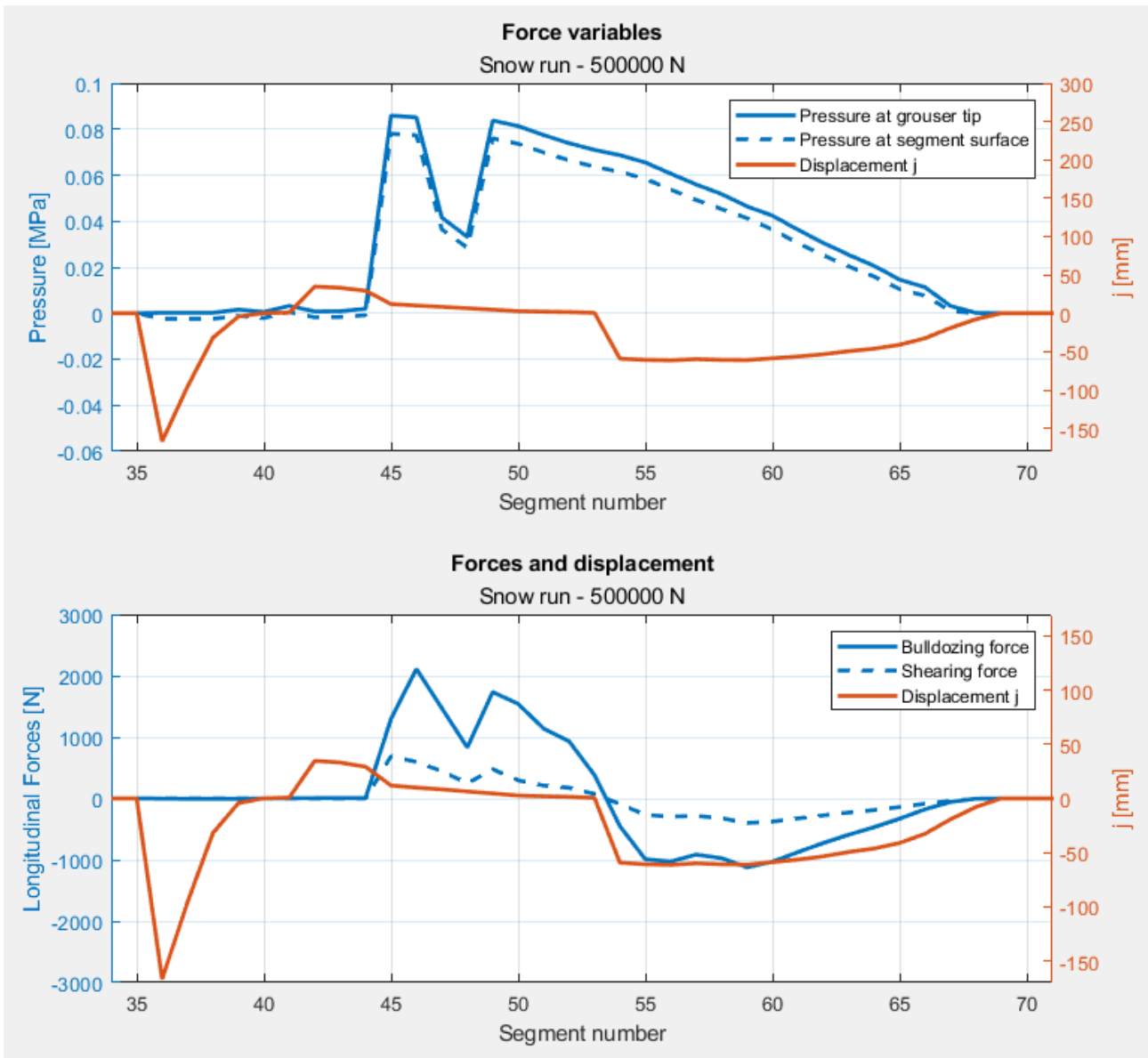


Figure 2.7.22 – Pressure and longitudinal forces with displacement j

Again, incrementally more stable and consistent.

Checking the torque provided by the sprocket at the chosen time step:

	Sprocket torque at 2.5s	
Sand - 40000 N tensioner	2.08E+03	Nm
Sand - 110000 N tensioner	1.83E+03	Nm
Sand - 500000 N tensioner	3.85E+03	Nm
Clay - 40000 N tensioner	3.59E+02	Nm
Clay - 110000 N tensioner	7.44E+02	Nm
Clay - 500000 N tensioner	2.61E+03	Nm
Snow - 40000 N tensioner	4.39E+03	Nm
Snow - 110000 N tensioner	3.05E+03	Nm
Snow - 500000 N tensioner	5.27E+03	Nm

Table 2.7.2 – Torque values at 2.5s

Interestingly, the torque varies quite a bit even if the vehicle is moving at the same speed in all simulations. For sand and snow, the minimum torque required is for the 110000 N tensioner force setup, while it's much higher for the 500000 N tensioner and still higher for the 40000 N tensioner, meaning a good balance of pressure distribution under the track and torque and power required to just move the vehicle in these soils is the middle value. For clay however, the lowest torque is the one associated with the lowest track tension.

2.7.1 Drawbar performance analysis

To better evaluate the performance of the vehicle with the variation of track tension, a study using the drawbar was conducted. The setup is the same as the analyses without the drawbar, with the addition of the drawbar pull force, so:

- Vehicle speed: 2 m/s or 7.2 km/h.
- Simulation time: 6 s.
- 3 different tensioner forces: 40000 N, 110000 N, 500000 N.
- Drawbar pull force: 20000 N.

Using the results coming from these analyses, the tractive efficiency in each configuration can be extracted.

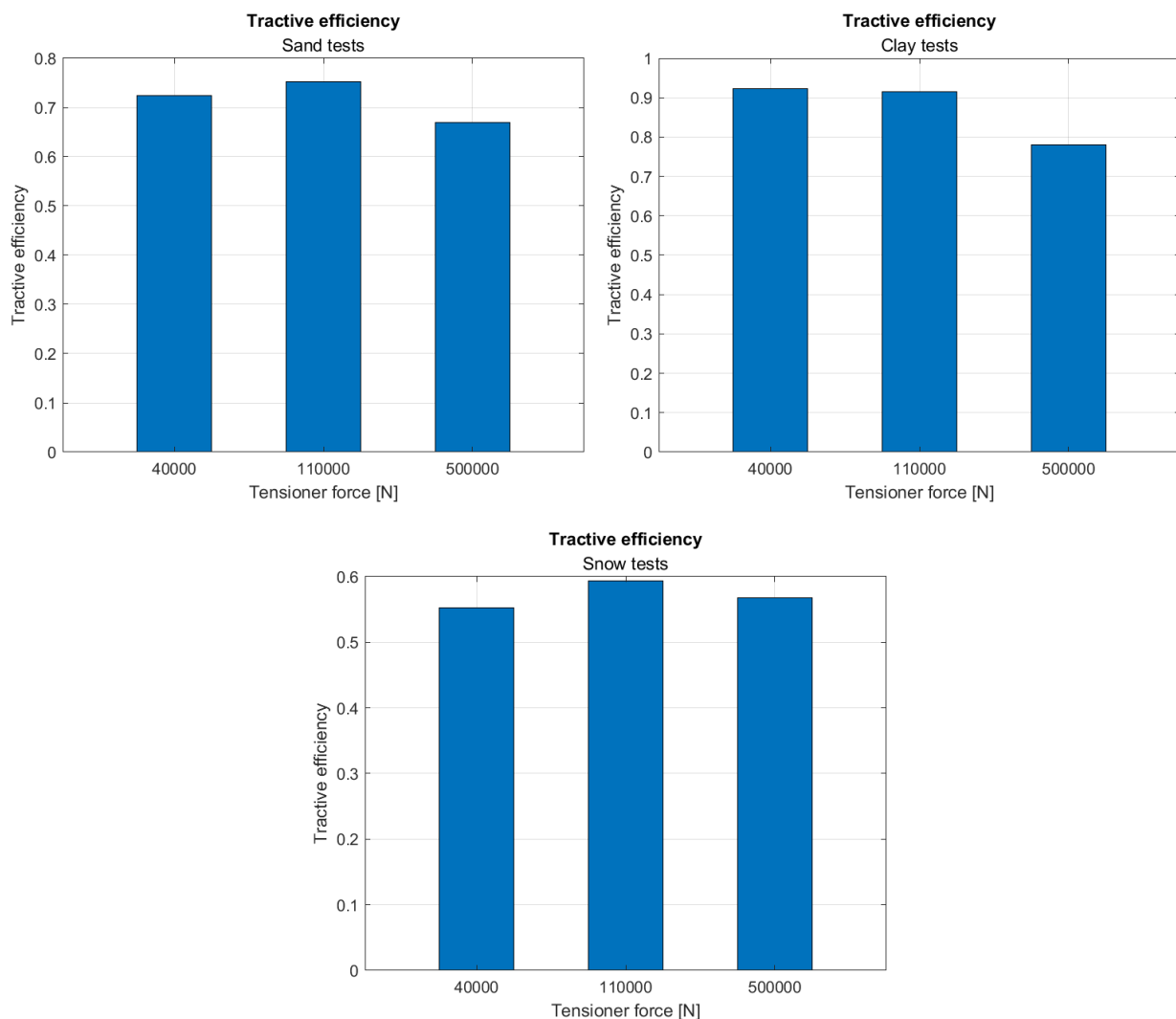


Figure 2.7.23 – Tractive efficiency in each run

What was previously seen with the torque variation is here clear. The best efficiencies for sand and snow are the 110000 N tensioner force setups. For clay instead, the lower force is slightly better.

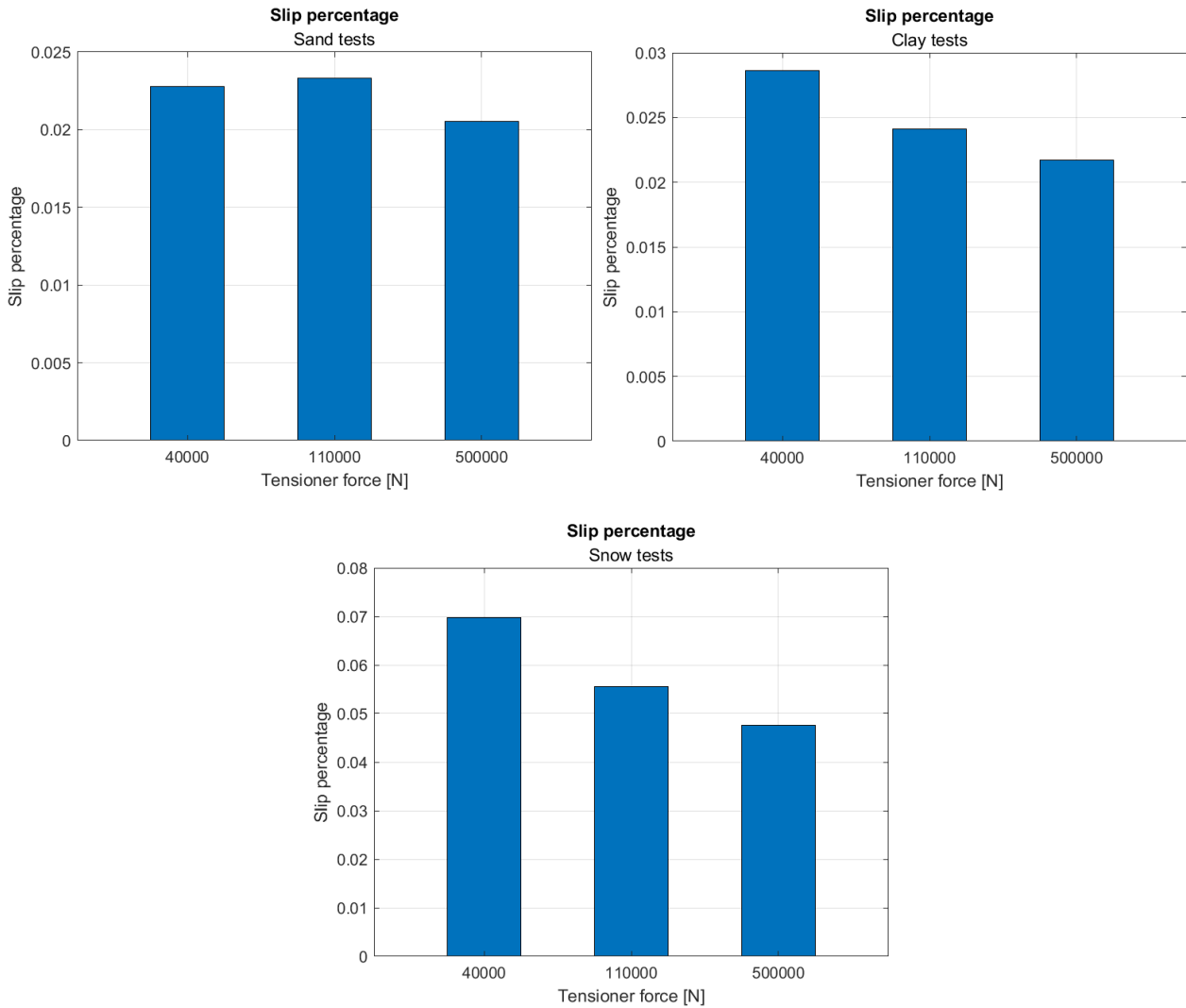


Figure 2.7.24 – Track slip percentage in each run

For all soils, the lowest slip happens at the highest tensioner force. This means that the sprocket wheel is rotating at lower velocity and therefore would, with the same torque generated, require less power and provide higher efficiency. However, as seen in table 2.6.1, the torque necessary in each case is much different, also in this case with a load applied:

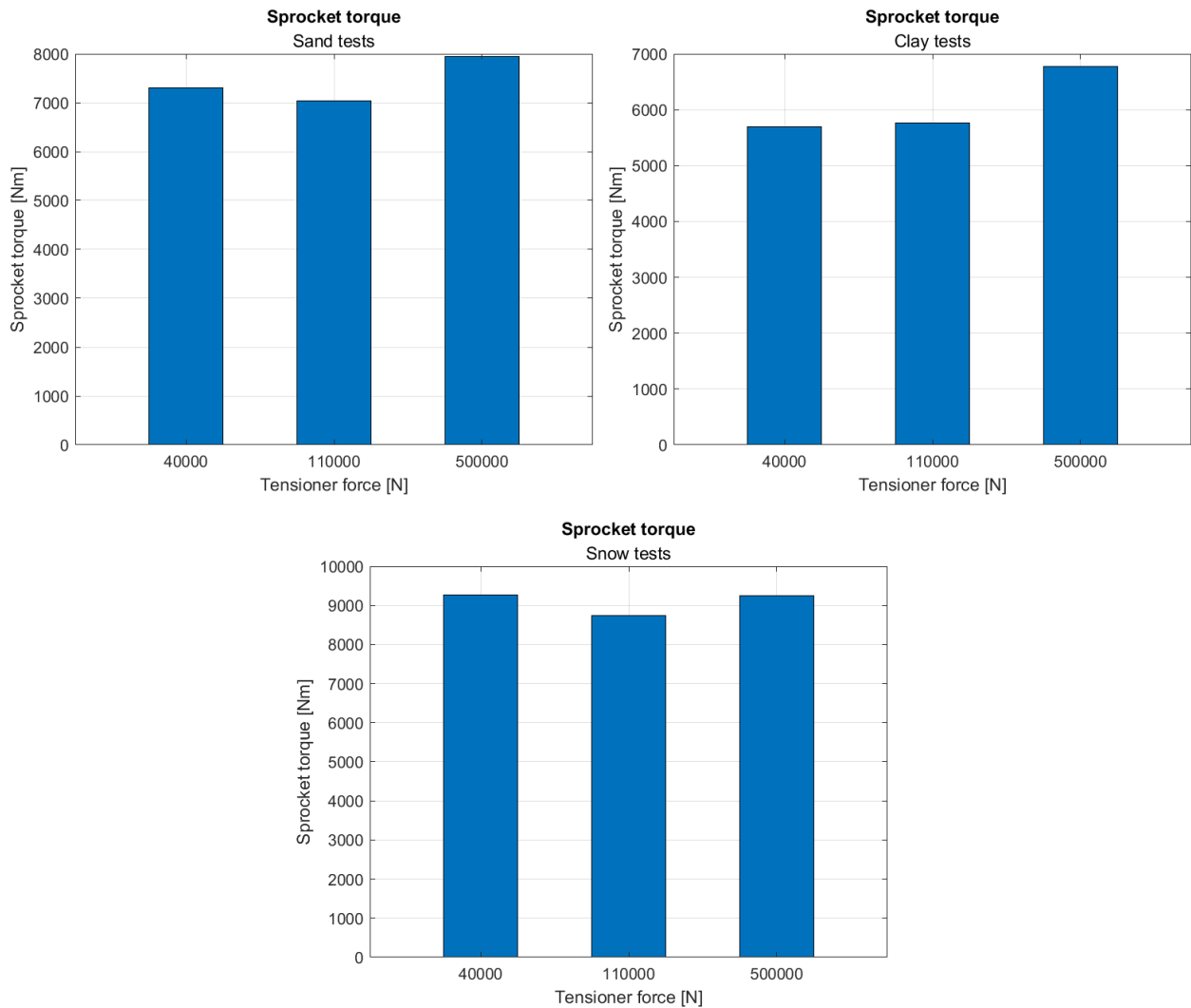


Figure 2.7.24 – Sprocket torque in each run

These results are in line with the ones from table 2.7.2, with an increase due to the load applied. Since the tank is moving at the same speed and the force applied is the same in every run, the efficiency depends only on torque and sprocket speed, so slip. In fact, for snow, the torque is almost the same for the 40000 N and 500000 N, but as seen in figure 2.7.20, the slip in the 40000 N run is much higher, and therefore the efficiency is lower.

In conclusion, the best setup force for the tensioner is 110000 N, which gives the best results for sand and snow, and comparable results for clay, making the tank able to cruise on all 3 terrains at high efficiencies.

Chapter 3 Conclusions

After utilizing the ATV software, it can be said that it provides a very useful tool to experiment with different combination of variables and geometry, making the user capable of optimizing the performance of the vehicle in a given situation.

In general, multibody simulation software saves a lot of time and cost, when the design of the vehicle is still in process, and allows to make assumptions and appropriate modifications before building a prototype. This makes the use of software in this and many other fields very advantageous.

Regarding ATV specifically, a tool to apply a constant load could be a great addition, and would require simply a slight adjustment of the current drawbar pull tool. Furthermore, the fact that damping isn't at all present in the calculation of longitudinal forces creates issues when analysing the steady state track forces of the vehicle without a load applied, since in some cases the segment slip can be negative and therefore generate negative forces, while in following time steps the behaviour is inverted, causing undamped oscillations in track forces. An addition of soil damping to better represent the forces generated by the track at any given moment would be a great asset, if appropriately supported by literature models in the near future.

Concluding, this document verified the positive effects of grousers in a tracked vehicle, while describing the many environment variables that are involved in the interactions between soft soils and rigid bodies, assessing the usefulness of simulation tools in the performance analyses of terramechanics.

Chapter 4 References

- [1] J. Y. Wong: Terramechanics and Off-Road Vehicle Engineering, 2nd ed., Elsevier Ltd., 2010
- [2] Adams Tracked Vehicle Toolkit Soft Soil Documentation, MSC Software Sweden AB, 2022
- [3] M. G. Bekker, Theory of land locomotion, Ann Arbor, The University of Michigan Press, 1956